Exsolution Mediated *In Situ* Alloying in Engineered Hercynite: A Promising Approach to Develop Catalysts for Sustainable Dry Reforming of Methane

Thesis submitted for the Degree of

DOCTOR OF PHILOSOPHY (SCIENCE)

Submitted By

Monotosh Bhattacharjee

Index No. 44/19/Chem./26

DEPARTMENT OF CHEMISTRY
JADAVPUR UNIVERSITY
KOLKATA – 700032
INDIA

AUGUST, 2025

JADAVPUR UNIVERSITY

KOLKATA – 700032, INDIA

Telephone: +91 33 2457 2767 (Office)
+91 8697671002 (Mobile)
E-mail : arup.gayen@jadavpuruniversity.in & agayenju@yahoo.com

Dr. Arup Gayen

PROFESSOR
PHYSICAL CHEMISTRY SECTION
DEPARTMENT OF CHEMISTRY

DATE: 27.08.2025

CERTIFICATE FROM THE SUPERVISORS

This is to certify that the thesis titled **"Exsolution Mediated *In Situ* Alloying in Engineered Hercynite: A Promising Approach to Develop Catalysts for Sustainable Dry Reforming of Methane"** submitted by **Mr. Monotosh Bhattacharjee** who got his name registered on **28th August, 2019** for the award of Ph.D. (Science) degree of Jadavpur University, is absolutely based upon his own work under the co-supervision of **Dr. Arup Gayen** and **Dr. Parthasarathi Bera** and neither this thesis nor any part of it has been submitted for either any degree/ diploma or any other academic award anywhere before.

Arup Gayen

---

1. Dr. Arup Gayen
Professor
Physical Chemistry Section
Department of Chemistry
Jadavpur University
Kolkata– 700 032
E-mail: arup.gayen@jadavpuruniversity.in

Dr. Arup Gayen
Professor
Department of Chemistry
Jadavpur University
Kolkata-700032

Parthasarathi Bera

---

2. Dr. Parthasarathi Bera
Professor, AcSIR and Senior Principal Scientist
Surface Engineering Division
CSIR–National Aerospace Laboratories
Bengaluru– 560017
E-mail: partho@nal.res.in

वैज्ञानिक / SCIENTIST
पृष्ठीया अभियांत्रिकी प्रभाग
SURFACE ENGINEERING DIVISION
सीएसआईआर राष्ट्रीय वायुसेना प्रयोगशालाएं
CSIR-National Aerospace Laboratories
बेंगलूरु/Bengaluru-560 017

DECLARATION

I hereby declare that the work embodied in the present thesis titled **"Exsolution Mediated *In Situ* Alloying in Engineered Hercynite: A Promising Approach to Develop Catalysts for Sustainable Dry Reforming of Methane"** is the result of investigations carried out by me in the Department of Chemistry of Jadavpur University under the co-supervision of **Dr. Arup Gayen**, Department of Chemistry, Jadavpur University and **Dr. Parthasarathi Bera**, Surface Engineering Division, CSIR–National Aerospace Laboratories, Bengaluru– 560017 and neither this thesis nor any part of this thesis has been submitted for any degree earlier anywhere.

In keeping with the general practice of reporting scientific observations, due acknowledgement has been made whenever the work described has been based on the findings of the other investigators. Any omission which might have occurred by oversight or error in judgment is regretted.

Date: 27.08.2025

Monotosh Bhattacharjee

(Monotosh Bhattacharjee)

Dedicated
To

All my Gurus and my Parents

Acknowledgements

"A grateful heart is a magnet of miracles"

The journey of writing this thesis has been one of the most rewarding experiences that brought me closer to my dream. There are so many people along the way, who supported and encouraged me consistently in the successful completion of this highest academic degree. It is impossible to put into words just how much their support means to me.

I am and will always be deeply grateful for the influencing support, expert guidance and the power of thoughtful analyses of my supervisor, Professor Arup Gayen. His constant inspiration was invaluable and truly helped me reach the finish line. I am deeply indebted to him for his inspiring enthusiasm, the trust he gave me to work freely, and his friendly demeanor. He not only taught me how to be a researcher but also inspired me to persevere through every challenge instilling a spirit of dynamism in me. To be honest, I am feeling blessed and fortunate enough to have the opportunity to work under the supervision of Prof. Gayen. He stood by me even in the most difficult moments of my life i.e., in every sense of the word, he has been a friend, a philosopher and a guide to me.

I would like to express my deepest gratitude to my co-supervisor, Professor Parthasarathi Bera. His intellectual curiosities, gracious guidance and unwavering support throughout my entire research journey were invaluable. I am truly thankful for his continuous monitoring and patient mentorship.

I cordially express my gratitude to the members of Research Advisory Committee (RAC) for their critical feedback and insightful suggestions that significantly shaped the theme of my thesis. Especially, I am very much thankful to the subject expert, Dr. Manas Kumar Panada, Jadavpur University for his critical assessment and useful suggestion in every RAC meeting held in my PhD tenure. Overall, their expertise and thoughtful critiques were instrumental in improving the overall quality of my work.

It is my honor to express my gratitude to Dr. Md. Motin Seikh, Visva Bharati University for his kind advice to join Professor Gayen's group to start and carry out my doctoral research. I am privileged enough to get a short exposure in his laboratory for my initial training for further exposure into greater domain. He was there from beginning in

every single moment of my journey with his special care and unforgettable endeavor to uplift the merit of my research.

My heartfelt thanks go to Dr. Prasanta Kumar Sinha, CSIR-CGCRI for his deep involvement and kind cooperation in my research work throughout this journey starting from the CGCRI days including the fruitful collaboration done from his end providing several high end instrumental facilities like HRTEM, ICP-AES and Raman spectroscopic analysis which helped me a lot to build up my thesis. His constant inspiration proved to be of immense help.

I am grateful to Professor Sounak Roy, BITS Pilani, Hyderabad campus for his supportive collaboration by providing us with XPS and TG-DTA measurements.

I would like to express my earnest sense of attitude to Professor Sara Colussi, University of Udine, Italy for her sincere attention in a critical situation of time bound revisionary research work.

My sincere thanks go to Dr. Bibhuti Bhusan Show, Jadavpur University for the fruitful scientific discussions in several critical issues during my doctoral research.

I wish to thank Dr. Srabanti Ghosh madam, CSIR-CGCRI for her valuable suggestion in a specific context during an investigation as a part of my research work.

I am very much thankful to Dr. Tapas Kumar Mandal, IIT Roorkee and his family for their cordial reception during my visit to his laboratory.

I express my thanks to the Section-In-Charges, Physical Chemistry Section, Heads of the Department of Chemistry and Deans of Science faculty for their kind cooperation in every time I needed and allowing me to access the general instrumental facilities during the entire tenure of my research work.

I would like to convey my deep admiration to Prof. S. C. Bhattacharya, Prof. S. K. Bhattacharya, Prof. K. K. Das, Prof. N. Chattopadhyay, Prof. A. Mahapatra, Dr. P. K. Mahapatra, Dr. B. Bhattacharjee, Prof. S. Ghosh, Prof. C. K. Mondal, Prof. S. Das, Prof. P. P. Parui, Dr. S. K. Ghosh, Dr. S. Bardhan and Dr. S. Mondal for their inspiration and motivation.

I am thankful to Mosaraf Da and Satyajit Da and other members of the Physical Chemistry Section for helping me in every possible way during my days at Jadavpur University.

Words are not enough to express my love for my labmates. I extend my gratitude to my brilliant colleagues, Kamalesh, Kalyan, Akbar, Trilochan, Chandan and Karan Di for the

countless hours of discussion, shared tea breaks, and for creating a supportive and fun-filled workspace in the laboratory. Their friendship made the long days feel short. Above all, the positive interactions and camaraderie with them had a significant impact on my research work. My special thanks go to Sourav, Akash, Tuhin, Koyel and Aishee for their company during their M. Sc. Project work. Thanks to Saborno of CGCRI for helping me a lot in the preparation of the very first draft of my maiden manuscript. I convey my thanks to Athira for their collaborative cooperation. I am also thankful to Akash of IIT (ISM) Dhanbad and Pratap of IACS for their unconditional support in my research.

I would like to express my hearty thanks to my dearest friend Dr. Debiprasad Roy of IACS, Kolkata for providing me the CHNS facility which is turned out to be very crucial for my research work.

I would like to convey my thanks to Ariful, Manotosh, Yasmin Di, Snigdha, Rini, Mainak, Sourav, Sayani, Chatan, Priyanka, Rakesh, Debmalya da, Debopam Da, Arnab Da, Mithun Da, Dasarath Da, Sabyasachi, Chandi, Pratima, Barnali, Taposhi, Madhusudan, kuntal, Monisha, Indrajit and other labmates for their cooperation and cheerful company. I am very much gratefull to my roommate Gopal and other hostelmates for the beautiful and loveable moments I shared with them in NPG cum RS hotel, Jadavpur University campus.

I am also deeply grateful to Smita madam for her warm hospitality, motherly care and affectionate support. I have been associated with cheerful moments with Sanjukta and Agniva. Moreover, I have been fortunate enough to receive the blessings of Mr. Haripada Gayen on several occasions.

I am also grateful to my dearest friends Jevan, Shruti, Anupam and Tanwi. Their unconditional moral support was a lifeline during the darkest moments of my life.

I have been further blessed by the love, affection and endless support by my family members, especially my mother, Mrs. Dali Bhattacharya and my beloved sister Ms. Suparna Bhattacharjee, inspiring me to push through every challenge in life. Without their inspiration and sacrifices I couldn’t have reached the shore of success. I would like to express my gratitude and gratefulness to the other family members for their wishes and blessings.

Finally, I thank the Science and Engineering Research Board (SERB), Government of India; Jigayasa 2.0 Scheme and CSIR-CGCRI for research fellowship and Jadavpur University for giving me such a great platform to pursue me doctoral research.

Contents

Chapter 5

Studies on the DRM behavior of combustion made $(NiMnCoCu)_xFe_{1-x}Al_2O_4$

Chapter 6

Exsolution-mediated in situ alloying: key findings and future outlook

Synopsis

Name of the scholar: **Monotosh Bhattacharjee**

Index No.: **44/19/Chem./26**

Title of the Thesis: **Exsolution Mediated *In Situ* Alloying in Engineered Hercynite: A Promising Approach to Develop Catalysts for Sustainable Dry Reforming of Methane**

The objective of the thesis is to design and synthesize some hercynite ($FeAl_2O_4$)-based catalysts, $(TM)_xFe_{1-x}Al_2O_4$ (where TM = Ni alone or in combination with other first row transition metals), capable of *in situ* alloying through co-exsolution, for sustainable dry (CO_2) reforming of methane (DRM) and provide a generalized idea for developing next generation DRM catalysts exploiting the 'exsolution mediated *in situ* alloying' technique.

DRM ($CH_4 + CO_2 \rightleftharpoons 2H_2 + 2CO$) is a thermocatalytic process that consumes two potent greenhouse gases, CO_2 and CH_4 to produce synthesis gas (also known as syngas, a mixture of H_2 and CO), a feedstock in the Fischer-Tropsch process. Additionally, this reaction has the required merits to be considered as a promising route for sustainable energy production. Despite its potential outcome, catalyst deactivation originating from sintering followed by carbon deposition are challenging issues for the commercialization of DRM process. Mostly explored catalysts are precious metals (Ru, Rh, Ir, Pd, and Pt), supported on a variety of materials, especially oxides. But their uses are limited because of scarcity and high cost. In this context, transition metals (mostly Ni) are viable substitution of the precious metals for DRM. Irrespective of high activity of Ni in DRM, there is a hurdle of interrelated issues viz., sintering and coking, as demonstrated by many researchers that over a threshold particle size of Ni, carbon formation is evident. The design and development of Ni-based catalysts with anti-sintering, anti-coking ability includes addition of other metal(s) (in various forms) as promoter. Alloying is a form of adding another metal to improve the electronic behaviour of Ni, which eventually assists in enhancing the performance of Ni-based catalysts in DRM. For alloying, reduction of the catalyst, particularly with H_2 is a common practice. In that case, dealloying of active phases in the DRM environment may hinder its applicability. To avoid the consumption of H_2 in prior reduction process and to prevent dealloying,

'exsolution mediated *in situ* alloying' may be effective for availing a hassle-free DRM. In this regard, hercynite, which is always challenging to synthesize in its pure phase, has purposefully been chosen for some judicial chemical tailoring towards robust DRM activity using Ni and other transition metals in different proportions which are discussed in various chapters of the thesis.

Chapter 1 provides a concise overview based on the literature survey on sustainable DRM taking into consideration the limiting issues of Ni-catalyzed DRM with a special featuring on alloying.

Chapter 2 enunciates at first the beauty of facile solution combustion synthesis (SCS) method utilized to prepare the different catalysts. The wide range of modern sophisticated characterization techniques are summarized that have been explored to observe the physicochemical nature of the catalysts and to provide comprehensive idea about structure-property relationship. These techniques include powder X-ray diffraction (PXRD), BET surface area measurement (S_{BET}), H_2-temperature programmed reduction (H_2-TPR), CO_2-temperature programmed oxidation (CO_2-TPO), inductively coupled plasma-atomic emission spectroscopy (ICP-AES), Chemical (CHNS) analysis, Raman spectroscopy, high resolution transmission electron microscopy (HRTEM), high-angle annular dark-field scanning tunneling electron microscopy (HAADF STEM), thermogravimetry-differential thermal analysis (TG-DTA) and X-ray photoelectron spectroscopy (XPS). The gas-solid heterogeneous catalyst testing protocols have been discussed at the end of this chapter.

Chapter 3 deals with investigation about the effect of chemical tailoring through simultaneous doping of Ni and Cu in the hercynite spinel. A series of nanodimensional (10–14 nm) hercynites has been synthesized following SCS method and the optimized sample, $Ni_{0.08}Cu_{0.07}Fe_{0.85}Al_2O_4$ (named as NCFAO8), is reported to exhibit noteworthy coke-free conversions of 97% and 99% for CH_4 and CO_2, respectively, with H_2/CO ratio of ~0.80 at a gas hourly space velocity (GHSV) of ~34000 mL g^{-1} h^{-1} at 800 °C. True potential of the catalyst has been evaluated over a range of temperatures and varying GHSVs. Additionally, this investigation highlights the structural evolution of the hercynite-based catalyst during time-on-stream activity behavior. Thorough characterization of the aged (after catalytic test for a prolonged duration of 100 h) vis-à-vis the as-prepared catalyst suggests *in situ* co-exsolution of the doped metal ions (Ni and Cu) and a certain portion of Fe from the catalyst leading to formation of NiCuFe trimetallic alloy and is accompanied by the formation of γ-Al_2O_3 along with the retention of pristine hercynite phase. Alloying of the active component

Ni with Cu, the two dopant ions, and host Fe in presence of the spinel ($FeAl_2O_4$ and γ-Al_2O_3) is shown to be beneficial in circumventing the difficulties of Ni-only catalysts in DRM. Interestingly, the residual carbon, present initially in the catalyst prepared with SCS method gets diminished in the course of reaction. Instead of coke deposition, substantial removal of the residual carbon in the DRM environment suggests NCFAO8, a promising next generation catalyst for DRM with sustainable coke resistant ability, which can be further extrapolated to simulated bio-gas reforming.

Chapter 4 discusses the study of DRM over the SCS-made Ni-doped hercynites, with general formula $Ni_xFe_{1-x}Al_2O_4$ (where, x = 0.2–0.5). All these catalysts show stable conversion behavior towards moderate temperature DRM reaction. It has also been noted that $Ni_{0.40}Fe_{0.60}Al_2O_4$ exhibits the highest DRM activity amongst all, after 20 h of continuous reaction without loss of activity. The catalyst shows nearly similar DRM activity up to 50 h run time of DRM. After the reaction, the aged phase of the catalyst has been recovered and found to contain the signature of NiFe alloying along with the retention of original hercynite phase. *In situ* alloying of the doped metal with host is again proved to be an effective way for entailing a sustainable moderate temperature DRM.

Chapter 5 comprises of the chemical tailoring of hercynite through simultaneous doping of Ni, Cu, Co, and Mn at the Fe-site using the ultra-fast SCS method followed by their activity test in catalytic DRM. No additional peak in the PXRD pattern of as-prepared catalyst confirms the structural flexibility of the hercynite in incorporating several transition metals into the spinel framework. The general formula of the catalysts is $(NiCuCoMn)_xFe_{1-x}Al_2O_4$ (x = 0.2 and 0.4). All these catalysts are shown to be very promising with respect to both conversions (CH_4 and CO_2) as well as H_2/CO ratio. Moreover, the diffraction pattern of 30 h aged catalyst clearly indicates the presence of *in situ* formed alloy.

Finally, the key research findings have been summarized in **Chapter 6** followed by highlighting certain significant insights in a conclusive manner. The plausible future directions have also been pointed out which are generalized in true sense in the crucial and developing field of “exsolution mediated *in situ* alloying” for sustainable DRM. The thesis is concluded with the briefing of research works that are underway and discussing of necessity of detailed investigations by high-end instruments and cutting-edge technologies, which may be availed in near future through collaborative research.

Chapter 1

A comprehensive overview on sustainable dry reforming of methane

1.1. Introduction

Due to rapid economic development and the continuous growth of the global population, energy demand has risen significantly over the past few decades, with fossil fuels remaining the primary source of energy, supplying approximately 80% of the world's needs. However, their combustion inevitably results in negative consequences, such as CO_2 emissions and global climate change. As a result, the urgent need for a renewable and environmentally friendly energy carrier has become increasingly evident. Hydrogen has attracted significant attention of researchers as an energy-efficient and clean fuel, thanks to its high energy content and net-zero carbon emission. Among the various hydrogen production methods, natural gas (NG) reforming is considered the primary approach, accounting for approximately 80–85 % of global hydrogen production. In recent years, natural gas exploitation has grown substantially, fueled by the discovery of new gas reserves and advancements in extraction technologies for unconventional natural gas (UNG), such as shale gas, methane clathrates, and biogas. This surge has, in turn, heightened interest in methane reforming technologies for hydrogen production. Steam reforming of methane (SRM) is currently the benchmark industrial process for H_2

production, accounting for approximately 80–85 % of global H_2 supply; however, it faces challenges such as high energy input due to reaction thermodynamics and the high specific heat capacity of water as well as issues related to catalyst stability. Compared to SRM, dry (CO_2) reforming of methane (DRM) has gained significant interest due to its ability to simultaneously converting two major greenhouse gases, CO_2 and CH_2, into synthesis gas (a mixture of H_2 and CO) in a single reaction, and the nearly equal stoichiometry of H_2 and CO (H_2/CO molar ratio ~ 1) in the product gas further extends its applicability beyond hydrogen production to various downstream processes such as Fischer-Tropsch synthesis, methanol synthesis and ammonia synthesis. Hence, this technology has attracted considerable attention as a promising approach for the valorization of CO_2 and the efficient use of natural gas.[1-6]

1.2. Potential of DRM over other reforming reactions

Except steam reforming, the DRM has been the subject of extensive study since 1928, when Fischer and Tropsch first explored it using a combination of Ni and Co catalysts.[7] Besides SRM and DRM, other widely studied technologies for the conversion of CH_4 to synthesis gas are autothermal reforming (ATR), partial oxidation (POM), combined reforming of methane (CRM) and tri-reforming of methane (TRM).[8] These reforming reactions differ in the oxidant used, final H_2/CO product ratio as well as energetics and kinetics of the reaction. On the other hand, reforming of CH_4 involving various combinations with O_2, H_2O and CO_2 is called ‘mixed’ reforming, and is usually employed to control H_2/CO ratio of the product stream simply by altering the ratio of H_2O, CO_2 and

O_2.[9] However, despite several limiting issues, Ross et al.[10] have shown that DRM incurs operating costs approximately 20% lower than those of other reforming processes.

1.3. Thermodynamics of DRM process: the limiting issues

In the DRM process, the primary reaction (Eq.1.1) is accompanied by six critical side reactions (Eq. 1.2 to Eq. 1.7) which are listed below.

DRM reaction: $CH_4 + CO_2 \rightleftharpoons CO + H_2$ ---------- (1.1)

Reverse water-Gas Shift (RWGS) reaction: $CO_2 + H_2 \rightleftharpoons CO + H_2O$ ---------- (1.2)

CH_4 decomposition reaction: $CH_4 \rightleftharpoons C + 2H_2$ ---------- (1.3)

CO disproportionation or Boudouard reaction: $2CO \rightleftharpoons C + CO_2$ ---------- (1.4)

CO_2 hydrogenation reaction: $CO_2 + 2H_2 \rightleftharpoons 2H_2O + C$ ---------- (1.5)

SRM reaction: $CH_4 + H_2O \rightleftharpoons CO + 3H_2$ ---------- (1.6)

CO hydrogenation reaction: $H_2 + CO \rightleftharpoons H_2O + C$ ---------- (1.7)

The DRM reaction is highly endothermic, and elevated temperatures above 727 °C are favorable for its progression. At high temperatures, the DRM reaction is typically accompanied by the reverse water-gas shift reaction, which consumes both the feed CO_2 and the produced H_2. As a result, CO_2 conversion is higher than CH_4 conversion, leading to a H_2/CO ratio of less than 1 (unity) in the resulting synthesis gas. Moreover, the water generated during the RWGS reaction can accelerate metal sintering, negatively impacting catalyst stability and performance. In addition, with increasing temperature the

contribution of the RWGS reaction, SRM, and carbon gasification (i.e., reverse Boudouard reaction) become more significant.[11, 8]

1.4. Benefits of Ni in catalytic DRM

Metals from groups VIII, IX, and X are generally active in DRM, with Ru, Rh, and Pt showing greater resistance to coke formation than other transition metals. The catalytic activity of noble metals in DRM follows the order: Rh > Ru > Ir > Pd > Pt. The superior performance of Rh, Ru, and Ir is attributed to their small particle size and high dispersion. Pd and Pt exhibit relatively lower activity in DRM due to high temperature sintering issues. However, their high costs and limited availability remain the main challenges, restricting their practical application. Key features for an industrial DRM catalyst include high activity, coke resistance, robustness, longevity, and minimal synthesis steps from commercially available precursors—though coke resistance is frequently overlooked. Considering these parameters, Ni, a non-noble metal, has emerged as a viable choice for DRM reactions. Despite the challenge of coking, Ni typically exhibits higher initial conversion(s) than Ru, Ir, Pd, and Pt.[12-19, 9]

1.5. Hurdle towards industrialization of DRM using Ni

Ni-based catalysts are susceptible to sintering at high operating temperatures of DRM, assisting carbon deposition, originating from methane cracking and other coke-forming reactions. As a consequence, the catalyst becomes poisoned due to blockage of the active sites. Carbonaceous deposits can chemisorb as strongly bonded single layers or physisorb

as multilayers and may completely encapsulate the active metal or plug micropores and/or mesopores, thereby severely hindering the accessibility of active sites to reacting substances. In the most severe cases, carbon may develop as cracking filaments that can lead to the destruction of the support material. These issues engender a decline in long-term stability, thereby significantly restraining their industrial application. Therefore, current research in DRM has engaged and should continue to focus on developing coke-resistant nickel-based catalysts.[20-29]

1.6. Rational development of Ni-based catalysts for DRM

1.6.1 Confined Ni catalysts

Rational catalyst design and synthesis can alleviate the challenges of sintering and carbon deposition on Ni-based catalysts. Great efforts have been put into developing new catalyst designs to overcome these challenges. For example, researchers are:

- developing structured catalysts (e.g., layered double hydroxides, perovskites, spinels, bimetallics, and solid solutions) that have strong metal-support interactions (SMSI).
- confining Ni metal within the cavities of mesoporous supports to restrict their growth.
- designing core/yolk-shell structures with a protective layer to prevent the active metal from sintering.[30-32]

Despite great advancements, several key problems with core-shell catalysts remain. For instance, methods for their efficient fabrication are limited and often not versatile. Furthermore, it is still difficult to precisely control the core size and shell thickness, and the

overall yield of the final catalyst is often low. Finally, a significant challenge is the shell-block effect, where the protective shell degrades the catalytic activity of the active metal core. These issues have limited the use of core-shell materials.[33]

1.6.2. Ni bimetallic and alloy catalysts

Developing bimetallic catalysts is a practical method to develop Ni-based DRM catalysts with coke-resistant ability. Combining Ni with other metals can readily change its surface properties to achieve better catalytic performance; known as synergistic effect. The structure of such Ni-based bimetallic particles can be a core–shell structure or alloy depending on their reduction potential although the relationship between reduction potential and structure is not always straightforward. For supported bimetallic materials, the structure also depends on the method of preparation. Several noble and non-noble (mostly transition metals) bimetallic formulations have been explored in DRM.[34]

1.6.2.1. Ni-noble metal formulations

Adding a minute quantity of noble metal can significantly boost the activity and carbon resistance of nickel-based catalysts. The underlying reasons behind this boosting are (i) improved reducibility due to H_2 spillover effect, (ii) "dilution" effect by noble metals leading to a higher metal dispersion and smaller metal particle size and (iii) modification of surface properties through surface reconstruction due to noble metal addition. [35-42, 34]

1.6.2.2. Ni-transition metal formulations

Besides noble metals, transition metals like Co, Fe and Cu have been incorporated into Ni-based catalysts to create bimetallic systems for DRM. The function of Co, Fe and Cu varies significantly within these bimetallic systems due to their inherent properties though other bimetallic systems based on Cr, Mn etc. have also been studied.[34]

NiCo with enhanced oxygen affinity: NiCo bimetallic systems with various supports and synthesis methods have been studied and the catalyst activity has been found to be highly dependent on the Ni/Co ratio and on the nature of the support. The coke resistant property of the NiCo bimetallic system can be attributed to the synergistic effect, good metal dispersion, high metallic surface, formation of different types of solid solutions and SMSI. Based on the overview of recent reports, it is evident that addition of a small amount of Co is sufficient to enhance the catalyst performance, whereas too much Co results in depressing the activity to lower than that of pristine Ni monometallic congener. The promotional effect of Co is primarily attributed to its strong affinity to oxygen species.[43-49]

NiFe with improved redox properties: NiFe catalysts always show an improved carbon resistance for DRM. The behavior of CO_2 oxidation and CH_4 reduction observed is consistent with a Mars–van Krevelen (MvK) mechanism. The presence and migration of FeO_x at the surface allows its reaction with deposited carbon. This fact could explain well the improved stability of bimetallic Ni-Fe catalysts via a $Fe^{2+}O/Fe^0$ redox cycle.[50-54]

NiCu with CO_2 activation ability: Partial substitution of Ni by Cu has been shown to promote DRM activity and increase the coke resistance ability of the catalyst. Cu content above a threshold limit suppresses the activation of CH_4, possibly due to competitive adsorption of CH_4 and slow dissociation kinetics over Cu atoms. Surface enrichment of Cu due to low surface energy compared to Ni may also decrease the number of active Ni sites on the surface and affect activity for higher amount of Cu loaded sample.[55-61]

1.6.3. Co-exsolved Ni-alloy nanoparticles: implication in DRM

Exsolution or co-exsolution, mostly explored for perovskite oxides, is a partial decomposition phenomenon where multiple cations diffuse from the bulk of a solid oxide precursor, primarily due to their well known defect chemistry and nucleate on the surface. The reversible co-exsolution mechanism of ABO_3 type perovskite oxides is emerging as an alternative and promising way for preparing alloy catalyst nanoparticles. The unique properties of exsolved alloy catalysts, including anti sintering property at high operating temperatures, improved dispersion and compositional malleability make them particularly useful for valorization of CO_2 and CH_4. However, the co-exsolution of metal components leading to formation of alloys is essentially achieved through reductive pretreatments and fundamental insight into the alloying mechanism is yet to be understood in a conclusive manner. However, the role of defect chemistry in exsolution process is apparent and perovskite oxide has been known to have the required merit to go through exsolution mediated alloying leading to a sustainable development in the field of DRM. Eventually, other systems like spinel oxide is underrated and yet to be explored in this regard. But

presence of some inherent defect is a primary criterion to show exsolution behavior i.e., while choosing an oxide support other than perovskite, it is desirable that the concerned system has the background of defect chemistry. Hercynite is one of the spinel oxides that is explored in several contexts due to its unique redox defects and may be considered as a model system to be studied in this regard.[62]

1.7. Engineering of hercynite spinel

1.7.1. Structural complexity of nano-dimensional hercynite

A typical mixed spinel oxide has the general structural formula of $(A_{1-i}B_i)(B_{2-i}A_i)O_4$ where the inversion factor 'i' lies in the range 0-1 according to the cation distribution between octahedral and tetrahedral sites. Depending on synthesis method or post synthetic treatment, hercynite may go through some sort of inversion i.e., Fe^{2+} can diffuse from tetrahedral site to octahedral site and Al^{3+} satisfy the vacancy created by Fe^{2+} which leads to inverse or mixed spinel.[63-70] It is very difficult to synthesize high-purity hercynite with high degree of crystallinity using routine chemical process. This is partly attributed to its complicated structure which requires high processing temperature. The inconsistency in valency of iron between its precursors including various ferric salts or Fe_2O_3 and that in $FeAl_2O_4$ (Fe^{2+}) also creates some difficulties.[71]

1.7.2. Applications of hercynite-based materials

Due to the highest abundance of aluminum and iron in the Earth's crust, hercynite is a relatively inexpensive spinel oxide and because of its excellent chemical stability,

mechanical properties and magnetic behavior it seems to be a suitable material for use in the field of heterogeneous catalysis. Although hercynite has received much attention as a photocatalyst for the degradation of pollutants like phenol, tetracycline, methylene blue[72-74] etc., it has also been employed for wastewater treatment.[75] The supercapacitive capabilities of hercynite-based materials has also been explored nowadays.[76] Moreover, hercynite is found to be a promising redox active material for solar thermochemical hydrogen (STCH) production[77], solar thermochemical fuel (STCF) production[78] and in enhanced oxygen evolution eletrocatalysis[79] due to its unique defect chemistry. Hercynite decorated catalysts are well envisaged for the purpose of energy production through various routes including (i) auto-thermal reforming of ethanol for hydrogen production[80], (ii) catalytic methane decomposition over Fe-Al_2O_3[81-83], (iii) syngas production through chemical looping combustion (CLC)[84] and dry reforming of the tar model compound[85]. Besides the aforementioned catalytic reactions, hercynite-based formulations have also been used in various catalytic aspects e.g., for CO_2 hydrogenation to linear α-olefins[86], as a support system in one pot annulation reactions[87, 88], as a magnetic nanocomposite catalyst for the selective esterification of chloroacetic acid[89] etc.

1.7.3. Scope of chemical tailoring in hercynite

High mechanical resistance, low temperature sinterability, high thermal stability, low surface acidity and high ability of cation diffusion ensure the selection of hercynite spinel oxides. Moreover, in last several years our group has been working on the synthesis and modification of hercynite-based catalysts followed by evaluation of their activity towards

various aspects including heterogeneous catalytic reactions.[90-93] The expertise to deal with hercynite-based compositions leading to its excellent methanol steam reforming activity and previous reports (as discussed above) of exhibiting superior activity in high temperature gas-solid heterogeneous catalysis in harsh reactions such as methane cracking, steam reforming, CO_2 hydrogenation, chemical looping etc. have prompted us to do further research about some chemical tailoring of the same to make it suitable for DRM, anticipating that other transition metals along with Ni will also have the similar type of metal-support interactions as is the case with Cu-doped hercynite.

1.7.4. Preparation of hercynite-based formulations: preference of solution combustion synthesis over other methods

The synthetic routes of Ni-based mixed metal oxides usually involve conventional methods like solid state synthesis, sol-gel, Pechini method, solution combustion synthesis (SCS), hydrothermal, co-precipitation, template/surfactant assisted precipitation, deposition−precipitation, solvothermal, impregnation, incipient wetness impregnation, microemulsion, sonochemical process, microwave combustion etc. Besides the well known solid state and soft chemical synthetic routes, other emerging preparation techniques are recently employed for the synthesis of Ni-based catalyst for DRM. They are plasma electrolytic oxidation, plasma spraying, evaporation-induced self-assembly (EISA), strong electrostatic adsorption (SEA), physical vapor deposition (PVD), chemical vapor deposition (CVD), atomic layer deposition (ALD) etc.

Based on our previous expertise in dealing with hercynite-based formulations, to address the issues of oxidation of hercynite based materials in oxidizing environment (oxidizes into Fe_3O_4, Fe_2O_3 etc.), while heat treatment is done, the facile SCS technique has been opted for the compositional engineering of $FeAl_2O_4$ as no additional heat treatment is required in the combustion route. Moreover, the added advantage of preparing catalyst materials within minutes using highly reproducible SCS make it suitable for synthesis and screening of numerous simple and complex mixed metal oxides with varying compositions for DRM. Even SCS has the required merits of providing various oxide-based materials with an ease, which are otherwise very difficult to prepare with high purity. High processing temperatures of oxide materials often lead to diminished surfaced area compromising with particle size and oxygen vacancy, whereas SCS has the capacity of producing nano-phasic materials with high surface area and enhanced oxygen vacancy, which is always found to be beneficial in heterogeneous catalysis, particularly in reforming reactions. By using different fuels, individually or in definite proportion in SCS, the particle size distribution can be varied and desired purpose can be contented. Moreover, nowadays SCS has been explored for controllable valence distribution. Hence SCS has the potential beauty and simplicity over other existing synthetic techniques, often encountered for the synthesis of Ni-based catalyst towards DRM.[94-115]

1. 8. Aim and rationale of the present investigation

From the foregoing discussion it is understandable that the dry reforming of methane holds significant relevance in the modern world due to its potential to address two of the most

pressing global challenges: climate change and the need for sustainable energy and chemical production and there is lot of scope towards design and development of effective catalysts for sustainable DRM. Especially the Ni-based catalysts are of prime importance for application in realistic DRM. But the prevailing issues of coking and deactivation need to be addressed through support engineering. Spinel oxides, especially Fe containing congeners are found to be superior due to their active participation in coke removal activity in the thermocatalytic DRM process. Hercynite is expected to be the most suitable support system for engineering of Ni-based DRM catalysts with below specific reasons:

- previous expertise to deal with hercynite-based compositions
- high methanol steam reforming activity with structural integrity retained in reducing environment
- unique redox defect chemistry
- flexibility of incorporating different transition metals
- anti-coking activity of Fe
- coke resistant DRM activity of Fe doped aluminate spinels like $MgAl_2O_4$.

In particular, hercynite engineering has been done through Ni incorporation, alone and in combination with other transition metals such as Cu, Co, Mn etc., using facile ultrafast SCS route for high and moderate temperature methane dry reforming. Thorough characterizations of the as-prepared vis-à-vis aged catalyst have been done using sophisticated instrumental techniques in a stepwise manner to reveal the structure-activity correlation so that suitable tailoring of the material properties can be done and a generalized conclusion can be drawn for further applicability of the materials.

References

1. Wang, H.; Diao, Y.; Gao, Z.; Smith, K. J.; Guo, X.; Ma, D.; Shi, C. H_2 Production from Methane Reforming over Molybdenum Carbide Catalysts: From Surface Properties and Reaction Mechanism to Catalyst Development. *ACS Catal.* **2022**, *12*, 15501-15528.

2. McFarland, E. Unconventional Chemistry for Unconventional Natural Gas. *Science* **2012**, *338*, 340-342.

3. Shi, Y.; Tian, X.; Deng, Z.; Shi, W.; Fan, W.; Wang, F. Review and Outlook of Confined Ni Catalysts for the Dry Reforming of Methane Reaction. *Energy Fuels* **2024**, *38*, 1633-1656.

4. Qiu, S.; Zhong, X.; Yang, Z.; Deng, Y.; Lai, Y.; Gao, X.; Kawi, S. Smart Designs of Zeolite-Based Catalysts for Dry Reforming of Methane: A Review. *Energy Fuels* **2024**, *38*, 8385-8405.

5. Bhaskaran, A.; Singh, S. A.; Reddy, B. M.; Roy, S. Integrated CO_2 Capture and Dry Reforming of CH_4 to Syngas: A Review. *Langmuir* **2024**, *40*, 14766-14778.

6. Yoon, Y.; You, H. M.; Kim, H. J.; Curnan, M. T.; Kim, K.; Han, J. W. Computational Catalyst Design for Dry Reforming of Methane: A Review. *Energy Fuels* **2022**, *36*, 9844-9865.

7. Fisher, F.; Tropsch, H. Conversion of methane into hydrogen and carbon monoxide. *Brennst. Chem.* **1928**, *9*, 39.

8. Huang, L.; Li, D.; Tian, D.; Jiang, L.; Li, Z.; Wang, H.; Li, K. Optimization of Ni-Based Catalysts for Dry Reforming of Methane via Alloy Design: A Review. *Energy Fuels* **2022**, *36*, 5102-5151.

9. Pakhare, D.; Spivey, J. A review of dry (CO_2) reforming of methane over noble metal catalysts. *Chem. Soc. Rev.,* **2014**, *43*, 7813.

10. Ross, J R.H. Natural gas reforming and CO_2 mitigation. *Catalysis Today* **2005,** *100*, 151–158.

11. Nikoo, M. K.; Amin, N. A. S. Thermodynamic analysis of carbon dioxide reforming of methane in view of solid carbon formation. *Fuel Processing Technology,* **2011,** *92*, 678–691.

12. Subramanian, S.; Song, Y.; Kim, D.; Yavuz, C. T. Redox and Nonredox CO_2 Utilization: Dry Reforming of Methane and Catalytic Cyclic Carbonate Formation. *ACS Energy Lett*. **2020**, *5*, 1689-1700.

13. Rezaei, M.; Alavil, S. M.; Sahebdelfar, S.; Yan, Z. Syngas Production by Methane Reforming with Carbon Dioxide on Noble Metal Catalysts. *Journal of Natural Gas Chemistry*, **2006,** *15*, 327-334.

14. Aramouni, N. A. K.; Touma, J. G.; Tarboush, B. A.; Zeaiter, J.; Ahmad, M. N. Catalyst design for dry reforming of methane: Analysis review. *Renewable and Sustainable Energy Reviews* **2018,** *82*, 2570–2585.

15. Jang, W. J.; Shim, J.; Kim, H.; Yoo, S.; Roh, H. A review on dry reforming of methane in aspect of catalytic properties. *Catalysis Today* **2019,** *324*, 15–26.

16. Li, D.; Nakagawa, Y.; Tomishige, K. Methane reforming to synthesis gas over Ni catalysts modified with noble metals. *Applied Catalysis A: General* **2011,** *408*, 1–24.

17. Houa, Z.; Chen, P.; Fang, H.; Zheng, X.; Yashima, T. Production of synthesis gas via methane reforming with CO_2 on noble metals and small amount of noble-(Rh-) promoted Ni catalysts. *Int. J. Hydrogen Energy***, 2006,** *31*, 555–561.

18. Guharoy, U.; Reina, T. R.; Liu, J.; Sun, Q.; Gu, S.; Cai, Q. A theoretical overview on the prevention of coking in dry reforming of methane using non-precious transition metal catalysts. *Journal of CO_2 Utilization* **2021,** *53*, 101728.

19. Seo, H. O. Recent Scientific Progress on Developing Supported Ni Catalysts for Dry (CO_2) Reforming of Methane. *Catalysts* **2018**, *8*, 110.

20. Muraza, O.; Galadima, A. A review on coke management during dry reforming of methane. *Int. J. Energy Res*. **2015**, *39*, 1196–1216.

21. Wang, Z.; Mei, Z.; Wang, L.; Wu, Q.; Xia, C.; Li, S.; Wang, T.; Liu, C. Insight into the activity of Ni-based thermal catalysts for dry reforming of methane. *J. Mater. Chem. A*, **2024**, *12*, 24802.

22. Hussien, G. S.; Polychronopoulou, K. A Review on the Different Aspects and Challenges of the Dry Reforming of Methane (DRM) Reaction. *Nanomaterials* **2022**, *12*, 3400.

23. Wu,L.; Xie, X.; Ren, H.; Gao, X. A short review on nickel-based catalysts in dry reforming of methane: Influences of oxygen defects on anti-coking property. *Materials Today: Proceedings* **2021,** *42*, 153–160.

24. Cai, Y.; Zhang, Y.; Zhang, X.; Wang, Y.; Zhao, Y.; Li, G.; Zhang, G. Recent Advances in Ni-Based Catalysts for CH_4-CO_2 Reforming (2013–2023). *Atmosphere* **2023**, *14*, 1323.

25. Zhu, H.; Chen, H.; Zhang, M.; Liang, C.; Duan, L. Recent advances in promoting dry reforming of methane using nickel-based catalysts. *Catal. Sci. Technol*., **2024**, *14*, 1712.

26. Wei, M.; Shi, X. Research Progress on Stability Control on Ni-Based Catalysts for Methane Dry Reforming. *Methane* **2024**, *3*, 86–102.

27. Gao, X.; Ge, Z.; Zhu, G.; Wang, Z.; Ashok, J.; Kawi, S. Anti-Coking and Anti-Sintering Ni/Al_2O_3 Catalysts in the Dry Reforming of Methane: Recent Progress and Prospects. *Catalysts* **2021**, *11*, 1003.

28. Xu, Z.; Park, E. D. Recent Advances in Coke Management for Dry Reforming of Methane over Ni-Based Catalysts. *Catalysts* **2024**, *14*, 176.

29. Gao, X.; Ashok, J.; Kawi, S. Smart Designs of Anti-Coking and Anti-Sintering Ni-Based Catalysts for Dry Reforming of Methane: A Recent Review. *Reactions* **2020**, *1*, 162–194

30. Wang, L.; Wang, F. Design Strategy, Synthesis, and Mechanism of Ni Catalysts for Methane Dry Reforming Reaction: Recent Advances and Future Perspectives. *Energy Fuels* **2022**, *36*, 5594−5621.

31. Xue, Y.; Xu, L.; Chen, M.; Wu, C.; Cheng, G.; Wang, N.; Hu, X. Constructing Ni-based confinement catalysts with advanced performances toward the CO_2 reforming of CH_4: state-of the-art review and perspectives. *Catal. Sci. Technol.*, **2021**, *11*, 6344.

32. Li, Z.; Wang, Z.; Kawi, S. Sintering and Coke Resistant Core/Yolk Shell Catalyst for Hydrocarbon Reforming. *ChemCatChem* **2019**, *11*, 202–224.

33. Arora, S.; Prasad, R. An overview on dry reforming of methane: strategies to reduce carbonaceous deactivation of catalysts. *RSC Adv*., **2016**, *6*, 108668.

34. Bian, Z.; Das, S.; Wai, M. H.; Hongmanorom, P.; Kawi, S. A Review on Bimetallic Nickel-Based Catalysts for CO_2 Reforming of Methane. *ChemPhysChem* **2017**, *18*, 3117 – 3134.

35. Zhao, R.; Cao, K.; Ye, R.; Tang, Y.; Du, C.; Liu, F.; Zhao, Y.; Chen, R.; Shan, B. Deciphering the stability mechanism of Pt-Ni/Al_2O_3 catalysts in syngas production via DRM. *Chemical Engineering Journal*, **2024**, *491*, 151966.

36. Liang, D.; Wang, Y.; Wang, Y.; Chen, M.; Xie, X.; Li, C.; Wang, J.; Yuan, L. Dry reforming of methane for syngas production over noble metals modified M-Ni@S-1 catalysts (M ¼ Pt, Pd, Ru, Au). *Int. J. Hydrogen Energy*, **2024**, *51*, 1002-1015.

37. Crisafulli, C.; Scire, S.; Maggiore, R.; Minico, S.; Galvagno, S. CO2 reforming of methane over Ni–Ru and Ni–Pd bimetallic catalysts. *Catalysis Letters*, **1999,** 59, 21–26.

38. Araiza, D. G.; Arcos, D. G.; Gómez-Cortés, A.; Díaz, G. Dry reforming of methane over Pt-Ni/CeO_2 catalysts: Effect of the metal composition on the stability. *Catalysis Today*, **2021,** *360*, 46–54.

39. Theofanidisa, S.; Pietersec, J.; Poelmana, H.; Longoa, A.; Sabbea, M. K.; Virginiee, M.; Detavernierf, C.; Marina, G. B.; Galvita, V. V. Effect of Rh in Ni-based catalysts on sulfur impurities during methane reforming. *Applied Catalysis B: Environmental*, **2020,** *267*, 118691.

40. Dai, C.; Zhang, S.; Zhang, A.; Song, C.; Shi, C.; Guo, X. Hollow zeolite encapsulated Ni–Pt bimetals for sintering and coking resistant dry reforming of methane. *J. Mater. Chem. A*, **2015**, *3*, 16461.

41. Liu, Y.; Li, D.; Li, T.; Guo, Y. MOF-derived Ni-Ir/CeO_2@SiO_2 catalyst with full spectrum utilization ability for anti-coking photothermal dry reforming of methane. *Journal of Alloys and Compounds,* **2025,** *1039*, 183091.

42. Jo´z´wiak, W. K.; Nowosielska, M.; Rynkowski, J. Reforming of methane with carbon dioxide over supported bimetallic catalysts containing Ni and noble metal I.

Characterization and activity of SiO_2 supported Ni–Rh catalysts. *Applied Catalysis A: General*, **2005,** *280*, 233–244.

43. Li, B.; Yuan, X.; Li, L.; Wang, X.; Li, B. Stabilizing Ni-Co Alloy on Bimodal Mesoporous Alumina to Enhance Carbon Resistance for Dry Reforming of Methane. *Ind. Eng. Chem. Res*. **2021**, *60*, 16874−16886.

44. Lyu, L.; Shengene, M.; Ma, Q.; Sun, J.; Gao, X.; Fan, H.; Zhang, J.; Zhao, T. Synergy of macro-meso bimodal pore and Ni-Co alloy for enhanced stability in dry reforming of methane. *Fuel*, **2022,** *310*, 122375.

45. Turap, Y.: Wang, I.; Fu, T.; Wu, Y.; Wang, Y.; Wang, W. Co-Ni alloy supported on CeO_2 as a bimetallic catalyst for dry reforming of methane. *Int. J. Hydrogen Energy*, **2020**, *45*, 6538-6548.

46. Wu, Z.; Yang, B.; Miao, S.; Liu, W.; Xie, J.; Lee, S.; Pellin, M. J.; Xiao, D.; Su, D.; Ma, D. Lattice Strained Ni-Co alloy as a High-Performance Catalyst for Catalytic Dry Reforming of Methane. *ACS Catal*. **2019**, *9*, 2693−2700.

47. Tang, W.; Cao, J.; Chen, C.; Jiang, W.; Chen, C.; He, Z.; Luan, K.; Zhao, X. Lignite-char-supported highly dispersed ultrasmall Ni-Co alloy for stably dry reforming of methane at low temperature. *Chemical Engineering Science*, **2023,** *281*, 119165.

48. Sheng, K.; Luan, D.; Jiang, H.; Zeng, F.; Wei, B.; Pang, F.; Ge, J. Ni_xCo_y Nanocatalyst Supported by ZrO_2 Hollow Sphere for Dry Reforming of Methane: Synergetic Catalysis by Ni and Co in Alloy. *ACS Appl. Mater. Interfaces* **2019**, *11*, 24078−24087.

49. Zhao, y.; Li, H.; Li, H. NiCo@SiO2 core-shell catalyst with high activity and long lifetime for CO2 conversion through DRM reaction. *Nano Energy*, **2018,** *45*, 101–108.

50. Yao, X.; Cheng, Q.; Attada, Y.; Ould-Chikh, S.; Ramírez, S.; Bai, X.; Mohamed, H.; Li, G.; Shterk, G.; Zheng, L.; Gascon, J.; Han, Y.; Bakr, O. M.; Castano, P. Atypical stability of exsolved Ni-Fe alloy nanoparticles on double layered perovskite for CO_2 dry reforming of methane. *Applied Catalysis B: Environmental*, **2023,** *328*, 122479.

51. Kim, S. M.; Abdala, P.; Margossian, T.; Hosseini, D.; Foppa, L.; Armutlulu, A.; Beek, W.; Comas-Vives, A.; Coperet, C.; Müller, C. Cooperativity and Dynamics Increase the Performance of NiFe Dry Reforming Catalysts. *J. Am. Chem. Soc*. **2017**, *139*, 1937−1949.

52. Theofanidis, S. A.; Galvita, V. V.; Poelman, h.; Dharanipragada, N. V. R. A.; Longo, A.; Meledina, M.; Tendeloo, G. V.; Detavernier, C.; Marin, G. B. Fe-Containing Magnesium Aluminate Support for Stability and Carbon Control during Methane Reforming. *ACS Catal.* **2018**, *8*, 5983−5995.

53. Song, Z.; Wang, Q.; Guo, C.; Li, S.; Yan, W.; Jiao, W.; Qiu, L.; Yan, X.; Li, R. Improved Effect of Fe on the Stable $NiFe/Al_2O_3$ Catalyst in Low Temperature Dry Reforming of Methane. *Ind. Eng. Chem. Res.* **2020**, *59*, 17250−17258.

54. Theofanidis, S. A.; Galvita, V. V.; Poelman, H.; Marin, G. B. Enhanced Carbon-Resistant Dry Reforming Fe-Ni Catalyst: Role of Fe. *ACS Catal*. **2015**, *5*, 3028−3039.

55. Yang, Y.; Lin, Y.;Yan, X.; Chen, F.; Shen, Q.; Zhang, L.; Yan, N. Cooperative Atom Motion in Ni−Cu Nanoparticles during the Structural Evolution and the Implication in the High-Temperature Catalyst Design. *ACS Appl. Energy Mater*. **2019**, *2*, 8894−8902.

56. Wu, T.; Cai, w.; Zhang, P.; Song, X.; Gao, L. $Cu–Ni@SiO_2$ alloy nanocomposites for methane dry reforming catalysis. *RSC Adv.*, **2013**, *3*, 23976.

57. Rezaei, R.; Moradi, G.; Sharifnia, S. Dry Reforming of Methane over Ni-Cu/Al_2O_3 Catalyst Coatings in a Microchannel Reactor: Modeling and Optimization Using Design of Experiments. *Energy Fuels* **2019**, *33*, 6689−6706.

58. Yu, X.; Zhang, F.; Chu, W. Effect of a second metal (Co, Cu, Mn or Zr) on nickel catalysts derived from hydrotalcites for the carbon dioxide reforming of methane. *RSC Adv*., **2016**, *6*, 7053.

59. Songa, K.; Lua, M.; Xua, S.; Chena, C.; Zhana, Y.; Lia, D.; Aua, C.; Jianga, L.; Tomishige, K. Effect of alloy composition on catalytic performance and coke-resistance property of Ni-Cu/Mg(Al)O catalysts for dry reforming of methane. *Applied Catalysis B: Environmental*, **2018,** *239*, 324–333.

60. Shi, y.; Han, K.; Wang, F. Ni−Cu Alloy Nanoparticles Confined by Physical Encapsulation with SiO_2 and Chemical Metal−Support Interaction with CeO_2 for Methane Dry Reforming. *Inorg. Chem*. **2022**, *61*, 15619−15628.

61. Han, K.; Wang, S.; Liu, Q.; Wang, F. Optimizing the Ni/Cu Ratio in Ni−Cu Nanoparticle Catalysts for Methane Dry Reforming. *ACS Appl. Nano Mater*. **2021**, *4*, 5340−5348.

62. Najimu, M.; Jo, S.; Gilliard-AbdulAziz , K. L. Co-Exsolution of Ni-Based Alloy Catalysts for the Valorization of Carbon Dioxide and Methane. *Acc. Chem. Res*. **2023**, *56*, 3132−3141.

63. Harrison, R. J.; Redfern, S. A. T.; O'neill, H. S.C. The temperature dependence of the cation distribution in synthetic hercynite ($FeAl_2O_4$) from in-situ neutron structure refinements . *Am. Min.* **1998**, *83*, 1092–109.

64. Dong, Y.; Lu, H.; Cui, J.; Yan, D.; Yin, F.; Li, D. Mechanical characteristics of $FeAl_2O_4$ and $AlFe_2O4$ spinel phases in coatings – A study combining experimental evaluation and first-principles calculations. *Ceram. Int*. **2017**, *43*, 16094–16100.

65. Tristan, N.; Hemberger, J.; Krimmel, A.; Nidda, H-A.; Tsurkan, V.; Loidl, A. Geometric frustration in the cubic spinels MAl_2O_4 (M=Co, Fe, and Mn). *Phys. Rev. B* **2005**, *72*, 174404.

66. Nakane, T.; Ishii, S.; Uchikoshi, T.; Naka, T. Influence of fabrication conditions on the structural characteristics and the magnetic properties of $FeAl_2O_4$. *J Am Ceram Soc.* **2023,** *106*, 2317–2325.

67. Cordova-Mayo, C.; Fernández-González, D.; Fernández, A.; Verdeja, L. F.; Castillo-Rodríguez, A.; Rodríguez-Castellanos, E. A.; Hernández-Reséndiz, M.; García-Quiñonez, L.; Gómez-Rodríguez, C. Synthesis of Al_2O_3−Fe_2O_3−$FeAl_2O_4$ Composites by Colloidal and Traditional Powder Routes of Nano-Al_2O_3−Fe_2O_3 Mixtures. *ACS Omega* **2025**, *10*, 6632−6642.

68. Yaqoob, M. M.; Hussain, S. S.; Riaz, S.; Naseem, S. Effect of Oxidation Temperature on Structural and Magnetic Properties of Al-doped Iron Oxide Thin Films. ***Mater****. Today: Proc.***2015**, *2*, 5400 – 5404.

69. Botta, P. M.; Mercader, R. C. Aglietti, E. F.; Lopez, J. M. Porto. Synthesis of Fe–$FeAl_2O_4$–Al_2O_3 by High-Energy Ball Milling of Al–Fe_3O_4 Mixtures. *Scr. Mater*. **2003**, *48*, 1093-1098.

70. Silva, J. M.; Araujo; J.F.D.F., Brocchi, E.; Solorzano, I.G. Micro Analytical and Magnetic Characterization of Aluminum-iron Spinel ($FeAl_2O_4$) Synthesized by Combustion Reaction. *Ceram. Int.* **2020**, *46*, 19052–19061.

71. Mu, H.; Li, F.; An, X.; Liu, R.; Li, Y.; Qianc, X.; Hu, Y. One-Step Synthesis, Electronic Structure, and Photocatalytic Activity of Earth-Abundant Visible-Light-Driven $FeAl_2O_4$. *Phys. Chem. Chem. Phys.* **2017**, *19*, 9392—9401.

72. Wang, J.; Yao, Z.; Yang, M.; Wang, Y.; Xia, Q.; Jiang, Z . A Fe3O4/FeAl2O4 composite coating via plasma electrolytic oxidation on Q235 carbon steel for Fenton-like degradation of phenol. *Environ Sci. Pollut. Res.* **2016,** *23*, 14927–14936.

73. Guo, M.; Han, Y.; Gao, H.; Xu, Z.; Wang, D.; Peng, Z.; Hou, H. Red mud-based biochar activated peroxydisulfate under visible light for tetracycline removal: Synergistic effect of $FeAl_2O_4$ photocatalysis. *Separation and Purification Technology* **2024,** *328*, 125078.

74. Chai, M.; Chen, X.; Zhao, Y.; Liu, R.; Zhao, J.; Li, F. Facile Ionic Liquid Combustion Synthesis and Visible-light Photocatalytic Ability of Mesoporous $FeAl_2O4$ with High Specific Surface Area. *Chem. Lett.* **2014**, *43*, 1743–1745

75. Kundea, G. B.; Sehgal, B. Eco-designed iron aluminate ($FeAl_2O_4$) free-standing mesoporous films and supported ultrafiltration membranes for wastewater treatment. *J. Environ. Chem. Eng.* **2020,** *8*, 104201.

76. Imran, M.; Alyousef, H. A.; Alrowaily, A.; Alotaibi, B. M.; Dahshan, A.; Al-Harbi, N.; Ahmad, K.; Saleem, M. I. Enhanced supercapacitive performance of $FeAl_2O_4$/g-CN nanocomposite for advanced energy storage systems. *Ceram. Int.* **2024,** *50*, 35313–35321.

77. Millican, S. L.; Clary, J. M.; Musgrave, C. B.; Lany, S. Redox Defect Thermochemistry of $FeAl_2O_4$ Hercynite in Water Splitting from First Principles Methods. *Chem. Mater*. **2022**, *34*, 519−528.

78. Millican, S. L.; Androshchuk, I.; Tran, J. T.; Trottier, R. M.; Bayon, A.; Salik, Y.; Idriss, H.; Musgrave, C. B.; Weimer, A. W. Oxidation kinetics of hercynite spinels for solar thermochemical fuel production. *Chem. Eng. J*. **2020**, *401*, 126015.

79. Chen, Y.; Xu, J.; Chen, y.; Wang, L.; Jiang, S.; Xie, Z.; Zhang, t.; Munroe, p.; Peng, s. Rapid Defect Engineering in FeCoNi/$FeAl_2O_4$ Hybrid for Enhanced Oxygen Evolution Catalysis: A Pathway to High-Performance Electrocatalysts. *Angew. Chem. Int. Ed*. **2024**, *163*, e202405372.

80. Huang, L.; Xie, J.; Chen, R.; Chu, D.; Chu, W.; Hsu, A. T. Effect of iron on durability of nickel-based catalysts in auto-thermal reforming of ethanol for hydrogen production. *Int. J. Hydrogen Energy*. **2008**, *33*, 7448 – 7456.

81. Zhou, L.; Enakonda, L. R.; Saih, Y.; Loptain, S.; Gary, D.; Del-Gallo, P.; Basset, J. Catalytic Methane Decomposition over Fe-Al_2O_3. *ChemSusChem*. **2016**, *9*, 1243 – 1248.

82. Kazemi,S.; Alavi, S. M.; Rezaei, M.; Akbari, E. Fabrication and evaluation of the Mn-promoted Ni/$FeAl_2O_4$ catalysts in the thermocatalytic decomposition of methane: Impact of various promoters. *Fuel* **2023,** *342*, 27797.

83 Kazemi,S.; Alavi, S. M.; Rezaei, M. Hydrogen production from CO_x-Free thermocatalytic decomposition of methane over the mesoporous iron aluminate spinel ($FeAl_2O_4$) nanopowder supported nickel catalysts. *Int. J. Hydrogen Energy*. **2022,** *47*, 18370-18383.

84. Rihko-Struckmann, L. K.; Datta, p.; Wenzel, M.; Sundmacher, K.; Dharanipragada, N. V. R. A.; Poelman, H.; Galvita, V. V.; Marin, G. B. Hydrogen and Carbon Monoxide Production by Chemical Looping over Iron-Aluminium Oxides. *Energy Technol*. **2016**, *4*, 304 – 313.

85. Qiu, S.; Liu, H.; Li, J.; Yao, S.; Wang, W.; Zhu, J.; Wu, Z.; Gao, E. Catalytic System of Y-Modified 15Fe−10Ni/Al_2O_3 Catalysts Used for Dry Reforming of the Tar Model Compound to Syngas. *Energy Fuels* **2025**, *39*, 1202−1215.

86. Xu, M.; Liu, X.; Cao, C.; Sun, Y.; Zhang, C.; Yang, Z.; Zhu, M.; Ding, X.; Liu, Y.; Tong, Z,; Xu, J. Ternary Fe−Zn−Al Spinel Catalyst for CO_2 Hydrogenation to Linear α-Olefins: Synergy Effects between Al and Zn. *ACS Sustainable Chem. Eng*. **2021**, *9*, 13818-13830.

87. Mohammadi, M.; Ghorbani-Choghamarani, A. A novel Hercynite-supported tetradentate Schiff base complex of manganese catalyzed one-pot annulation reactions. *Appl Organomet. Chem*. **2022,** *36*, 6905.

88. Mohammadi, M.; Mansouri, G. Synthesis and Characterization of a Hercynite-Supported Copper(II) Complex Based on 1,10-Phenanthroline-5,6-dione and Acetylacetone Building Blocks and Its Catalytic Application in Annulation Reactions. *Langmuir* **2024**, *40*, 22773−22786.

89. Nikseresht, A.; Karami, M.; Mohammadi, M. Phosphotungstic Acid-Supported Hercynite: A Magnetic Nanocomposite Catalyst for the Selective Esterifcation of Chloroacetic Acid. *Langmuir* **2024**, *40*, 18512-18524.

90. Maiti, S.; Llorca, J.; Dominguez, M.; Colussi, S.; Trovarelli, A.; Priolkar, R. K.; Aquilanti, G.; Gayen, A. Combustion Synthesized Copper-ion Substituted $FeAl_2O_4$ ($Cu_{0.1}Fe_{0.9}Al_2O_4$): A Superior Catalyst for Methanol Steam Reforming Compared to its Impregnated Analogue. *J. Power Sources.* **2016**, *304*, 319–331.

91. Mistri, R.; Maiti, S.; Llorca, J.; Dominguez, M.; Mandal, T. K.; Mohanty, P.; Raya, B. C.; Gayen, A. Copper Ion Substituted Hercynite ($Cu_{0.03}Fe_{0.97}Al_2O_4$): A Highly Active

Catalyst for Liquid Phase Oxidation of Cyclohexane. *Appl. Catal. A: Gen.* **2014**, *485*, 40–50.

92. Maiti, S.; Das, D.; Pal, K.; Llorca, J.; Soler, L.; Colussi, S.; Trovarelli, A.; Priolkar, R. K.; Sarode, P. R.; Asakura, K.; Seikh, M. M.; Gayen, A. Methanol Steam Reforming Behavior of Sol-gel Synthesized Nanodimensional CuxFe1-x Al2O4 Hercynites. *Appl. Catal. A: Gen.* **2019**, *570*, 73–83.

93. Maiti, S.; Kundu. A. K.; Lebedev, O. I.; Bera, P.; Anandan, C.; Gayen, A.; Seikh, M. M. Synthesis and Magnetic Properties of Nanodimensional $Fe_{1-x}Cu_xAl_2O_4$ ($0.3 \leq x \leq 0.8$). *RSC Adv.* **2015**, *5*, 83809–83817.

94. Kingsley, J. J.; Patil, K. C. A Novel Combustion Process for the Synthesis of Fine Particle α-Alumina and Related Oxide *Materials. Mater. Lett.* **1988**, *6*, 427−432.

95. Varma, A.; Mukasyan, A. S,; Rogachev, A. S.; Manukyan, K. V. Solution Combustion Synthesis of Nanoscale Materials. *Chem. Rev*. **2016**, *116*, 14493−14586.

96. Aruna, S. T.; Muthuraman, M.; Patil, K. C. Combustion synthesis and properties of strontium substituted lanthanum manganites $La_{1-x}Sr_xMnO_3$ ($0 \leq x \leq 0.3$). *J. Mater. Chem.*, **1997**, *7*, 2499–2503.

97. Ekambaram, S.; Patil, K. C. Combustion Synthesis of Yttria. *J. Mater. Chem.*, **1995**, *5*, 905-908.

98. Patil, K. C.; Aruna, S.T.; Mimani, T. Combustion synthesis: an update. *Curr. Opin. Solid State Mater. Sci*. **2002**, *6*, 507–512

99. Hedge, M. S.; Madras, G.; Patil, K. C. Noble Metal Ionic Catalysts. *Acc. Chem. Res.* **2009**, *42*, 704-712.

100. Patil, K. C.; Aruna, S. T.; Ekambaram, S. Combustion synthesis. Combustion synthesis Patil, Aruna and Ekambaram.

101. Colussi, S.; Gayen, A.; Llorca, J.; Leitenburg, C.; Dolcetti, G.; Trovarelli, A. Catalytic Performance of Solution Combustion Synthesized Alumina- and Ceria-Supported Pt and Pd Nanoparticles for the Combustion of Propane and Dimethyl Ether (DME). *Ind. Eng. Chem. Res*. **2012**, *51*, 7510–7517.

102. Romanovski, V.; Sdobnyakov, N.; Roslyakov, S.; Kolosov, A.; Podbolotov, K.; Savina, K.; Kwapinski, W.; Moskovskikh, D,; Khort, A. Bimetallic CuNi Nanoparticle Formation: Solution Combustion Synthesis and Molecular Dynamic Approaches. *Inorg. Chem*. **2024**, *63*, 24844−24854.

103. Voskanyan, A. A.; Chan, K.; Li, C. V. Colloidal Solution Combustion Synthesis: Toward Mass Production of a Crystalline Uniform Mesoporous CeO_2 Catalyst with Tunable Porosity. *Chem. Mater*. **2016**, *28*, 2768−2775.

104. Cross, A.; Kumar, A.; Wolf, E. E.; Mukasyan, A. S. Combustion Synthesis of a Nickel Supported Catalyst: Effect of Metal Distribution on the Activity during Ethanol Decomposition. *Ind. Eng. Chem. Res*. **2012**, *51*, 12004−12008.

105. Deshpande, K.; Mukasyan, A,; Varma, A. Direct Synthesis of Iron Oxide Nanopowders by the Combustion Approach: Reaction Mechanism and Properties. *Chem.* Mater. **2004**, *16*, 24.

106. Manabayeva, A. M.; Mäki-Arvela, P.; Vajglová, Z.; Martinéz-Klimov, M.; Tirri, T.; Baizhumanova, T. S.; Grigor'eva, V. P.; Zhumabek, M.; Aubakirov, Y. A.; Simakova, I.; Murzin, D.; Tungatarova, S. A. Dry Reforming of Methane over Ni−Fe−Al Catalysts

Prepared by Solution Combustion Synthesis. *Ind. Eng. Chem. Res*. **2023**, *62*, 11439−11455.

107. Halder, S.; Roy, S.; Roy, S.; Chakraborty, C. Enriching Oxygen Vacancy in Co_3O_4 by Solution Combustion Synthesis for Enhanced Supercapacitive Property. *J. Phys. Chem. C* **2023**, *127*, 18279−18290.

108. Cross, A.; Roslyakov, S.; Manukyan, K. V.; Rouvimov, S.; Rogachev, A. S.; Kovalev, D.; Wolf, E. E.; Mukasyan, A. S. In Situ Preparation of Highly Stable Ni-Based Supported Catalysts by Solution Combustion Synthesis. *J. Phys. Chem. C* **2014**, *118*, 26191−26198.

109. Zuo, C.; Liu, H.; Wang, Y.; Chen, J.; Yang, H.; Yuan, X.; Yue, G. One-Step Preparation of Trinary Co(III)/Co(II)/Co(0) Bifunctional Catalysts with Controllable Co Valence Distribution via Solution Combustion Synthesis and Its Application to Oxygen Reduction and Evolution in Zinc−Air Batteries. *Inorg. Chem*. **2025**, *64*, 9093−9101.

110. Khort, A.; Podbolotov, K.; Serrano-García, R.; Gun'ko, Y. One-Step Solution Combustion Synthesis of Cobalt Nanopowder in Air Atmosphere: The Fuel Effect. *Inorg. Chem*. **2018**, *57*, 1464−1473.

111. Barbato, P. S.; Colussi, S.; Benedetto, A. D.; Landi, G.; Lisi, L.; Llorca, J.; Trovarelli, A. Origin of High Activity and Selectivity of CuO/CeO_2 Catalysts Prepared by Solution Combustion Synthesis in CO-PROX Reaction. *J. Phys. Chem. C* **2016**, *120*, 13039−13048.

112. Hossain, M. K.; Sarker, H. P.; Sotelo, P.; Dang, U.; Rodríguez-Gutierrez, I.; Blawat, J.; Vali, A.; Xie, W.; Oskam, G.; Huda, M. N.; Macaluso, R. T.; Rajeshwar, K. Phase-Pure

Copper Vanadate (α-CuV_2O_6): Solution Combustion Synthesis and Characterization. *Chem. Mater*. **2020**, *32*, 6247−6255.

113. Manukyan, K. V.; Cross, A.; Roslyakov, S.; Rouvimov, S.; Rogachev, A. S.; Wolf, E.; Mukasyan, A. S. Solution Combustion Synthesis of Nano-Crystalline Metallic Materials: Mechanistic Studies. *J. Phys. Chem*. C **2013**, *117*, 24417−24427.

114. Sathiskumar, P. S.; Thomas, C. R.; Madras, G. Solution Combustion Synthesis of Nanosized Copper Chromite and Its Use as a Burn Rate Modifier in Solid Propellants. *Ind. Eng. Chem. Res*. **2012**, *51*, 10108−10116.

115. Jia, M.; Deng, R.; Li, F.; Xu, K.; Ye, Y.; Wang, Z.; Yang, H.; Wang, X. Solution Combustion Synthesis of a $Y_{0.87}Ba_{0.1}Zr_{0.03}O_{1.465}$ Catalyst for Highly Efficient NO Direct Decomposition at High Temperatures. *Energy Fuels* **2023**, *37*, 19704−19714.

Chapter 2

Synthetic processes, characterization techniques and DRM activity test of the materials

2.1. Introduction

The development of catalytic formulations as well as application of these formulations to the synthesis of industrially important products is indeed a very challenging to the experimentalist. For industrial application of the catalyst, it should have reached the highest attainable quality and could perform at the optimum and possibly lowest cost level. Thus the design and manufacturing processes of the materials play crucial role for it to become a good catalyst. The development of solid catalyst requires knowledge of several parameters which have great influence on the catalyst performance. Main objective of the catalyst developments is optimization of various different catalyst properties. In the recent years, novel concept of nanotechnology has been used to synthesize solid oxide materials with well defined structural characteristics. Among variety of nanostructured oxides hercynite is one important material as elaborated in chapter 1.

Besides, detail characterization of the synthesized materials is a vital part of the material science. This is the key to unravel the structure-property correlation. The hercynite being an attractive material a number of divers characterization techniques are needed to explore the relationship of the activity pattern with the structure.

This chapter discusses the SCS method, opted for the synthesis of hercynite-based materials presented in this thesis, followed by the details of experimental techniques used for their charecterizations.

2.2. Chemicals used for synthesis of catalyst materials

To prepare the spinel oxide (hercynite) based catalyst materials of this research work, corresponding nitrate salts of metal, $Ni(NO_3)_2.6H_2O$ (98%), $Cu(NO_3)_2.3H_2O$ (99%), $Fe(NO_3)_3.6H_2O$ (98%), $Al(NO_3)_3.9H_2O$ (98.5%), $Co(NO_3)_2.6H_2O$ (97%), $Mn(NO_3)_2.4H_2O$ (97%) were taken and oxalyldihydrazide ($C_2H_6N_4O_2$, ODH) was used as the fuel as well as complexing agent in the solution combustion synthesis. All the nitrate salts were purchased from Merck and used without any further treatment. ODH was prepared by the reaction of hydrazine hydrate with diethyl oxalate in an aqueous solution under ice-cooled condition. Millipore water (ultra-pure water) was used as the solvent in the synthetic procedure.

2.3. Solution combustion synthesis of the catalysts

2.3.1. Ni and Cu co-doped hercynite

Nanocrystalline $Ni_xCu_{0.07}Fe_{0.93-x}Al_2O_4$ (corresponding to x= 0, 0.02, 0.04, 0.06, 0.08 and 0.10 that are named respectively as CFAO, NCFAO2, NCFAO4, NCFAO6, NCFAO8 and NCFAO10) as well as $FeAl_2O_4$ and $Ni_{0.08}Fe_{0.92}Al_2O_4$, named respectively as FAO and NFAO, were synthesized through facile solution combustion method using metal nitrate salts as precursors and oxalyldihydrazide as the fuel in a muffle furnace preheated at ~350 °C.[1] The preparation of $Ni_{0.08}Cu_{0.07}Fe_{0.85}Al_2O_4$ (i.e., NCFAO8) involves the combustion of the metal nitrates $Ni(NO_3)_2.6H_2O$, $Cu(NO_3)_2.3H_2O$, $Fe(NO_3)_3{\cdot}9H_2O$, $Al(NO_3)_3{\cdot}9H_2O$ with ODH, taken in a molar ratio 0.08:0.07:0.85:2:4.425, at the ignition temperature of the redox

mixture. The synthetic process is shown schematically in **Scheme 2.1**. In a typical synthesis of NCFAO8, stoichiometric amounts of (0.1162 g of $Ni(NO_3)_2.6H_2O$ (98%), 0.0845 g of $Cu(NO_3)_2.3H_2O$ (99%), 1.7170 g of $Fe(NO_3)_3.9H_2O$ (98 %), 3.7513 g of $Al(NO_3)_3.9H_2O$ (98.5 %), and 2.6151 g of ODH were taken in a borosilicate dish and dissolved in ~50 mL of distilled water through heating in a mantle. The redox mixture was then introduced into the preheated muffle furnace. The solution underwent dehydration through frothing and foaming and at the point of complete dehydration the surface got ignited and burnt with a flame to form the required oxide material within one minute.

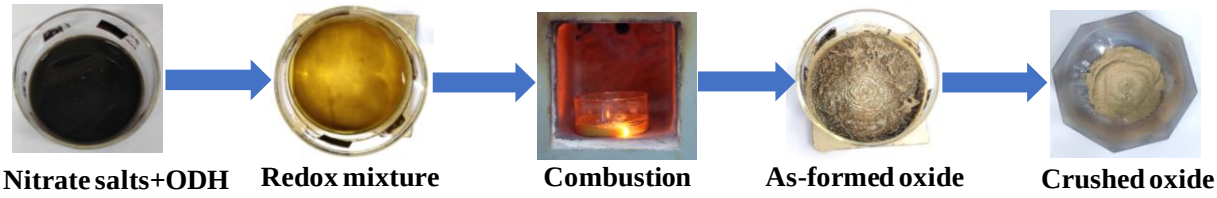

Scheme 2.1. Schematic diagram of solution combustion synthesis of NCFAO8.

2.3.2 Ni-doped hercynite

The hercynite materials, $Ni_xFe_{1-x}Al_2O_4$ (where x= 0.3, 0.4 and 0.5 and denoted as NFAOn, where n= 30, 40 and 50; the at.% of Ni doped in the hercynite) were also prepared by SCS process. Typically, for the preparation of $Ni_{0.50}Fe_{0.50}Al_2O_4$, 0.3635g of $Ni(NO_3)_2.6H_2O$, 0.505g of $Fe(NO_3)_3.9H_2O$, 1.8756g of $Al(NO_3)_3.9H_2O$, and 1.2558 g of ODH were taken in a borosilicate dish and dissolved in ~50 mL of distilled water through heating in a mantle. The redox mixture was then introduced into the preheated muffle furnace. The solution undergoes complete dehydration and eventually the surface got ignited and then burnt with a flame to form the required oxide material within one minute. Similarly the other Ni-doped hercynite were prepared.

2.3.3 Ni, Cu, Co and Mn-doped hercynite

The multimetal hercynite, $(NiCuCoMn)_xFe_{1-4x}Al_2O_4$ where x= 0.05-0.10 were also prepared by a the traditional SCS method. In a typical preparation of $(NiCuCoMn)_{0.1}Fe_{0.6}Al_2O_4$, 0.0969g of $Ni(NO_3)_2.6H_2O$, 0.0805g of $Cu(NO_3)_2.3H_2O$, 0.0969g of $Co(NO_3)_2.6H_2O$, 0.0836g of $Mn(NO_3)_2.4H_2O$, 0.808g of $Fe(NO_3)_3.6H_2O$, 2.5008g of $Al(NO_3)_3.9H_2O$, and 1.6942g of ODH were taken in a borosilicate dish and dissolved at first with ~60 mL Millipore water and then introduced in a preheated muffle furnace when dehydration took place. At the point of complete dryness, the surface of the resulting redox mixture got ignited and then burnt to form the desired multimetal doped oxide materials.

2.4. Material characterizations

This part provides a detailed discussion of all the characterization methods used to study the chemical and physical characteristics of the synthesized materials. Initially, the phase purity of the synthesized samples was confirmed from powder X-ray diffraction (PXRD) analysis. BET surface area measurement gave the specific surface areas (S_{BET}) of different samples and porosity data of the materials. A preliminary DRM test was performed to decide the most active catalyst amongst all the synthesized materials. After that, the final catalyst material has been characterized by high resolution transmission electron microscopy (HRTEM), high-angle annular dark-field scanning transmission electron microscopy (HAADF-STEM) and energy dispersive X-ray spectroscopy/ analysis (EDX/ EDS) study, X-ray photoelectron spectroscopy (XPS), H_2 temperature programmed reduction (H_2-TPR), CO_2 temperature programmed desorption (CO_2-TPD), thermogravimetry-differential thermal analysis (TG/DTA), carbon, hydrogen, nitrogen, and sulfur (CHNS) analysis, inductively coupled plasma - atomic emission spectrometry (ICP-AES) analysis, and Raman analysis.

2.4.1. Powder X-ray diffraction study

The bulk phase information was gathered using powder X-ray diffraction data recorded on a Bruker D8 Advance X-ray diffractometer with Cu Kα radiation operating at 40 kV and 40 mA using 1D position-sensitive LYNXEYE detector. The XRD patterns were collected in the 2θ range 10°-80° at a scan rate of 0.5-2 s per step, depending on the requirement.

2.4.2. Specific BET surface area (S_{BET}) study

N_2 adsorption-desorption isotherms were recorded with Autosorb iQ2 (Quantachrome Inc.) instrument. Before the measurement, all the samples were outgassed at 130 °C under 0.3 torr vacuum for 6 h with a FLOVAC degasser tube. The pore volume and pore size distributions of the samples were calculated by the NLDFT method. The specific surface area (S_{BET}) of the catalysts was measured by the multipoint BET method.

2.4.3. High-resolution transmission electron microscopy study

Microstructural analysis was done using high resolution transmission electron microscope (HRTEM; FEI, USA) operating at 200 kV.

2.4.4. HAADF-STEM and EDX study

EDS mapping of the as-prepared and aged catalysts was performed using high angle annular dark field scanning transmission electron microscope (HAADF-STEM; Thermo Scientific Talos F200X G2).

2.4.5. X-ray photoelectron spectroscopy study

The surface characterization of the as-prepared and aged samples were examined by using X-ray photoelectron spectroscopy. The experiments are performed in a Thermo Scientific K-

Alpha surface analysis spectrometer fitted with a monochromatic Al Kα radiation (1486.6 eV) as an X-ray source and operated at 12 kV and 6 mA. The binding energy of C 1s (284.8 eV) was used to calibrate the binding energies. Peak Fit v4.12 software was employed for the curve fitting.

2.4.6. H_2 temperature programmed reduction

H_2-TPR experiment was performed with a Chemstar TPx (Quantachrome Inc.) equipped with a thermal conductivity detector (TCD) taking 20 mg of sample in a U-shaped quartz tube. For H_2-TPR, a pretreatment of the sample was done at 200 °C with a hold time of 30 min using a Ar flow of 20 mL min^{-1}. H_2/Ar gas mixture (10% v/v) was then introduced with a flow rate of 50 mL min^{-1} and the continuous H_2 uptake was monitored by the TCD from ambient temperature to 900 °C with a ramp rate of 10 °C min^{-1}.

2.4.7. CO_2 temperature programmed desorption

CO_2-TPD experiments were performed with the same Chemstar TPx (Quantachrome Inc.) equipped with a TCD taking 20 mg of sample in a U-shaped quartz tube. For CO_2-TPD, a pretreatment of the sample was done at 200 °C with a hold time of 30 min using a He flow of 20 mL min^{-1}. CO_2/He gas mixture (10% v/v) was then introduced with a flow rate of 50 mL min^{-1} for 1 h, followed by a flushing with He flow of 20 mL min^{-1} for 1 h at 30 °C. Finally, TPD was conducted by heating the sample from room temperature to 900 °C with a rate of 10 °C min^{-1}.

2.4.8. Thermogravimetry-differential thermal analysis

TG-DTA analysis of the aged catalyst was performed in a Shimadzu DTG-60 under zero air flow from room temperature to 900 °C with the heating rate of 10 °C min^{-1}.

2.4.9. CHNS analysis

The CHNS analysis was performed for few selected samples using Elementar (Germany) Vario Micro cube instrument.

2.4.10. ICP-AES analysis

The chemical analysis was performed with inductively coupled plasma-atomic emission spectroscopy (ICP-AES, Spectro Analytical).

2.4.11. Raman analysis

The Raman spectrum of a few selected materials was obtained using a Micro Raman Spectrometer (Model: Renishaw inVia Reflex, UK) equipped with a 514 nm diode laser source and a 20x objective lens.

2.5. DRM activity test

The DRM activities of synthesized materials were evaluated in a reaction set up fabricated in the laboratory (see **Scheme 2.2**).[2] All the gases (reactant and carrier) pass through 1/8-inch stainless steel tube to prevent any chemical reaction. The gas flow rates were monitored by thermal mass flow controllers (MFC, Bronkhorst High-Tech BV). After leaving the MFC, the gas can go in any of the three available directions: (i) to the microreactor for DRM, or (ii) to

the bypass line for the analysis of gas mixture or (iii) directly to a bubble flow meter (BFM) for checking the set value of the flow rates with the manually determined value.

Scheme 2.2. The reaction setup for conducting gas-solid heterogeneous catalytic experiments.

Initially, a pellet was made from the as-prepared catalyst powder, which was then crushed to get 85–100 mesh before being put through a catalytic test. A down flow quartz micro-reactor with an inner diameter of 6 mm was used to carry out the DRM reaction at atmospheric pressure. In a typical catalytic test, 100 mg of solid catalyst was packed on a layer of quartz wool in the micro-reactor and placed in a vertical tube furnace. A K-type thermocouple (Omega, UK) positioned closely in contact with the catalyst bed was utilized to monitor the actual reaction temperature, while the temperature of the furnace was controlled by a thyristor-powered Eurotherm PID controller (model 2416). The flow rates of the calibration gas mixtures and other reaction conditions were as follows: 10 mL of 10% CH_4 in He, 10 mL of 10% CO_2 in He, 37 mL of pure He (carrier gas), 800 °C and GHSV= 34000 mL g^{-1} h^{-1} (for materials in chapter 3); 25 mL of 10% CH_4 in N_2, 25 mL of 10% CO_2 in N_2, pure N_2 (carrier gas), 800 °C and GHSV= 30000 mL g^{-1} h^{-1} (for materials in chapter 4); and 25 mL of 10% CH_4 in N_2, 25 mL of 10% CO_2 in N_2, pure N_2 (carrier gas), 700 °C and GHSV= 30000 mL g^{-1} h^{-1} (for materials in chapter 5) so as to ensure the CH_4/CO_2 molar ratio as per

DRM stoichiometry. The preliminary tests of all the materials were carried out at different temperatures ranging from 500 to 800 °C to optimize the reaction temperature. Further tests, like the durability tests were subsequently carried out at temperature(s) based on the preliminary data. The outgoing gases were detected and analyzed using an OMNI^{Star} gas analysis system equipped with a quadrupole mass spectrometer, where the characteristic m/z (m = mass of the gas, z = charge on the ion) value of the constituent gases (*X*) is acquired. The catalytic activities were computed using the conversions of CH_4, CO_2, and H_2/CO molar ratio. The CH_4 and CO_2 conversions were calculated using the following conversion formula (Eq. 2.1 and 2.2) by taking the initial (i.e., before reaction, $A_{X,\,in}$) and steady-state (after 1 h of reaching the target temperature of T °C, $A_{X,\,out}$) ion current values for each component, which correspond to a fixed value of m/z. This is because the ion current is directly proportional to the concentration of the gas analysed. The relevant mass signals (m/z), which were set in the instrument to be 2 amu for H_2, 4 amu for He, 16 amu for CH_4, 18 amu for H_2O, 28 amu for CO, and 44 amu for CO_2, were used to analyse the outlet gas composition. The H_2/CO ratio is obtained by calculating the simple ratio (Eq. 2.3) of their individual ion current values, H_2/CO, which has a theoretical value of one for the DRM reaction. The gas composition was also analyzed using a Nucon 5765 gas chromatograph (GC), New Delhi, India, for which the feed gas composition was maintained to be the same, while Ar was used as the carrier gas.

$$CH_4\ conversion = \frac{A_{CH\,4,in} - A_{CH\,4,out}}{A_{CH\,4,in}} \times 100\% \text{ -------- (2.1)}$$

$$CO_2\ conversion = \frac{A_{CO\,2,in} - A_{CO\,2,out}}{A_{CO\,2,in}} \times 100\% \text{ -------- (2.2)}$$

$$\frac{H_2}{CO}\ molar\ ratio = \frac{A_{H\,2,out}}{A_{CO\,,out}} \text{ ---------- (2.3)}$$

References

1. Maiti, S.; Llorca, J.; Dominguez, M.; Colussi, S.; Trovarelli, A.; Priolkar, R. K.; Aquilanti, G.; Gayen, A. Combustion Synthesized Copper-ion Substituted $FeAl_2O_4$ ($Cu_{0.1}Fe_{0.9}Al_2O_4$): A Superior Catalyst for Methanol Steam Reforming Compared to its Impregnated Analogue. *J. Power Sources.* **2016**, *304*, 319–331.

2. Hossain, A.; Bhattacharjee, M.; Ghorai, K.; Llorca, J.; Vasundhara, M.; Roy, S.; Bera, P.; Seikh, M. M.; Gayen, A. High Activity in the Dry Reforming of Methane using a Thermally Switchable Double Perovskite and In Situ Generated Molecular Level Nanocomposite. Phys. *Chem. Chem. Phys.* **2024**, *26*, 5447−5465.

Chapter 3

Studies on the DRM activity behavior of Ni and Cu co-doped hercynite

3.1. Introduction

As detailed in chapter 1, DRM not only reveals a prospective technology towards the GHG management, it has an added advantage of producing synthesis gas that can be introduced in Fischer-Tropsch synthesis for the production of higher hydrocarbons[1-5].

Nickel is the primary choice of researchers in this aspect because of its low cost, easy availability and high activity. Sintering and agglomeration at high operating temperatures lead to catalyst deactivation through severe coke deposition and subsequent pore-clogging as the activity of the catalyst is highly sensitive to the particle size and dispersion of the active phase[6-8]. Various efforts have been devoted to understand the facts, like metal support interaction[9], surface acidity/basicity[10, 11], oxygen vacancies mechanism, encapsulation of Ni metal within a shell[9, 12] and most importantly, introduction of a second metal component as a promoter along with the active metal counterpart[13] or alloying of Ni[14, 15], which play a crucial role for the betterment of activity and stability of the catalyst.

Previous studies have shown that a very useful and economic approach to enhance the stability of Ni-based catalyst is alloying of Ni with another transition metal such as Cu, Fe, Co etc. by prior reduction of the as-prepared catalyst[16-24]. There is hardly any example of synthesis

strategy of alloy-based catalyst that devoid of the prior reduction step[25]. To address these issues, *in situ* generation of Ni-based alloy might be an effective way to avoid the prior reduction step as a prerequisite. A very timely initiative in this regard is to explore the exsolution phenomenon properly to avail the desired alloy. It is evident from many reports that exsolved particles are silent to coking or/and agglomeration as compared to their deposited analogues[26, 27]. Recent researches have revealed that the extra stability of the exsolved particles is due to the fact that, they are partially embedded over the surface of the parent oxide and are not allowed to move freely which actually causes the active metal to agglomerate[28]. The well-known defect chemistry of perovskite oxide materials allow them to exhibit exsolution phenomena in proper redox condition[29-33] but this is not a general practice with the spinel system showing exsolution behavior, except a few examples[34, 35]. We have already discussed the unique defect chemistry[36] of hercynite spinel that has been purposefully explored in this work.

We have been working on the synthesis and modification of hercynite-based catalysts for the last one decade and evaluated their activity towards various heterogeneous catalytic reactions[37-40]. Our studies have demonstrated that the doping of a small percentage of copper introduces good crystallinity to solution combustion synthesized hercynite, whereas it is amorphous or poorly crystalline in its purest form[41]. We were successful to show that 10 at.% copper doped hercynite has a promising activity towards methanol steam reforming (MSR) with excellent time on stream behaviour[37]. Our expertise to deal with hercynite-based compositions and the excellent MSR activity of these systems have prompted us to explore further the chemical tailoring of the hercynite structure so as to make it suitable for the dry reforming of methane.

In this chapter, we have presented the synthesis, characterization and catalytic activity of rationally designed Ni and Cu co-doped hercynite, $Ni_xCu_{0.07}Fe_{0.93-x}Al_2O_4$ (x= 0, 0.02, 0.04, 0.06, 0.08, and 0.10) corresponding to total metal (Ni+Cu) doping percentage up to 17 at.% by a facile one step solution combustion synthesis. Based on the previous findings that 7-10 at. % of Cu is good enough for MSR, we have fixed the amount of Cu-loading in all the compositions at. 7 at.%, while varied the Ni-loading from 0 to 10 at.%. $FeAl_2O_4$ and $Ni_{0.08}Fe_{0.92}Al_2O_4$ have also been synthesized for comparison with Ni and Cu codoped hercynite. Among all the samples, the nominal composition $Ni_{0.08}Cu_{0.07}Fe_{0.85}Al_2O_4$ appears to be the most active, coking free and highly durable DRM catalyst at GHSV of 34000 mL g^{-1} h^{-1} at ~800 °C. To the best of our knowledge, this is the first report on the synthesis of hercynite-based material which offers *in situ* generated (exsolution mediated) NiCuFe ternary alloy exhibiting excellent methane dry reforming activity with high durability and potential coke resistant ability. Above all, the high thermal stability and pronounced defect chemistry of hercynite allows the substantial retention of the pristine phase over the exsoluted phases in the harsh DRM environment.

3.2. Results and Discussion

3.2.1 Powder XRD studies

Hercynite spinel phase formation is evident for all the as-prepared samples, as shown in **Figure 3.1**, which is well matched with JCPDS PDF# 34-0192. Thus, Ni and Cu get incorporated in the $FeAl_2O_4$ lattice. As no noticeable diffraction peaks due to CuO and/or NiO are identified, it may be concluded that even if these phases are formed they are negligible enough to escape the detection limit of powder XRD. The crystallite size of the as-prepared samples lies in the range

10-14 nm as obtained from the Scherrer's equation. All the powder patterns were analyzed by pattern matching to extract the cell parameters. There is minuscule change in the cell parameters with the increase in Ni content (see **Figure 3.2**). However, the overall change in cell volume is less than 1%. It is within the error limit for estimation of cell parameters from the powder pattern, more specifically when the diffraction peaks are very broad. Thus we can conclude that there is no noticeable change in cell constant with the increase in Ni or Cu doping.

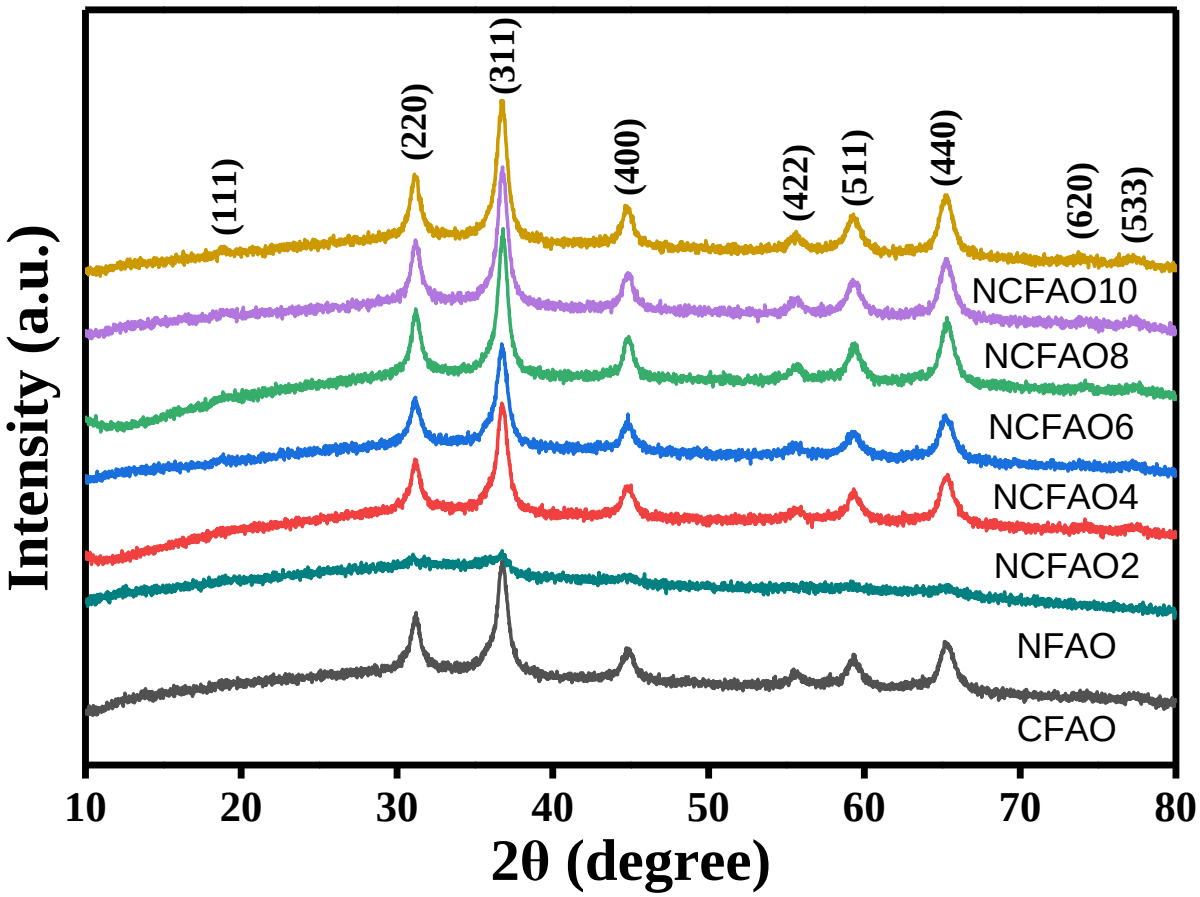

Figure 3.1. PXRD patterns of the as-prepared Cu doped, Ni doped and Cu, Ni co-doped $FeAl_2O_4$ system.

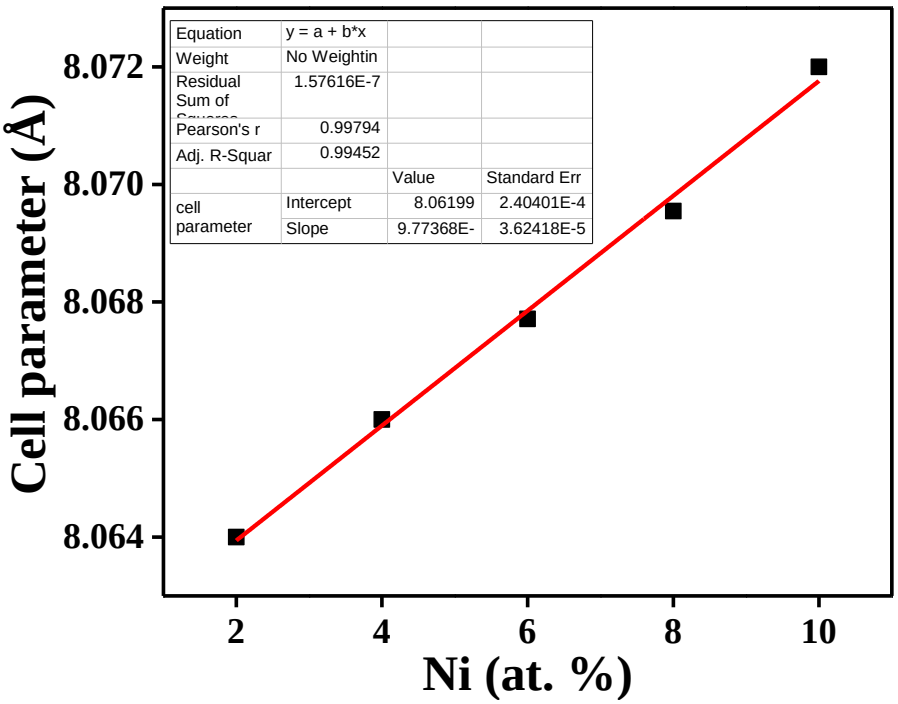

Figure 3.2. Change in the cell parameters of copper doped hercynite (CFAO) with Ni content.

3.2.2. BET studies

The specific BET surface areas along the porosity data of selected as-prepared samples and aged sample of this study are included in **Table 3.1**. The nature of adsorption-desorption isotherms (see **Figure 3.3**) indicates mesoporous nature of the materials although pore sizes of the concerned materials lie within 2 nm. The Cu-only catalyst has a higher surface area than the Ni and Cu co-doped hercynite catalyst. Upon 100 h aging in harsh DRM environment, the surface area of NCFAO8 is reduced to some extent (by 7 $m^2 g^{-1}$). This means that formation of alumina and NiCuFe alloy does not change the surface area of the best performing sample significantly. The anti-sintering behavior of the catalyst is thus evident from surface area analysis that is a highly desirable property of Ni-based catalyst employed in high temperature DRM process.

Table 3.1: BET surface area and porosity data of as-prepared samples.

Sample name	Surface area ($m^2 g^{-1}$)	Pore volume ($cm^3 g^{-1}$)	Pore size (nm)
CFAO	55	0.18	1.38
NCFAO2	53	0.14	1.44
NCFAO4	49	0.13	1.38
NCFAO6	47	0.13	2.07
NCFAO8	48	0.11	1.38
NCFAO10	50	0.13	2.07
Aged NCFAO8	41	0.13	1.38

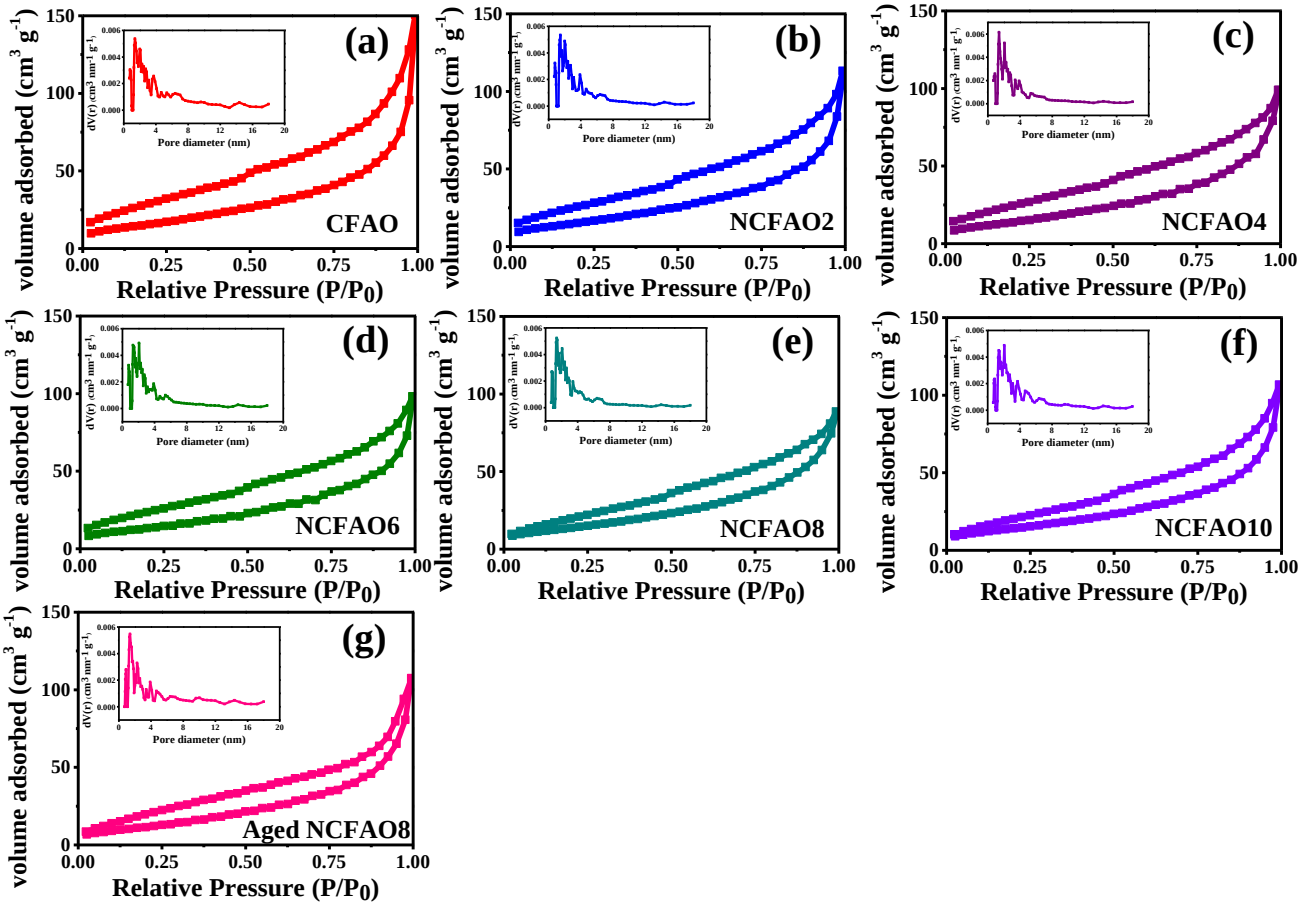

Figure 3.3. Nitrogen adsorption–desorption isotherms and pore size distribution curves of (a-f) NCFAOn (n= 0, 2, 4, 6, 8, 10) and (g) aged NCFAO8 samples.

3.2.3. Screening of the as-prepared materials

Catalytic activities of all the materials have been checked preliminarily for 10 h each to sort out the optimized sample. Preliminary tests, including blank test and DRM test using pure hercynite as the sample, confirmed no activity contributed either from the chromel-alumel thermocouple (containing 90 % of Ni in it and is inserted in the catalyst bed) or from the support oxide of the catalyst system. DRM activity of the materials varies with Ni loading in the hercynite and it follows the order CFAO< NFAO< NCFAO2< NCFAO4< NCFAO6< NCFAO8 ≈ NCFAO10 (**Figure 3.4**). The 8% Ni-doped congener CNFAO8 is found to be the most active formulation. The CH_4 and CO_2 conversions for NCFAO8 were 97 % and 99 %, respectively, with a H_2/CO ratio 0.80. Upon increasing the Ni content, there was no further improvement in activity for NCFAO10. This is because of the fact that the CH_4 and CO_2 conversions for both the NCFAO8 and NCFAO10 catalysts reached approximately to the theoretical value of equilibrium conversion (~99% for both CH_4 and CO_2 calculated using the software HSC5.1 (Outocompu), see **Figure 3.5(a)**) under the chosen reaction conditions of this study. Additionally, the values of apparent activation energies (E_a) of CH_4 (99.8 kJ mol^{-1}) and CO_2 (90.4 kJ mol^{-1}) calculated from the Arrhenius plot (see **Figure 3.5(b)**) in the temperature range 530 °C to 580 °C, after prior activation of the NCFAO8 catalyst at 800 °C, lie well in the typical E_a range of other state of the art DRM catalysts. Finally, the NCFAO8 has been selected for the long term activity and durability test. Consequently, the necessary characterizations have been carried out for this optimized formulation in its as-prepared and aged forms.

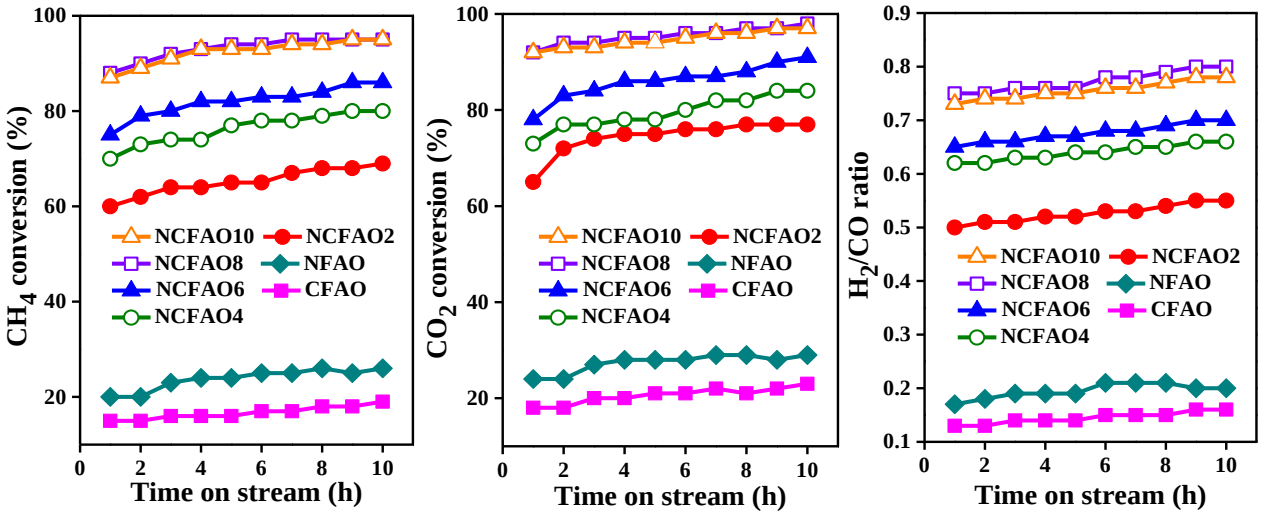

Figure 3.4. Comparison of the catalytic conversions of (a) CH_4 and (b) CO_2 and (c) H_2/CO ratio of the Ni and Cu co-doped $FeAl_2O_4$ systems (Reaction condition: 10 mL of 10% CH_4 in He, 10 mL of 10% CO_2 in He, 37 mL of pure He (carrier gas), 800 °C and GHSV= 34000 mL g^{-1} h^{-1}).

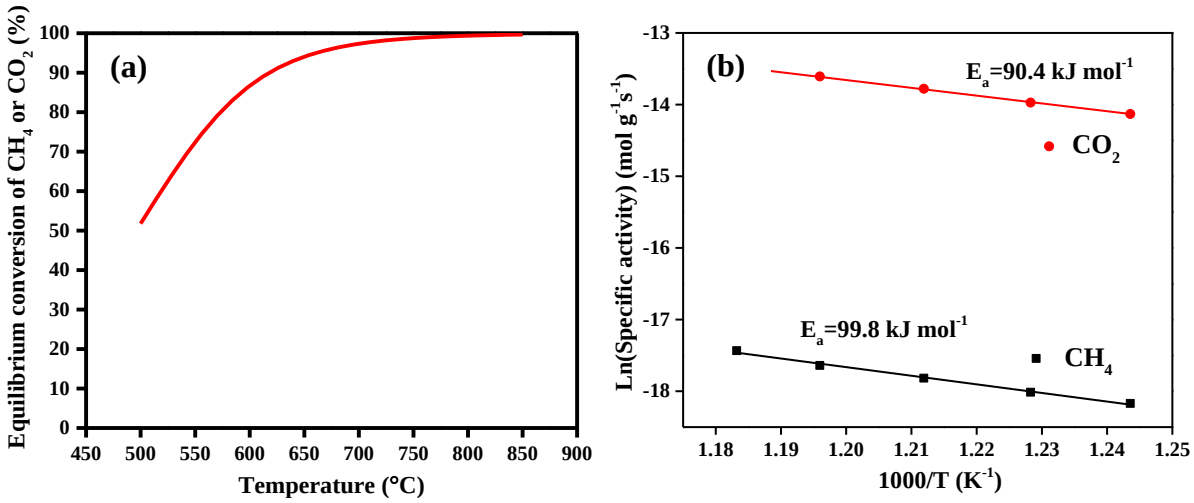

Figure 3.5. (a) Theoretical equilibrium conversion vs temperature plot calculated using the software HSC5.1 (Outocompu) and (b) Arrhenius plots for calculating the values of apparent activation energy for CH_4 and CO_2 (Reaction condition: 10 mL of 10% CH_4 in He, 10 mL of 10% CO_2 in He, 37 mL of pure He (carrier gas), 800 °C and GHSV= 34000 mL g^{-1} h^{-1}).

3.2.4. Time on stream behavior and effects of temperature and GHSV variations

Long-term activity of NCFAO8 catalyst in reforming environment has been evaluated by 100 h of continuous monitoring of conversions and H_2/CO ratio (**Figure 3.6**). Remarkably, NCFAO8 demonstrated a conversion of 97 % for CH_4 and 99 % for CO_2 and H_2/CO ratio gets stabilized at around 0.80 during this long span of durability at 800 °C. In order to assess the durability of the catalyst at a lower temperature, the long-term activity was also tested at 750 °C. The CH_4 and CO_2 conversions get reduced to 78 % and 84 %, respectively with the decrease of H_2/CO molar ratio to ~0.74. Slightly more conversion (~2% at 800 °C) of CO_2 than that of CH_4 can be attributed to the occurrence of reverse water gas shift reaction (RWGSR) which is a strong competitor of DRM. As expected, the lag in conversion is more when the reforming is done at the lower temperature of 750 °C. The CH_4 and CO_2 conversions and H_2/CO molar ratios were also investigated at further lower temperatures of 650 °C and 700 °C at 34000 mL g^{-1} h^{-1} (see **Figure** 3.**7** and **Table 3.2**) and at higher GHSVs of 68000 and 102000 and mL g^{-1} h^{-1} at 800 °C (see **Figure** 3.**8** and **Table 3.2**). The trend is as per expectation, the CH_4 and CO_2 conversions decreased respectively to 26-65 % and 34-69 %, while the H_2/CO molar ratios get stabilized in the range 0.55-0.68. The deviation of H_2/CO ratio from unity, more when the temperature is lowered, can be accounted for by taking the RWGSR into consideration. There was no appreciable loss of activity before termination of the reaction after 100 h. Intrinsic activities are also calculated for this catalyst with respect to Ni and have been listed in **Table 3.3**. A comparison of hercynite-based NCFAO8 catalyst with other state of the art Ni and Ni-alloy based DRM catalysts suggest promising activity behavior of the NCFAO8 catalyst (see **Table 3.4**) in the context of (a) facile one step synthetic route of catalyst preparation as well as (b)

potential coke resistant ability and (c) long term stable conversion without loss of activity over a wide range of temperatures as elaborated afterwords. The 100 h used sample at 800 °C, collected after cooling to room temperature in helium flow is termed as aged catalyst. A thorough characterization of the aged catalyst has been performed subsequently and compared with the findings on the as-prepared catalyst to elucidate the structure-activity correlation of the catalyst system.

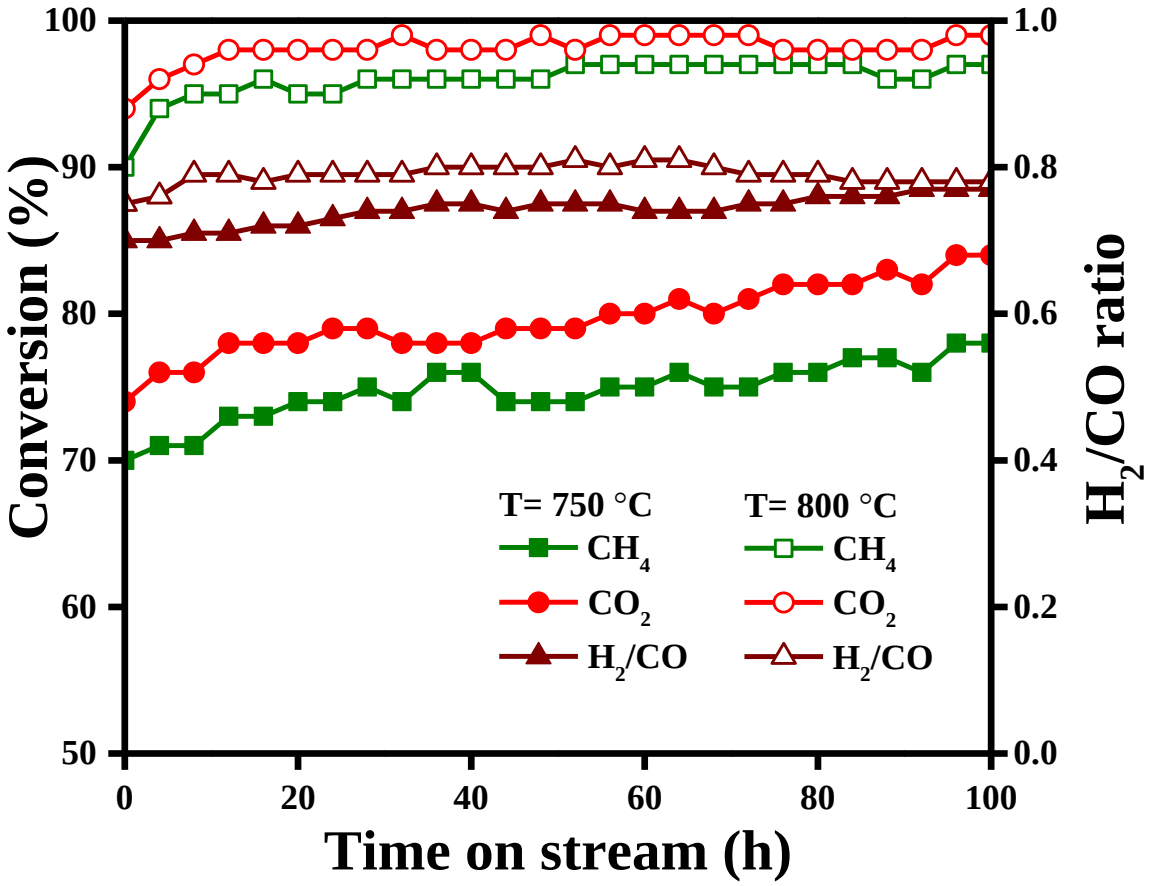

Figure 3.6. Time on stream behavior of NCFAO8 at 750 °C and 800 °C (Other reaction conditions: 10 mL of 10% CH_4 in He, 10 mL of 10% CO_2 in He, 37 mL of pure He (carrier gas) and GHSV= 34000 mL g^{-1} h^{-1}).

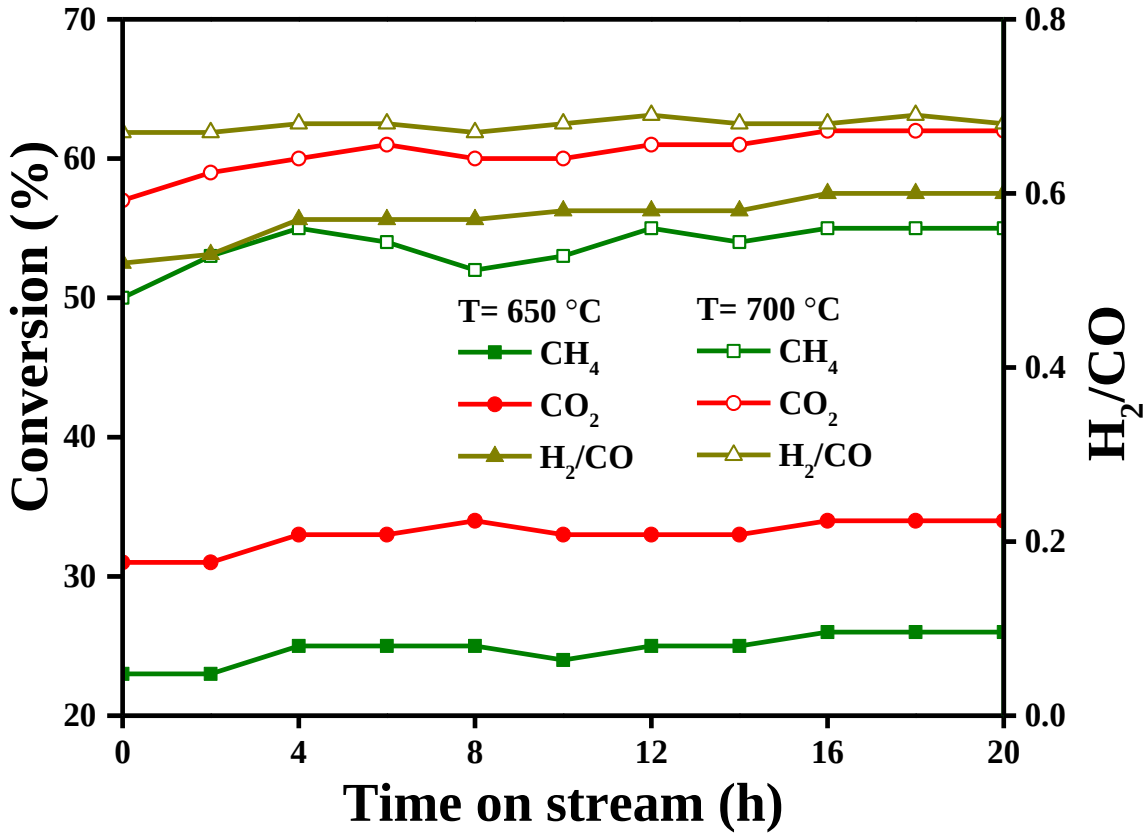

Figure 3.7. Effect of temperature variation (650 °C and 700 °C) on the CH_4, CO_2 conversions and H_2/CO ratio at 34000 mL g^{-1} h^{-1} (Reacting gas composition: 10 mL of 10% CH_4 in He, 10 mL of 10% CO_2 in He, 37 mL of pure He as carrier gas).

Table 3.2. Variation in CH_4 and CO_2 conversions and H_2/CO molar ratios at different temperatures and GHSVs.

GHSV (mL g^{-1} h^{-1})	Temperature (°C)	CH_4 conversion (%)	CO_2 conversion (%)	H_2/CO molar ratio
34000	650	26	34	0.60
34000	700	55	62	0.68
68000	800	65	69	0.63
102000	800	57	62	0.55

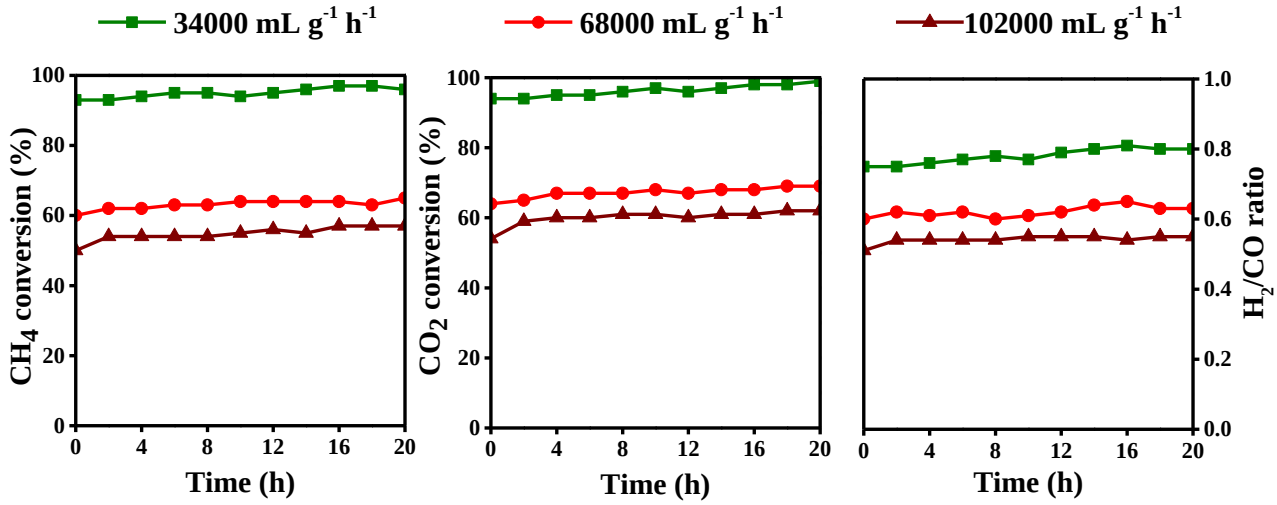

Figure 3.8. Effect of GHSV variation on the CH_4, CO_2 conversions and H_2/CO ratio at 800 °C.

Table 3.3. Table of intrinsic activities of the NCFAO8 catalyst at 800 °C.

Intrinsic activity	**CH_4**	**CO_2**
Reaction rate (mmol g^{-1} s^{-1})	0.288	0.297
Turnover frequency (s^{-1})	1.69×10^{-2}	1.74×10^{-2}
Activity (mmol m^{-2} s^{-1})	3.74×10^{-3}	3.86×10^{-3}

3.2.5. Identification of the phase(s) in the aged NCFAO8

The structural evolution on ageing of the CNFAO8 catalyst have been assessed at first from the powder XRD analysis, as shown in **Figure 3.9(a)**. A careful analysis of the diffraction peaks of aged catalyst indicates that the peaks at 2θ values 31.2°, 36.7°, 44.7°, 48.7°, 55.4°, 59.1°, 64.9° and 76.9° correspond to (220), (311), (400), (331), (422), (511), (440) and (533) planes and are well-matched with the pristine hercynite phase. The diffraction peaks marked with ∗ on the right side of the hercynite phase related peaks correspond to γ-Al_2O_3. PXRD data of the catalyst sample (collected after cooling in helium flow to room temperature) recorded after 2 h of stable

conversion confirms the formation of NiO (without any signature of CuO or the corresponding metal components) along with the starting hercynite spinel phase (**Figure 3.9(b)**).

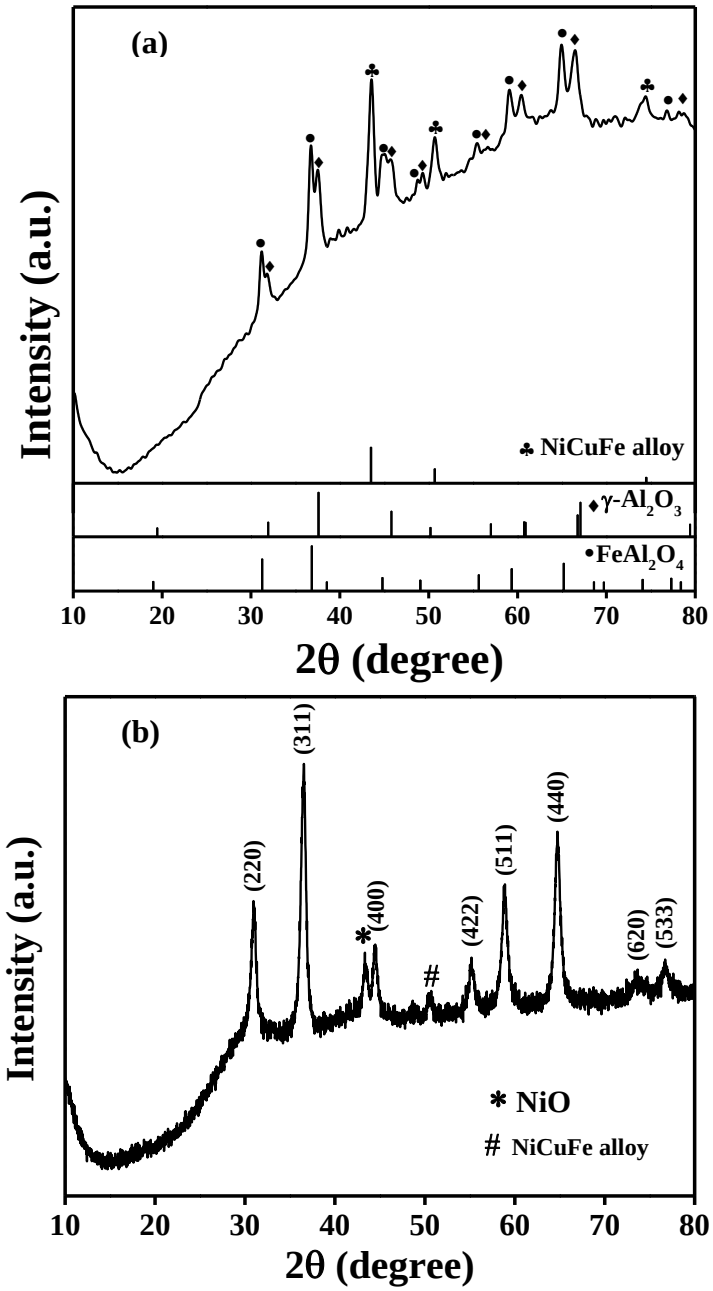

Figure 3.9. (a) Diffraction pattern of the 100 h aged NCFAO8 catalyst where spinel phase remains intact along with the formation of NiCuFe alloy and γ-Al_2O_3 phases and (b) powder XRD pattern of NCFAO8 sample collected after 2 h of DRM reaction at 800 °C.

Thus, by comparing the diffraction pattern of this intermediate catalyst with those of as-prepared and aged catalysts, we can propose that exsolution of nickel (apparently occurs at first) along with copper and a portion of iron occurs in the DRM environment. These exsolved phases eventually lead to the formation of NiCuFe alloy (the peaks identified with ♣ in **Figure 3.9(a)**) without any detectable NiO/CuO phases. The signature of alloying is also observed after ~2 h of DRM. Increasing and gradually higher background intensity in the diffraction pattern seems to be contributed from X-ray fluorescence from Ni and Fe in NiCuFe alloy. The average Scherrer sizes of hercynite and γ-Al_2O_3 are 14±2and 12±2, respectively, while the NiCuFe alloy particles have the average size of 10±2 nm. Etsell et al.[42] have explored the exsolution of CuNi alloy through the reduction (by H_2) of Cu-Ni-Al oxide solid solution . Their studies suggest exsolution of NiO initially, followed by Cu with the increase in temperature that subsequently form CuNi alloy. The release of aluminium in the form of γ-Al_2O_3 in this work is mediated through the above exsolution process so as to maintain the structural integrity of the pristine hercynite. No crystalline carbon phase is also detected in the aged sample.

3.2.6. H_2 temperature programmed reduction (H_2-TPR) analysis

To get further insights about the structure as well as reducibility of the NCFAO8 catalyst, H_2-TPR analysis of the as-prepared catalyst was done, followed by PXRD analysis of the resulting sample. The TPR profile of the sample (see **Figure 3.10(a)**) comprised of mainly one broad peak centered at ~460 °C, along with some small humps. Interestingly, the XRD pattern of the H_2-reduced catalyst (see **Figure 3.10(b)**) suggests no noticeable change in the parent spinel structure, indicating no signature of sintering and the particle size remains similar (8±2 nm) to the other forms of the catalyst. This structural integrity of the catalyst indicates that

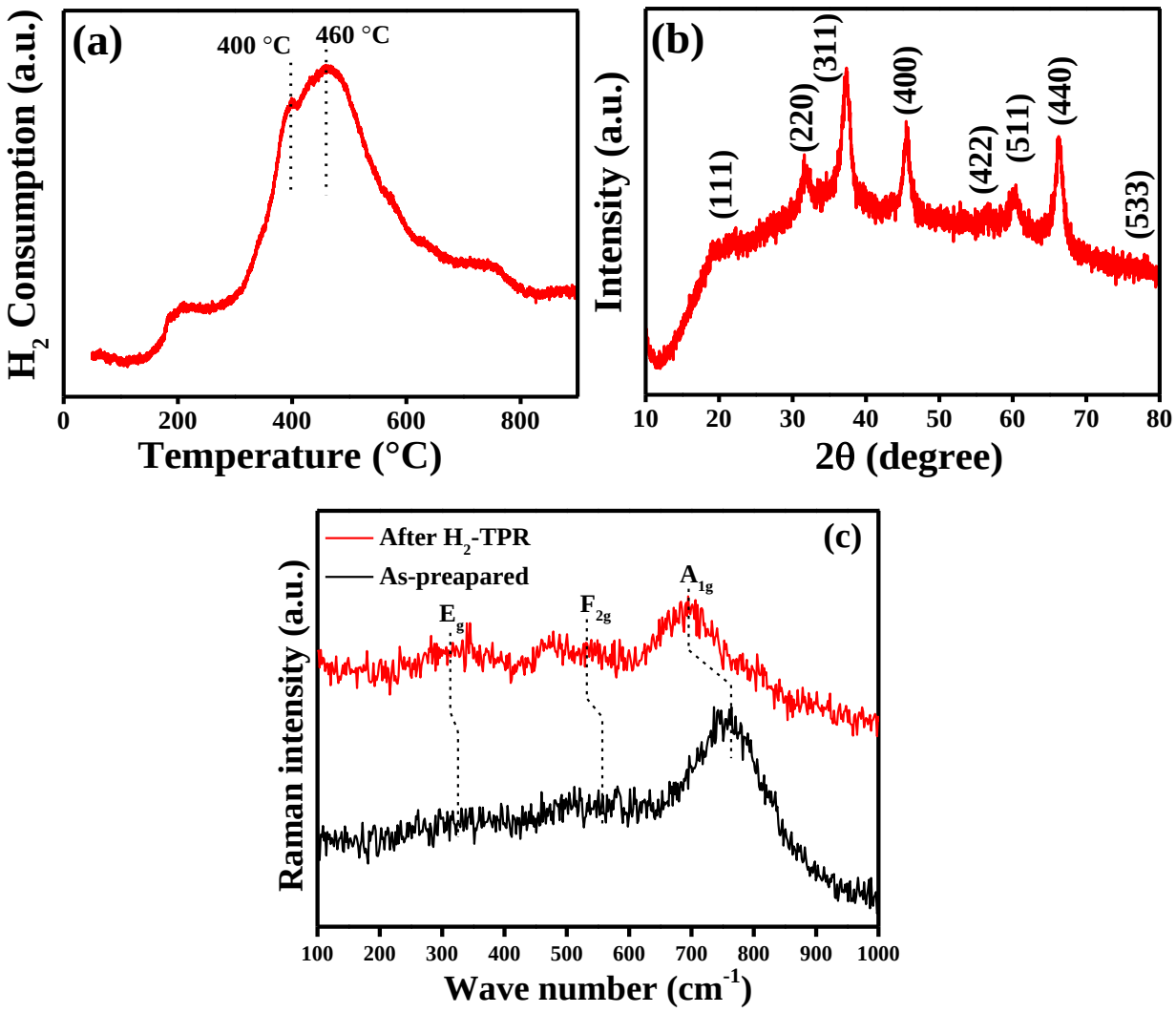

Figure 3.10. Reduction behavior and post reduction product analysis of the NCFAO8 catalyst: (a) H_2-TPR profile of NCFAO8, (b) PXRD of the sample collected after H_2-TPR and (c) Raman spectra of NCFAO8 before (as-prepared catalyst) and after H_2-TPR reduction.

the broad hydrogen consumption peak (~460 °C) is possibly due to surface oxygen reduction, while the small hump centered at ~ 400 °C, might be due to the reduction of a minute fraction of Ni^{2+} that cannot be ruled out for this complex catalyst system. This is very much expected for the hercynite-based catalyst that is quite stable in reducing H_2 environment. It is pertinent to mention

that the scenario is different for the hercynite catalyst doped only with copper. In an earlier report[37], we have shown formation of Cu, Fe, AlO, $Al_{2.667}O$ phases after H_2-TPR of the 10 at.% Cu-doped $FeAl_2O_4$ catalyst. Thus, when Ni is doped along with Cu, as in the Ni and Cu co-doped hercynite catalyst (NCFAO8), the stability increases (in comparison to the Cu-only catalyst), thereby maintaining the structural integrity up to ~800 °C in H_2-TPR analysis.

The Raman spectra of the NCFAO8 sample collected after H_2-TPR along with that of the as-prepared catalyst are shown in **Figure 3.10(c)**. The peculiar peak due to hercynite phase is the broad and intense A_{1g} mode (at ~759 cm^{-1}) in close similarly with the earlier report by Lottici et al.[43] The other peaks, although not well-defined, that could be identified are centered at ~562 cm^{-1} and at ~325 cm^{-1} for the F_{2g} and E_g modes, respectively. A signature of a small shoulder (~697 cm^{-1}) at the lower wavenumber side of the A_{1g} mode may be attributed to cation disorder in the spinel structure. There is a shift of ~60 cm^{-1} of the A_{1g} mode in the case of H_2-TPR sample pointing to change in the local environment like creation of oxide-ion vacancy in the hercynite structure. It is to be noted that no structural change is evident from the powder XRD pattern of the H_2-TPR treated NCFAO8, neither there is any signature of individual oxides of the metal components. So, Raman study presumably points to structural integrity of the main hercynite phase, although we have already noted that NiCuFe alloy is formed through *in situ* coexsolution in the DRM atmosphere.

3.2.7. TEM-HRTEM, EDS, HAADF-STEM mapping of as-prepared and aged NCFAO8

The transmission electron microscopy analysis of as-prepared NCFAO8 under low resolution is shown in **Figure 3.11(a)**, while **Figure 3.11(b)** shows a high-magnification image that reveals a

six-membered ring-shaped structure with a crystallite size of approximately ~17 nm and a lattice fringe of 2.77 Å, which corresponds to the (220) plane of doped hercynite, NCFAO8. **Figure 3.11(c,d)** further illustrates the fast Fourier transform (FFT) and inverse fast Fourier transform (IFFT) images, respectively of the (220) plane. For the aged NCFAO8, **Figure 11(e,f**) present the low- and high-resolution TEM images, respectively. Two sets of FFT and IFFT images corresponding to the HRTEM image are shown in **Figure 3.11(e-i**). Distinct lattice fringes with spacings of 2.03 Å and 2.08 Å correspond respectively to the (400) and (111) planes of pristine hercynite and NiCuFe alloy (see **Figure 3.11(g,h**)), while the fringe spacing of 2.33 Å correspond to the (311) plane of γ-Al_2O_3 (see **Figure 3.11(i,j**)) in the aged catalyst. The selected area electron diffraction (SAED) pattern (**Figure 3.11(k**)) exhibits concentric circles, confirming the polycrystalline nature of the synthesized NCFAO8.

The diffraction rings correspond to d-spacings of 0.2860, 0.2434, 0.2018, 0.1665, 0.1568, and 0.1435 nm, which align with the (220), (311), (400), (422), (511), and (440) crystallographic planes, respectively. These values are in good agreement with the X-ray diffraction analysis of the sample (see **Figure 3.1**). The SAED pattern of aged NCFAO8 (**Figure 3.11(l))** reveals the presence of (220), (311), (400), (422), (511), and (440) crystallographic planes of the spinel structure. The sharper dot pattern in the SAED image indicates a higher crystallinity in the aged sample compared to the as-synthesized NCFAO8. It may also be pointed out that the TEM image of as-prepared catalyst (see **Figure 3.11(a)**) apparently suggests the presence of residual carbon in between the interfaces of the catalyst particles. Interestingly, a similar type of residual carbon is seemingly absent in the TEM image of the aged catalyst (see **Figure 3.11(e)**) that is in conformity with the enhanced crystallinity on ageing of the catalyst.

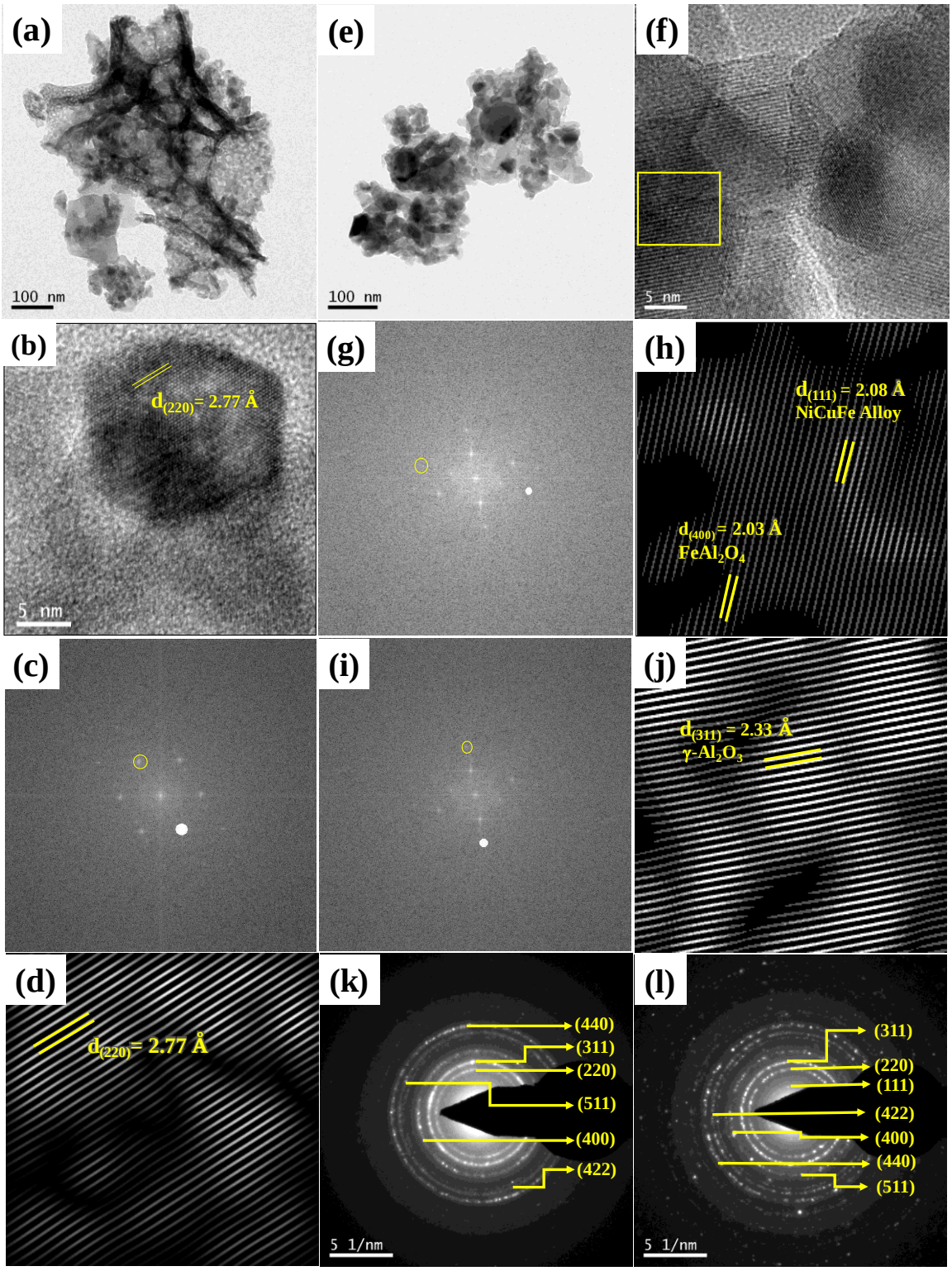

Figure 3.11. TEM-HRTEM images, FFT and IFFT analyses and SAED patterns of (a-d and k) as-prepared and (e-j and l) aged NCFAO8 catalysts.

The energy dispersive spectroscopy (EDS) analyses (see **Figure 3.12**) of both the as-prepared and aged samples of NCFAO8 confirm presence of all the expected elements Ni, Cu, Fe, Al, and O in the material. It is to be noted that atomic percentage of Cu is very high than the expected result due to the contribution from the Cu-grid to the EDS signal of Cu, barring us to talk about the elemental composition. Hence, ICP-AES analysis of the as-prepared sample was carried out that revealed the actual mass% of Ni to be 2.48, Cu to be 2.36, Fe to be 26.90 and Al to be 27.85 which are in good agreement with the expected stoichiometry of the NCFAO8 catalyst.

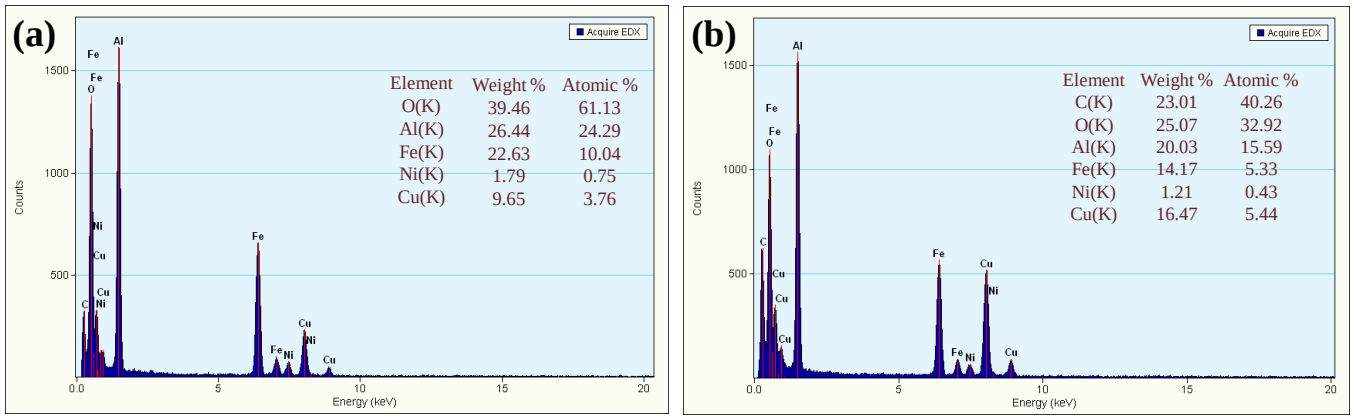

Figure 3.12. Elemental compositions of (a) as-prepared and (b) aged NCFAO8 catalyst obtained from energy dispersive X-ray spectroscopy (EDS) analyses.

According to the EDS elemental mapping (see **Figure 3.13**), Ni, Cu, and Fe are homogeneously distributed in the two forms of the NCFAO8 catalyst. Specifically, in the aged catalyst, these elements are localized within specific regions, providing direct evidence for the formation of NiCuFe alloy. This is in conformity with the diffraction pattern of the aged NCFAO8 catalyst. Elemental mapping for Al, O and combined mapping of as-prepared and aged NCFAO8 catalyst also show homogeneity of the various elements (see **Figure 3.14**).

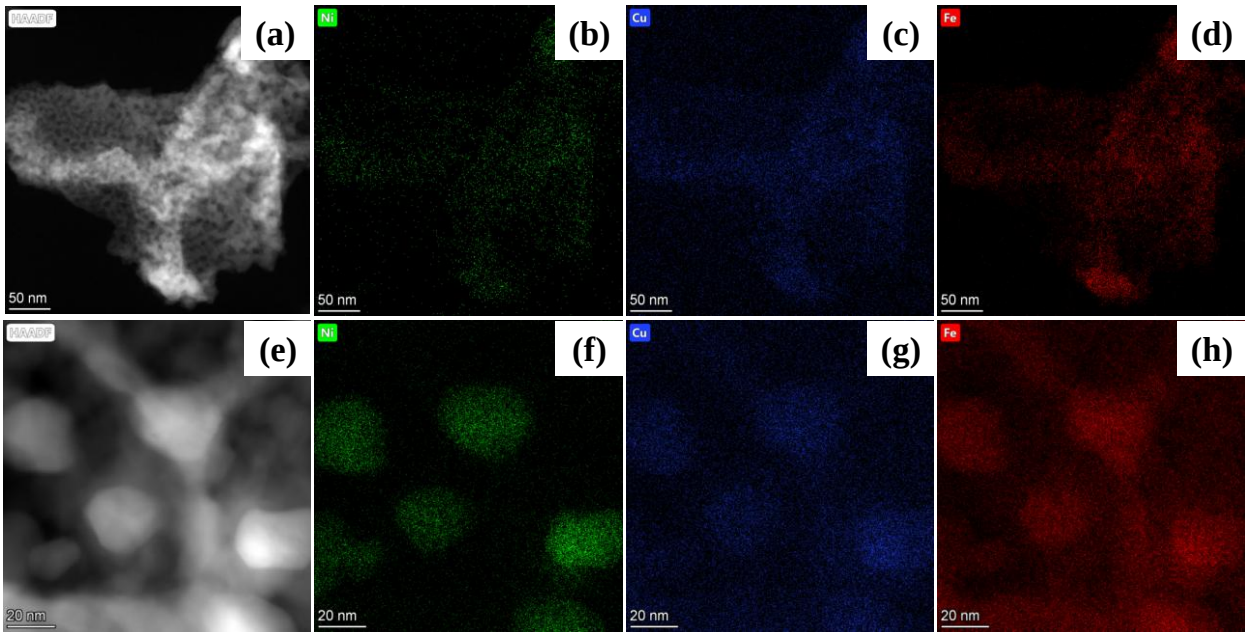

Figure 3.13. HAADF-STEM images of (a) as-prepared and (e) aged NCFAO8 catalyst and elemental mapping of Ni, Cu and Fe in (b-d) as-prepared (before alloying) and (f-h) aged NCFAO8 catalyst (after alloying).

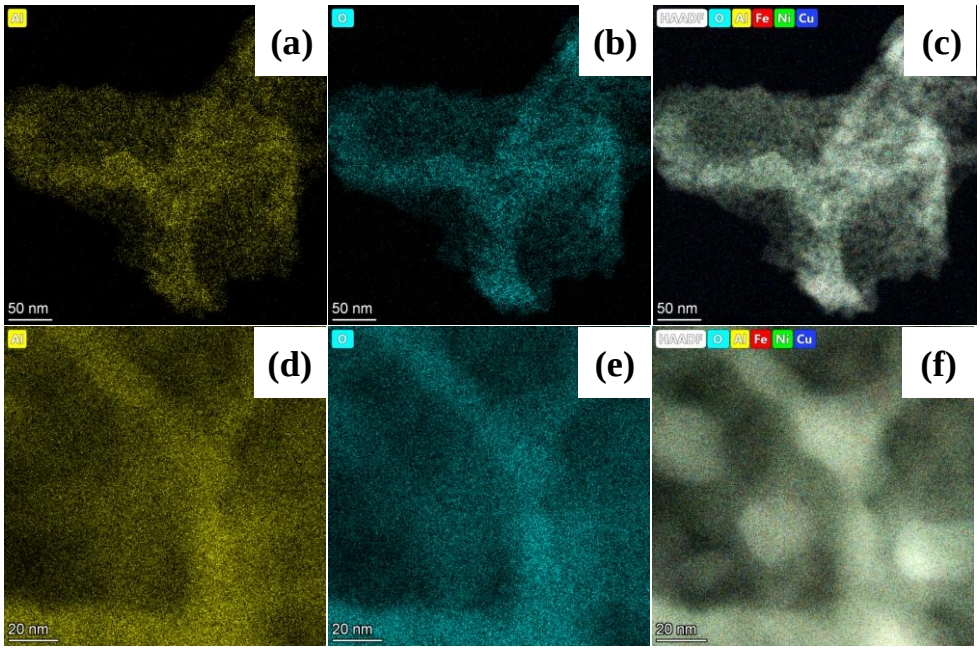

Figure 3.14. Elemental mapping for Al, O as well as combined mapping of (a-c) as-prepared and (d-f) aged NCFAO8 catalyst.

3.2.8. XPS studies

XPS analyses have been utilized to characterize NCFAO8 to understand the composition and bonding nature of the constituent elements. Al 2p, Fe 2p, Ni 2p and Cu 2p core level spectra of as-prepared NCFAO8 catalysts are presented in **Figure 3.15**. The Al 2p core level spectra of as-prepared catalyst is observed to be asymmetric and is curve-fitted into component species as displayed in **Figure 3.15(a)**. Observed peak at 74.4 eV in as-prepared catalyst corresponds to octahedral Al^{3+} species present in the catalyst, while a weak component peak in the lower binding energy region at 73.4 eV indicates the presence of tetrahedral component of Al^{3+} species[44]. Fe 2p core level spectrum is observed to be broad in as-prepared catalyst sample indicating the presence of multiple Fe-species in the sample and they are curve-fitted into component species as shown in **Figure 3.15(b)**. Fe $2p_{3/2,1/2}$ peaks observed at 709.5, 722.9 and 710.8,724.6 eV in curve-fitted Fe 2p core level spectrum of as-prepared sample along with characteristic satellite peaks at 717.2 and 730.7 eV are assigned for octahedral and tetrahedral Fe^{2+} species, respectively[45]. Ni $2p_{3/2}$ component peaks in broad Ni 2p core level spectrum of as-prepared catalyst are observed at 854.7 and 856.3 eV as presented in **Figure 3.15(c)** are assigned respectively to Ni^{2+} in octahedral and tetrahedral sites in the doped hercynite catalyst[45]. The Cu 2p core level spectrum of as-prepared catalyst is broad indicating the presence of different Cu species which is decomposed into different component peaks by curve-fitting and is displayed in **Figure 3.15(d)**. Accordingly, Cu $2p_{3/2,1/2}$ peaks at 933.5 and 953.4 eV with characteristic satellite peaks at 941.4, 943.8, and 962.3 eV and spin-orbit separation of 19.9 eV correspond to Cu^{2+} species present in the catalyst. In addition, weak component $2p_{3/2,1/2}$ peaks at 935.8 and 955.7 eV are also found in the Cu 2p core level spectrum. It has been reported in the literature that Cu 2p binding energy decreases on increasing the coordination number with oxygen ions from

tetrahedral to octahedral sites. Therefore, Cu $2p_{3/2,1/2}$ peaks at 933.5 and 953.4 eV are assigned for Cu^{2+} species in octahedral sites, while the spin-orbit doublets at 935.8 and 955.7 eV stand for Cu^{2+} in tetrahedral sites of the hercynite structure.[44] Core level spectra of Al 2p, Fe 2p, Ni 2p, and Cu 2p in aged catalyst are shown in **Figure 3.15 (e-h)**. In the aged catalyst, intensity of lower binding energy peak in Al 2p core level spectrum is found to decrease as displayed in

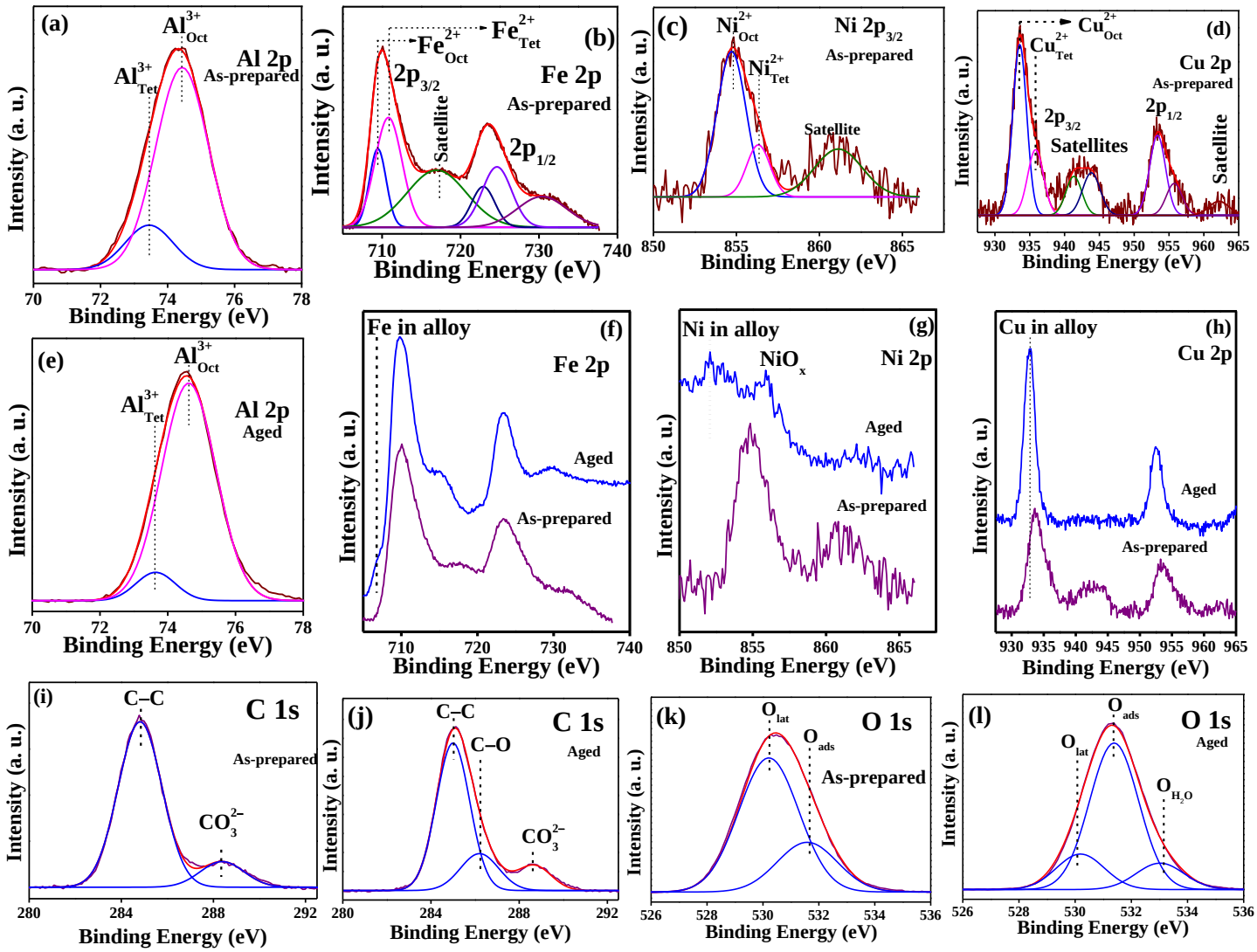

Figure 3.15. XPS core-level regions of (a, e) Al 2p, (b, f) Fe 2p, (c, g) Ni 2p, (d, h) Cu 2p, (i, j) C 1s and (k, l) O 1s in as-prepared and aged NCFAO8 catalyst.

Figure 3.15(e). Fe 2p core level spectrum in the aged catalyst along with that of as-prepared catalyst is shown in **Figure 3.15(f)**. It is to be noted that spectral envelopes of both the catalysts look different. Weak peaks are surfaced in the lower binding energy region and peak widths of the main peaks are reduced. Weak spin-orbit peaks at 707.4 and 720.3 eV are attributed to Fe alloy species formed during DRM process and observed peaks at 709.8 and 723.6 eV correspond to Fe^{2+} species. Similar to Fe 2p core level spectrum of aged catalyst, spectral nature of Ni $2p_{3/2}$ core level of this catalyst is different from as-prepared catalyst which is presented in **Figure 3.15 (g)**. A discerned peak around 853 eV is assigned to Ni alloy present in the aged catalyst. A higher binding energy peak at 855.8 eV along with a satellite peak at 862 eV is attributed to NiO_x species. In Cu 2p core level spectrum of the aged catalyst as displayed in **Figure 3.15(h)** along with that of the as-prepared catalyst, intense Cu $2p_{3/2,1/2}$ peaks at 932.8 and 952.1 eV in the lower binding energy region of the spectrum are observed, which can be ascribed to either metallic Cu or Cu alloy species. Spectral tail in the higher binding energy region can be due to presence of CuO_x species. It is also to be mentioned that satellite peaks are absent in the aged catalyst compared to as-prepared catalyst. Further, there is formation of NiCuFe alloy as per the XRD, HRETM and STEM HAADF findings of the aged catalyst. In the view of this, lower binding energy peaks observed in Ni 2p and Cu 2p core level spectra of aged catalyst may be associated with NiCuFe alloy. During DRM condition, Ni, Cu and Fe come out from the spinel catalyst forming the alloy species. C 1s core level spectra of as-prepared and aged catalysts are presented in **Figure 3.15(i, j)**. The as-prepared sample shows mainly C–C bond at 284.8 eV along with a weak peak at 288.4 eV corresponding to carbonate species. However, in the aged sample, oxidized carbon (C–O bond) at 286.3 eV is also observed along with C–C bond and carbonate species. **Figure 3.15(k, l)** presents O 1s core level spectra of as-prepared and aged samples.

Spectra are curve-fitted into component species as the spectra are broad in nature. Core level spectrum of as-prepared catalyst contains lattice oxygen component peak at 530.2 eV and a peak at 531.6 eV corresponding to adsorbed oxygen species. However, in the spectrum of aged sample, peak intensity of adsorbed species gets increased and a new component peak at 533.1 eV is also observed which is attributed to adsorbed water species. These findings indicate the change in oxygen species on the surface of the aged catalyst during DRM condition.

It is very clear that the intensities of Cu 2p peaks are much higher than those of Fe 2p and Ni $2p_{3/2}$ in the aged catalyst. This may be ascribed to surface segregation of copper in NiCuFe alloy particles. We have already noted that nickel is presumably the first to get exsolved as NiO that is followed by CuO, FeO_x and γ-Al_2O_3 exsolution. The NiO, CuO and FeO_x oxides then experience *in situ* reduction in the reforming environment and form the NiCuFe alloy. An intimate nanocomposite of this NiCuFe alloy with the parent hercynite and γ-Al_2O_3 phases prevents sintering of the alloy particles so as to ensure the stable conversion behavior of the hercynite-based catalyst system.

3.2.9. CHNS analysis of the as-prepared and aged NCFAO8

The results of CHN analyses have confirmed that the as-prepared NCFAO8 contains 3.91 mass% of carbon, whereas after 100 h of aging the amount of carbon is reduced to almost one third of the original value at 1.39%. This unusual result correlates well with the findings of TEM analyses that clearly show reduction of residual carbon subsequent to ageing in the DRM atmosphere. In a previous study, it has been shown that combustion synthesized materials contain a certain amount of amorphous carbon in it due to incomplete oxidation of organic residues, which can be removed either by thermal treatment in an oxidizing environment or by

chemical treatment[46]. But these pretreatments may have adverse outcomes like growth of crystallites together with a decrease in surface area. We thus deliberately used the as-prepared sample without any pretreatment and looked at the outcome. The decrease in carbon content on ageing can be well accounted for by a coke-free conversion in DRM that is accompanied by continuous removal of the carbon present inherently in the as-prepared catalyst. In this context, it can be said that the carbon is amorphous by nature and hence gets removed in the course of DRM. Moreover, both X-ray diffraction and microstructural analysis suggest absence of any crystalline phase of carbon in the as-prepared as well as aged NCFAO8, which again confirms the amorphous nature of the carbon.

3.2.10. TGA-DTA analysis of the aged NCFAO8

The thermogravimetry-differential thermal analyses of the aged catalyst carried out in zero air flow from room temperature to ~900 °C is shown in **Figure 3.16**. Four stages of mass change may be noted from the TGA profile. The preliminary loss of mass is due to the combined effect of the vaporization of absorbed water (and in line with DTA profile, desorption of water being endothermic) together with the onset of oxidation of amorphous carbon. This is followed by a slow increase of mass, which is presumably due to beginning of oxidation of NiCuFe alloy to the component oxides[47] together with the oxidation of remaining carbon, because the amorphous coke is generally oxidized within 350 °C. In the third stage, from ~320 °C to ~600 °C, the oxidation of alloy is completed and is accompanied by an additional contribution from the oxidation of iron to FeO and/or Fe_3O_4 spinel phase[48], which is reflected by an increase in slope in the TGA profile. In the final stage, i.e., beyond 600 °C, the increase in mass may be ascribed to further oxidation of iron from FeO and/or Fe_3O_4 to Fe_2O_3.

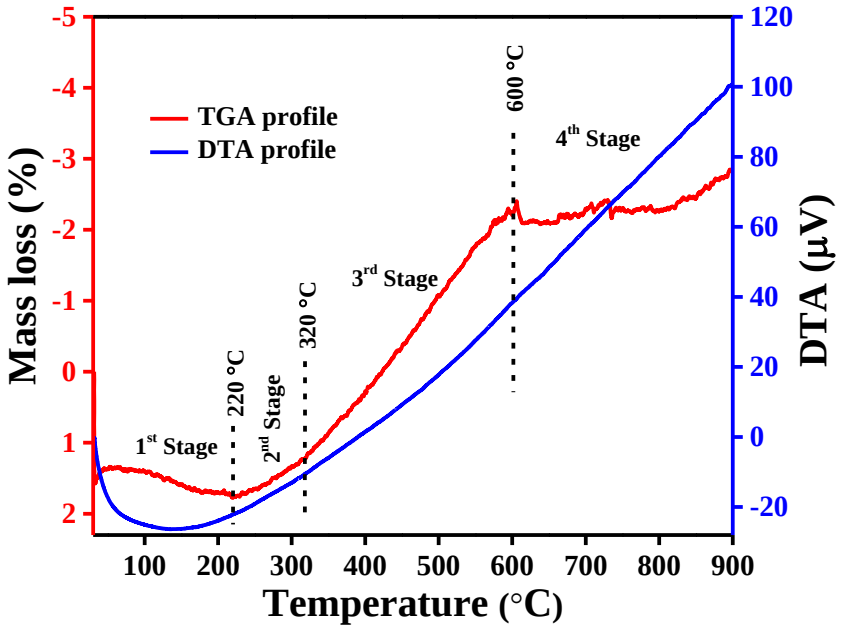

Figure 3.16. TGA-DTA curves of aged NCFAO8 catalyst in zero air flow.

3.2.11. Structure-activity correlation

The improvement of redox behavior and sintering resistance of the alloys are reported to increase the activity and stability of the catalyst[47, 17]. K. Han et al.[47] have reported that the CH_x are completely decomposed to C atoms on the Ni nanoparticles and are dissolved into nanoparticle framework of the Ni-Cu/SiO_2 catalyst prepared by electrostatic adsorption of Ni−ammonia complexes of Ni and Cu on SiO_2. After a certain time the dissolved C atoms grow as carbon nanotubes over the Ni nanoparticles. The Cu decorated Cu-Ni alloy nanoparticles influence CH_x decomposition through the formation of activated O atoms (from CO_2 activation by Cu) that gasifies the CH_x to CO and H. This property of Cu-Ni alloy has been reported to be responsible for the long term DRM process without any observable peak of carbon nanotube. Alongside Cu, Fe is also expected to be involved in coke removal activities through Fe/FeO_x redox cycle as demonstrated by Theofenidis et al. [21] and Kim et al. [49] The first group has explored the role of Fe

in DRM and has proposed that the reaction over NiFe-based catalysts can be described by a Mars-van Krevelen mechanism where CH_4 is activated on Ni sites to form H_2 and surface carbon, while Fe gets oxidized to FeO_x (dealloying/segregation) by CO_2 and the deposited carbon is subsequently been reoxidized to CO by lattice oxygen of FeO_x. According to Muller et al., absence of any signature of FeO in the XRD pattern can be well explained by taking into consideration that FeO is formed as miniature domains of a few atomic layer covering a fraction of the Ni-rich particle surface, thereby ensuring a close proximity of the coke removal (FeO) and CH_4 activation (Ni) sites. Eventually the pronounced effect of segregation of Fe from the NiFe alloy i.e., dealloying restricts its use in DRM. In another study, Theofenidis et al.[50] have explored that a third metal Pd can suppress the preferential segregation of Fe from NiFe alloy. Following them, Jin et al.[51, 52] have replaced Pd by Cu for studying the structural evolution of NiCuFe alloy which indeed comes out to be an excellent trimetalic combination with improved stability and coke resistant ability. As a logical corollary to the previous outcomes, presently concerned NiCuFe is supposed to have the combined efficiency of both NiCu and NiFe alloys.

In regard to the crucial role played by Fe in mitigating coke formation, Theofenidis et al.[53] have mentioned the importance of Fe incorporation in the $MgFe_xAl_{2-x}O_4$ (Ni/$MgFe_xAl_{2-x}O_4$) matrix. In accordance with their findings, the coke-resistance ability of the NCFAO8 catalyst can partially be attributed to the remaining hercynite phase, which is a classic example of cation antisite defects due to the cation inversion and/or off-stoichiometry of the cation, as a result of which local oxygen vacancies are created[36]. Luo et al.[11] have extensively investigated the role of defect sites in γ-Al_2O_3 in facilitating DRM process and have reported that this defect sites catalyze the reaction by increasing the adsorption and activation ability of CO_2 molecule. This CO_2 activation also indirectly facilitates the CH_4 activation. They have shown that the CO_2-TPD

profile shows a weak adsorption peak of CO_2 at around 100 °C for the pure γ-Al_2O_3 phase, while two additional desorption peaks are observed for the defect γ-Al_2O_3 phase, namely a high temperature desorption peak at nearly 600 °C and another desorption peak at about 350 °C, which have been attributed to the defect sites in γ-Al_2O_3 and for Ni impregnation, respectively. In line with their findings, it is reasonable to propose that such defect sites should be present in the *in situ* generated γ-Al_2O_3 of the present NCFAO8 catalyst. To corroborate the aspect of *in situ* generation of oxygen defect, CO_2-TPD analysis of the 100 h aged sample was carried out (**Figure 3.17**). The TPD profile shows CO_2 desorption peaks at higher temperatures of ~410 °C, ~550 °C and ~680 °C along with a weak CO_2 adsorption peak at a much lower temperature of ~87 °C. Considering the identified phases associated with the aged NCFAO8 catalyst, it may be proposed that the desorption peaks at ~550 °C and ~680 °C are originated from the spinel phases $FeAl_2O_4$ and defect γ-Al_2O_3 phase, while the peak at ~410 °C may be due to the NiCuFe alloy. As a result, this defect containing γ-Al_2O_3 phase helps in CO_2 adsorption and activation eventually assisting indirect CH_4 activation. This oxygen defects present in hercynite and γ-Al_2O_3 phases of NCFAO8 catalyst also help in CO_2 activation process through adsorption of CO_2 molecules[54]. In the presently reported hercynite-based NiCuFe alloy catalyst, Ni takes care of CH_x decomposition to C atoms, while CO_2 activation gets facilitated by surface enriched Cu, while Fe (both as a part of the alloy and the hercynite) has the potential ability in removing coke in unison, eventually leading to long term coke-free DRM[55-60] activity of the NCFAO8 catalyst.

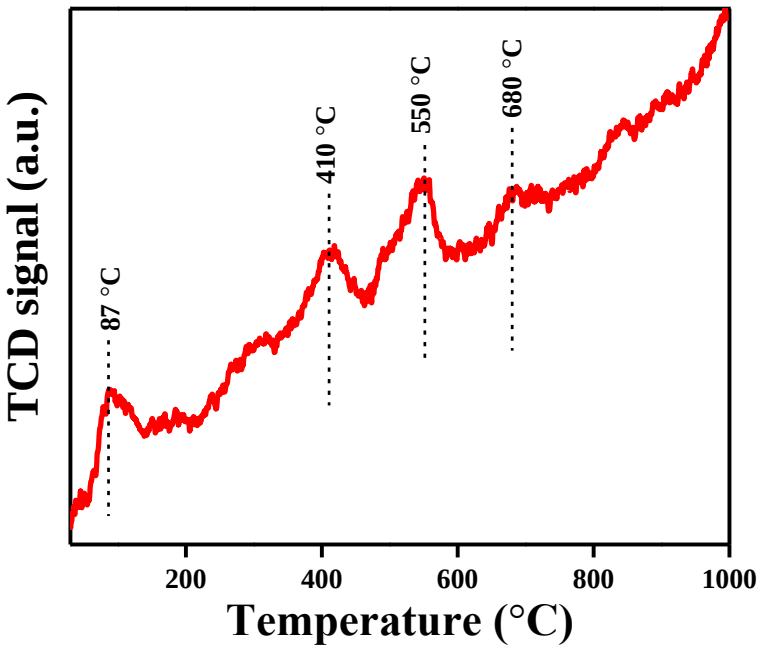

Figure 3.17. CO_2-TPD profile of the aged NCFAO8 catalyst.

3.3. Summary

In this study we have shown highly reproducible, simple, cost-effective solution combustion synthesis method as a suitable method to prepare Ni and Cu co-doped hercynite spinel. NCFAO8 shows very high CH_4 and CO_2 conversion efficiencies at 800 °C and GHSV of 34000 mL g^{-1} h^{-1} without any appreciable loss of activity. Additionally this report highlights a hercynite-based catalyst capable of offering *in situ* generated Ni-based multicomponent alloy entailing apparently coke-free DRM. In true sense, NCFAO8 acts as the precursor for *in situ* generation of NiCuFe termetallic alloy, the main carrier of the reaction along with γ-Al_2O_3 and hercynite. Herein, the beauty of the catalyst lies in the fact that the improvisation of the active metal and support system occur simultaneously during the progress of the reaction and may be projected as a suitable contender for industrialization of the currently immature DRM technique. It may also be

proposed that modifications of hercynite system may further be studied as a fertile ground for other catalytic reactions through suitable tailoring of its chemical composition.

References

1. Kahle, L. C. S.; Roussière, T.; Maier, L.; Delgado, K. H.; Wasserschaff, G.; Schunk, S. A.; Deutschmann, O. Methane Dry Reforming at High Temperature and Elevated Pressure: Impact of Gas-Phase Reactions. *Ind. Eng. Chem. Res.* **2013**, *52*, 11920-11930.

2. Lu, Y.; Kang, L.; Guo, D.; Zhao, Y.; Zhao, Y.; Wang, S.; and Ma, X. Double-Site Doping of a V Promoter on Ni_x-V-MgAl Catalysts for the DRM Reaction: Simultaneous Effect on CH_4 and CO_2 Activation. *ACS Catal.* **2021**, *11*, 8749-8765.

3. Komarala, E. P.; Dabbawala, A. A.; Harfouche, M.; Vasiliades, M. A.; Charisiou, N.; Anjum, D. H.; Mao, S.; Rueping, M.; Baker, M. A.; Goula, M. A.; Efstathiou, A. M.; Polychronopoulou, K. Tune and turn the pyrolysis of metal organic frameworks towards stable supported nickel catalysts for the dry reforming of methane. *Appl. Surf. Sci.* **2024,** *666*, 160388.

4. Dahan, M.; Komarala, E.; Fadeev, L.; Chinnam, A. K.; Shlomovich, A.; Lipstman, S.; Padi, S. P.; Haustein, H.; Gozin, M.; Rosen, B. A. Methane dry reforming catalyst prepared by the co-deflagration of high-nitrogen energetic complexes. *J. Mater. Chem. A*, **2019**, *7*, 141.

5. Buharon, M.; Singh, S.; Komarala, E. P.; Rosen, B. A. Expanding possibilities for solid-phase crystallization by exsolving tunable Pd–NiO core– shell nanostructures. *CrystEngComm*, **2018**, *20*, 6372.

6. Ojeda-Niño, O. H.; Gracia, F.; Daza, C. Role of Pr on Ni-Mg-Al Mixed Oxides Synthesized by Microwave-Assisted Self-Combustion for Dry Reforming of Methane. *Ind. Eng. Chem. Res.* **2019**, *58*, 7909-7921.

7. Qi, R.; An, L.; Guo, Y.; Zhang, R.; and Wang, Z. In Situ Fabrication of Ultrasmall Ni Nanoparticles from $Ni(OH)_2$ Precursors for Efficient CO_2 Reforming of Methane. *Ind. Eng. Chem. Res.* **2022**, *61*, 198-206.

8. Guo,Y.; Li, Y.; Ning, Y.; Liu, Q.; Tian, L.; Zhang, R.; Fu, Q.; and Wang, Z. CO_2 Reforming of Methane over a Highly Dispersed Ni/Mg-Al-O Catalyst Prepared by a Facile and Green Method. *Ind. Eng. Chem. Res*. **2020**, *59,* 15506-15514.

9. Dong, J.; Fu, Q.; Li, H.; Xiao, J.; Yang, B.; Zhang, B.; Bai, Y.;Song, T.; Zhang, R.; Gao, L.; Cai, J.; Zhang, H.; Liu, Z.; Bao, X. Reaction-Induced Strong Metal-Support Interactions between Metalsand Inert Boron Nitride Nanosheets. *J. Am. Chem.Soc*. **2020**, *142*, 17167-17174.

10. Ray, D.; Chawdhury, P.; and Subrahmanyam, C. Promising Utilization of CO_2 for Syngas Production over Mg^{2+} and Ce^{2+}-Promoted Ni/γ-Al_2O_3 Assisted by Nonthermal Plasma. *ACS Omega* **2020**, *5,* 14040-14050.

11. Zhang, Y.; Zu, Y.; He, D.; Liang, J.; Zhu, L.; Mei, Y.; Luo, Y. The tailored role of "defect" sites on γ-alumina: A key to yield an efficient methane dry reforming catalyst with superior nickel utilization. *Appl. Catal. B Environ*. **2022**, *315,* 121539.

12. Lim, Z.; Tu, J.; Zhou, F.; Xu, Y.; Chen, B. Anti-coking Ni encapsulated in SiO_2 via one pot reverse microemulsion method as a versatile catalyst for CO_2 methane reforming. *J. CO_2 Util.* **2023**, *67,* 102341-102351.

13. Kim, J.; Seo, J.; Jang, W.; and Lee, K. Effect of Sr Incorporation and Ni Exsolution on Coke Resistance of the Ni/Sr-Al_2O_3 Catalyst for Dry Reforming of Methane. *ACS Sustainable Chem. Eng.* **2023**, *11,* 17415-17424.

14. Huang, L.; Li, D.; Tian, D.; Jiang, L.; Li, Z.; Wang, H.; and Li, K. Optimization of Ni-Based Catalysts for Dry Reforming of Methane via Alloy Design: A Review. *Energy Fuels* **2022**, *36*, 5102-5151.

15. Torimoto, M.; and Sekine, Y. Effects of alloying for steam or dry reforming of methane: a review of recent studies. *Catal. Sci. Technol*., **2022**, *12*, 3387.

16. Zhukova, A.; Fionov, Y.; Semenova, S.; Khaibullin, S.; Chuklina, S.; Maslakov, K.; Zhukov, D.; Isaikina, O.; Mushtakov, A.; and Fionov, A. Ethanol Dry Reforming for Hydrogen-Rich Syngas Production over Cu-Promoted Ni/Al_2O_3-ZrO_2 *Catalysts. J. Phys. Chem. C* **2024**, *128*, 20177-20194.

17. Yang, Y.; Lin, Y. A.; Yan, X. Y.; Chen, F.; Shen, Q.; Zhang, L.; and Yan, N. Cooperative Atom Motion in Ni-Cu Nanoparticles during the Structural Evolution and the Implication in the High-Temperature Catalyst Design. *ACS Appl. Energy Mater*. **2019**, *2*, 8894-8902.

18. Xiao, Z.; Hou, F.; Zhang, J.; Zheng, Q.; Xu, j.; Pan, L.; Wang, L.; Zou, J.; Zhang, X.; and Li, G. Methane Dry Reforming by Ni-Cu Nanoalloys Anchored on Periclase-Phase $MgAlO_x$ Nanosheets for Enhanced Syngas Production. *ACS Appl. Mater. Interfaces* **2021**, *13*, 48838-48854.

19. Shi, Y.; Han, K.; and Wang, F. Ni-Cu Alloy Nanoparticles Confined by Physical Encapsulation with SiO_2 and Chemical Metal-Support Interaction with CeO_2 for Methane Dry Reforming. *Inorg. Chem.* **2022**, *61*, 15619-15628.

20. Yao, X.; Cheng, Q.; Attada, Y.; Ould-Chikh, S.; Ramírez, A.; Bai, X.; Mohamed, H. O.; Li, G.; Shterk, G.; Zheng, L.; Gascon, J.; Han, Y.; Bakr, O. M.; a, Castano, P. A typical stability of exsolved Ni-Fe alloy nanoparticles on double layered perovskite for CO_2 dry reforming of methane. *Appl. Catal. B Environ* **2023**, *328*, 122479.

21. Theofanidis, S. A.; Galvita, V. V.; Poelman, H.; Dharanipragada, N. V. R. A.; Longo, A.; Meledina, M.; Tendeloo, G. V.; Detavernier, C.; and Marin, G. B. Fe Containing Magnesium Aluminate Support for Stability and Carbon Control during Methane Reforming. *ACS Catal.* **2018**, *8*, 5983-5995.

22. Li, B.; Yuan, X.; Li, L.; Wang, X.; and Li, B. Stabilizing Ni-Co Alloy on Bimodal Mesoporous Alumina to Enhance Carbon Resistance for Dry Reforming of Methane. *Ind. Eng. Chem. Res.* **2021**, *60*, 16874-16886.

23. Wu, Z.; Yang, B.; Miao, S.; Liu, W.; Xie, J.; Lee, S.; Pellin, M. J.; Xiao, D.; Su, D.; and Ma, D. Lattice Strained Ni-Co alloy as a High-Performance Catalyst for Catalytic Dry Reforming of Methane. *ACS Catal*. **2019**, *9*, 2693-2700.

24. Sheng, k.; Luan, D.; Jiang, H.; Zeng, F.; Wei, B.; Pang, F.; and Ge, J. Ni xCoy Nanocatalyst Supported by ZrO_2 Hollow Sphere for Dry Reforming of Methane: Synergetic Catalysis by Ni and Co in Alloy. *ACS Appl. Mater. Interfaces* **2019**, *11*, 24078-24087.

25. Manabayeva, A. M.; Mäki-Arvela, P.; Vajglová, Z.; Martinéz-Klimov, M.; Tirri, T.; Baizhumanova, T. S.; Grigor'eva, V. P.; Zhumabek, M.; Aubakirov, Y. A.; Simakova, I. L.; Murzin, D. Y.; and Tungatarova, S. A. Dry Reforming of Methane over Ni-Fe-Al Catalysts Prepared by Solution Combustion Synthesis. *Ind. Eng. Chem. Res.* **2023**, *62*, 11439-11455.

26. Neagu, D.; Oh, T.; Miller, D. N.; Me´nard, H.; Bukhari, S. M.; Gamble, S. R.; Gorte, R. J.; Vohs, J. M.; & Irvine, J. T. S. Nano-socketed nickel particles with enhanced coking resistance grown in situ by redox exsolution. *Nat. Commun*. **2015**, *6*, No. 8120.

27. Jeong, H; Kim, Y. H.; Won, B.; Jeon, H.; Park, C.; Myung, J. Emerging Exsolution Materials for Diverse Energy Applications: Design, Mechanism, and Future Prospects. *Chem. Mater*. **2023**, *35,* 3745-3764.

28. Marin, C. M.; Popczun, E. J.; Nguyen-Phan, T.; Tafen, D. N.; Alfonso, D.; Waluyo, I.; Hunt, A.; Kauffman, D. R. Designing perovskite catalysts for controlled active-site exsolution in the microwave dry reforming of methane. *Appl. Catal. B Environ.* **2021**, *284,* 119711.

29. Shah, S.; Sayono, S.; Ynzunza, J.; Pan, R.; Xu, M.; Pan, X.; Gilliard-AbdulAziz, K. L. The effects of stoichiometry on the properties of exsolved Ni-Fe alloy nanoparticles for dry methane reforming. *AIChE J*. **2020**; *66,* e17078.

30. Shah, S.; Xu, M.; Pan, X.; and Gilliard-Abdulaziz, K. L. Exsolution of Embedded Ni-Fe-Co Nanoparticles: Implications for Dry Reforming of Methane. *ACS Appl. Nano Mater*. **2021**, *4*, 8626-8636.

31. Shah, S.; Xu, M.; Pan, X.; and Gilliard-Abdulaziz, K. L. Complex Alloy and Heterostructure Nanoparticles Derived from Perovskite Oxide Precursors for Catalytic Dry Methane Reforming. *ACS Appl. Nano Mater.* **2022**, *5,* 17476-17481.

32. Shah, S.; Hong, J.; Cruz, L.; Wasantwisut, S.; Bare, S. R.; and Gilliard-AbdulAziz, K. L. Dynamic Tracking of NiFe Smart Catalysts using *In Situ* X-Ray Absorption Spectroscopy for the Dry Methane Reforming Reaction. *ACS Catal.* **2023**, *13,* 3990-4002.

33. Najimu, M.; Jo, S.; and Gilliard-AbdulAziz, K. L. Co-Exsolution of Ni-Based Alloy Catalysts for the Valorization of Carbon Dioxide and Methane. *Acc. Chem. Res.* **2023**, *56,* 3132-3141.

34. Zhao, J.; Bao, J.; Yang, S.; Niu, Q.; Xie, R.; Zhang, Q.; Chen, M.; Zhang, P.; and Dai, S. Exsolution-Dissolution of Supported Metals on High-Entropy $Co_3MnNiCuZnO_x$: Toward Sintering-Resistant Catalysis. *ACS Catal.* **2021**, *11*, 12247-12257.

35. Zeng, D.; Qiu, Y.; Peng, S.; Chen, C.; Zeng, J.; Zhang, S.; and Xiao, R. Enhanced hydrogen production performance through controllable redox exsolution within $CoFeAlO_x$ spinel oxygen carrier materials. *J. Mater. Chem. A*, **2018**, *6*, 11306.

36. Millican, S. L.; Clary, J. M.; Musgrave, C. V.; Lany, S. Redox Defect Thermochemistry of $FeAl_2O_4$ Hercynite in Water Splitting from First-Principles Methods. *Chem. Mater*. **2022**, *34*, 519-528.

37. Maiti, S.; Llorca, J.; Dominguez, M.; Colussi, S.; Trovarelli, A.; Priolkar, K. R.; Aquilanti, G.; Gayen, A. Combustion synthesized copper-ion substituted $FeAl_2O_4$ ($Cu_{0.1}Fe_{0.9}Al_2O_4$): A superior catalyst for methanol steam reforming compared to its impregnated analogue. *J. Power Sources*. **2016**, *304*, 319–331.

38. Mistri, R.; Maiti, S.; Llorca, J.; Dominguez, M.; Mandal, T. K.; Mohanty, P.; Raya, B. C.; Gayen, A. Copper Ion Substituted Hercynite ($Cu_{0.03}Fe_{0.97}Al_2O_4$): A Highly Active Catalyst for Liquid Phase Oxidation of Cyclohexane. *Appl. Catal. A: Gen***. 2014**, *485*, 40–50.

39. Maiti, S.; Das, D.; Pal, K.; Llorca, J.; Soler, L.; Colussi, S.; Trovarelli, A.; Priolkar, K. R.; Sarode, P.R.; Asakura, K.; Seikh, M. M.; Gayen, A. Methanol steam reforming behavior of sol-gel synthesized nanodimensional $CuxFe_{1-x}Al_2O_4$ hercynites. *Appl. Catal. A: Gen.* **2019**, *570*, 73–83.

40. Maiti, S.; Kundu, A. K.; Lebedev, O. I.; Bera, P.; Anandan, C.; Gayen, A.; and Seikh, M. M. Synthesis and magnetic properties of nanodimensional $Fe_{1-x}Cu_xAl_2O_4$ ($0.3 \leq x \leq 0.8$). *RSC Adv*., **2015**, *5*, 83809.

41. Mu, H.; Li, F.; An, X.; Liu, R.; Li, Y.; Qianc, X.; Hu, Y. One-Step Synthesis, Electronic Structure, and Photocatalytic Activity of Earth-Abundant Visible-Light-Driven $FeAl_2O_4$. *Phys. Chem. Chem. Phys.* **2017**, *19,* 9392—9401.

42. Naghash, A. R.; Etsell T. H.; Xu, S. XRD and XPS Study of Cu-Ni Interactions on Reduced Copper-Nickel-Aluminum Oxide Solid Solution Catalysts. *Chem. Mater*. **2006**, *18,* 2480-2488.

43. D'Ippolito, V.; Andreozzi, G. B.; Bersanib, D.; Lottici, P. P. Raman fingerprint of chromate, aluminate and ferrite spinels. J. Raman Spectrosc. **2015**, *46,* 1255–1264

44. Pal, K.; Dey, A.; Jana, R.; Ray, P. P.; Bera, P.; Kumar, L.; Mandal, T. K.; Mohanty, P.; Seikh, M.. M.; Gayen, A. Citrate Combustion Synthesized Al-Doped $CaCu_3Ti_4O_{12}$ Quadruple Perovskite: Synthesis, Characterization and Multifunctional Properties. *Phys. Chem. Chem. Phys*. **2020**, *22*, 3499−3511.

45. Bera, P.; Lakshmi, R. V.; Prakash, B. H.; Tiwari, K.; Shukla, A.; Kundu, A. K.; Biswas, K.; Barshilia, H. C. Solution Combustion Synthesis, Characterization, Magnetic, and Dielectric Properties of $CoFe_2O_4$ and $Co_{0.5}M_{0.5}Fe_2O_4$ (M = Mn, Ni, and Zn). *Phys. Chem. Chem. Phys*. **2020**, *22*, 20087−20106.

46. Ianos, R.; Lazau, R.; Lazau, I.; Pacurariu, C.Chemical oxidation of residual carbon from $ZnAl_2O_4$ powders prepared by combustion synthesis. *J. Eur. Ceram. Soc.*. 2012, *32.* 1605–1611.

47. Han, K.; Wang, S.; Liu, Q.; Wang, F. Optimizing the Ni/Cu Ratio in Ni-Cu Nanoparticle Catalysts for Methane Dry Reforming. *ACS Appl. Nano Mater*. **2021**, *4,* 5340-5348.

48. Li, X.; Wang, H.; Zhou, Q.; Qi, T.; Liu, G.; Peng, Z. Phase Transformation of Hercynite During the Oxidative Roasting Process. *JOM,* **2020,** *72,* 10.

49. Kim, S. M.; Abdala, P. M.; Margossian, T.; Hosseini, D.; Foppa, L.; Armutlulu, A.; Beek, W. V.; Comas-Vives, A.; Coperet, C.; Müller, C. Cooperativity and Dynamics Increase the Performance of NiFe Dry Reforming Catalysts. *J. Am. Chem. Soc.* **2017,** *139,* 1937-1949.

50. Theofanidis, S. A.; Galvita, V. V.; Sabbe, M.; Poelman, H.; Detavernier, C.; Marin, G. B. Controlling the stability of a Fe–Ni reforming catalyst: Structural organization of the active components Appl. Catal. B: Environ. **2017,** *209,* 405–416.

51. Jin, F.; Fu, Y.; Kong,W.; Wang, J.; Cai, F.; Yuan, C.; Pan, B.; Zhang, J.; Sun, Y. Stable Trimetallic NiFeCu Catalysts with High Carbon Resistance for Dry Reforming of Methane. *ChemPlusChem* **2020**, *85,* 1120 –1128.

52. Jin, F.; Fub, Y.; Kong, W.; Wang, J, Caib, F.; Zhangb, J.; Xu, J. Dry reforming of methane over trimetallic NiFeCu alloy catalysts *Chem. Phys. Lett.* **2020,** *750,* 137491.

53. Theofanidis, A.; Galvita, V. V.; Poelman, H.; Dharanipragada, N. V. R. A.; Longo, A.; Meledina, M.; Tendeloo, G.V.; Detavernier, C.; Marin, G. B. Fe-Containing Magnesium Aluminate Support for Stability and Carbon Control during Methane Reforming Stavros *ACS Catal.* **2018**, *8,* 5983-5995.

54. Yentekakis, I. V.; Panagiotopoulou, P.; Artemakis, G. A review of recent efforts to promote dry reforming of methane (DRM) to syngas production via bimetallic catalyst formulations. *Appl. Catal. B Environ:* **2021,** *296,*120210.

55. Padi, S. P.; Shelly, L.; Komarala, E. P.; Schweke, D.; Hayun, S.; Rosen, B. A. Coke-free methane dry reforming over nano-sized NiO-CeO_2 solid solution after exsolution. *Catal. Commun*. **2020,** *138,* 105951.

56. Yu, J.; Le, T.; Jing, D.; Stavitski, E.; Hunter, N.; Lalit, K.; Leshchev, D.; Resasco, D. E.; Sargent, E. H.; Wang, B.; Huang, W. Balancing elementary steps enables coke-free dry reforming of methane. *Nat. Commun.* **2023,** *14*, 7514.

57. Akri, M.; Zhao, S.; Li, X.; Zang, K.; Lee, A. F.; Isaacs, M. A.; Xi, W.; Gangarajula, Y.; Luo, J.; Ren, Y.; Cui, Y.; Li, L.; Su, Y.; Pan, X.; Wen, W.; Pan, Y.; Wilson, K.; Li, L.; Qiao, B.; Ishii, H.; Liao, Y.; Wang, Wang, Y.; Zhang, T. Atomically dispersed nickel as coke-resistant active sites for methane dry reforming. *Nat. Commun.* **2019,** *10*, 5181.

58. Sorcar, S.; Das, J.; Komarala, E.P. ; Fadeev, L.; Rosen, B.A.; Gozin. M. Design of coke-free methane dry reforming catalysts by molecular tuning of nitrogen-rich combustion precursors. *Mater. Today Chem.* **2022,** *24*, 100765.

59. Manavi, N.; Liu, B. Mitigating Coke Formations for Dry Reforming of Methane on Dual Site Catalysts: A Microkinetic Modeling Study. *J. Phys. Chem. C* **2023**, *127*, 2274−2284.

60. Kim , S. B.; Eissa , A.; Kim, M.; Goda, E. S.; Youn, J. R.; Lee, K. Sustainable Synthesis of a Highly Stable and Coke-Free Ni@CeO2 Catalyst for the Efficient Carbon Dioxide Reforming of Methane. *Catal.* **2022**, *12*, 423.

Chapter 4

DRM behavior of solution combustion synthesized $Ni_xFe_{1-x}Al_2O_4$

4.1. Introduction

In **Chapter 3** we have shown that hercynite has the flexibility of incorporating several transition metals into the 'A'/'Fe' site of its spinel framework and the doped metals along with the host Fe are co-exsolved in the harsh DRM environment forming NiCuFe ternary alloy.[1] Contextually, the role of the individual component in the alloy (Ni, Cu and Fe) has been discussed in conclusive manner in the previous chapter. From mechanistic point of view, based on the extensive studies done on NiFe bimetallic system including our work, it is clear that the NiFe bimetallic alloy formulation is a very promising combination for coke resistance in DRM.[2-17]

In a previous study, Theofanidis et al.[18,19] have shown that the NiFe alloy catalyzed DRM goes through Mars-van Krevelen mechanism in which Fe plays a crucial role by taking part in a redox cycle operating between deposited carbon, Fe and CO_2 that oxidizes the deposited coke into CO and increases the longevity of the Ni-based catalyst in harsh DRM environment. Again, according to kinetic studies and coke gasification kinetics done by Tingting Zhang et al.[20], Fe increases the alloy particle's surface oxyphilicity by balancing the otherwise strong carbon affinity of the Ni surface leading to transformation

of the surface carbon from refractory type to soft type, that is easily gasified by CO_2. They have also concluded that Fe slowed down the rate of coke deposition and speed up the rate of surface coke gasification without altering the reaction mechanism and the kinetic properties of the Ni catalyst used. But the inherent issues of Fe oxidation (in NiFe) i.e., dealloying in presence of CO_2, as revealed by Sung Min Kim et al.[21] restricts the use of NiFe alloy towards thermocatalytic DRM process in more harsh and demanding situations. Fe, not only in the metallic form (as in the alloy) but also in the spinel framework can play a controlling role in the CH_4 conversion and coke removal activity. This dealloying issue is supposed to be partially solvable by adding a third metal[22]. But there is another possibility of trade off between activity and stability due to confinement of the active metal Ni in the core shell (shell block effect) made by the third metal. Su Li et al.[23] in a valuable study, have tried to break the trade-off between the activity and the coke deposition through tailoring the d-band center of Ni via Fe-doping, matching with the energy level of CH_4* dehydrogenation, but is far away from that of the over-cleavage of CH_x*. This prevailing issue can be addressed by taking help of the exsolved[24] and *in situ* grown[25] miniscule alloy with strong metal support interaction. Ni incorporation in the hercynite and subsequent exposure in DRM may be a desired solution in this respect.

We have already shown in chapter 3 that 8 at.% Ni is not sufficient enough to introduce that much crystallinity in hercynite system compared to its Cu-doped analogue. Additionally, we have also seen that 8 at.% Ni-doped hercynite, $Ni_{0.08}FeAl_2O_4$ (labeled as NFAO8) exhibit low activity towards DRM compared to its Cu, Ni co-doped congener (NCFAO8) for a feed gas ratio (CH_4: CO_2: carrier gas) of 1: 1: 54. Now to understand the role of Ni in developing crystallinity in hercynite, it is reasonable to increase the extent of

Ni-loading starting with a justifiable amount. Moreover, mimicking the harsh realistic DRM condition, where the feed gas concentration is very high (we have deliberately used the feed gas ratio as 1:1:18 in our present investigation) or when the GHSV is more demanding, the concentration of the active metal matters. As we know from our previous investigation, with an increase in feed gas concentration or GHSV of the process, the rate of conversion increases and vice versa. It is also demanding that for higher feed gas concentration in DRM (which is required for commercial purposes), Ni concentration must be higher in hercynite than that in the previous study (8 at.%). With the decrease in operating temperature, the conversion also decreases which can be compensated by higher active metal (Ni here) loading.

Keeping in mind the aforementioned factors like crystallinity, diminished activity (due to feed gas concentration, GHSV and operating temperature), the trade-off between activity and stability along with the prevailing dealloying issue of Fe, we have synthesized $Ni_xFe_{1-x}Al_2O_4$ (where x = 0.30 to 0.50 that are designated as NFAOX where X= 30-50) using ultrafast SCS method and subsequently employed in catalytic DRM over a low-moderate temperature range[26, 27] with a prior intuition of NiFe alloying through co-exsolution of dopant Ni and Fe in the hercynite host in the reaction medium. Among all the samples, NFAOX exhibits very promising dry reforming activity over 50 h of time on stream activity and hence revealing the prospect of alloy-based DRM catalyst with high activity and durability.

4.2. Results and Discussion

4.2.1. Powder XRD studies

The powder XRD patterns of Ni-doped $FeAl_2O_4$ catalysts are shown in **Figure 4.1**. Formation of the hercynite spinel phase is clearly evident from the well matched diffraction peaks of JCPDS PDF# 34-0192. No noticeable peak of NiO could be identified in the PXRD pattern, which point to successful doping of Ni in hercynite. The crystallite size of the as-prepared sample is 15-25 nm as obtained from Scherrer's equation indicating nano-dimensional nature of the synthesized materials.

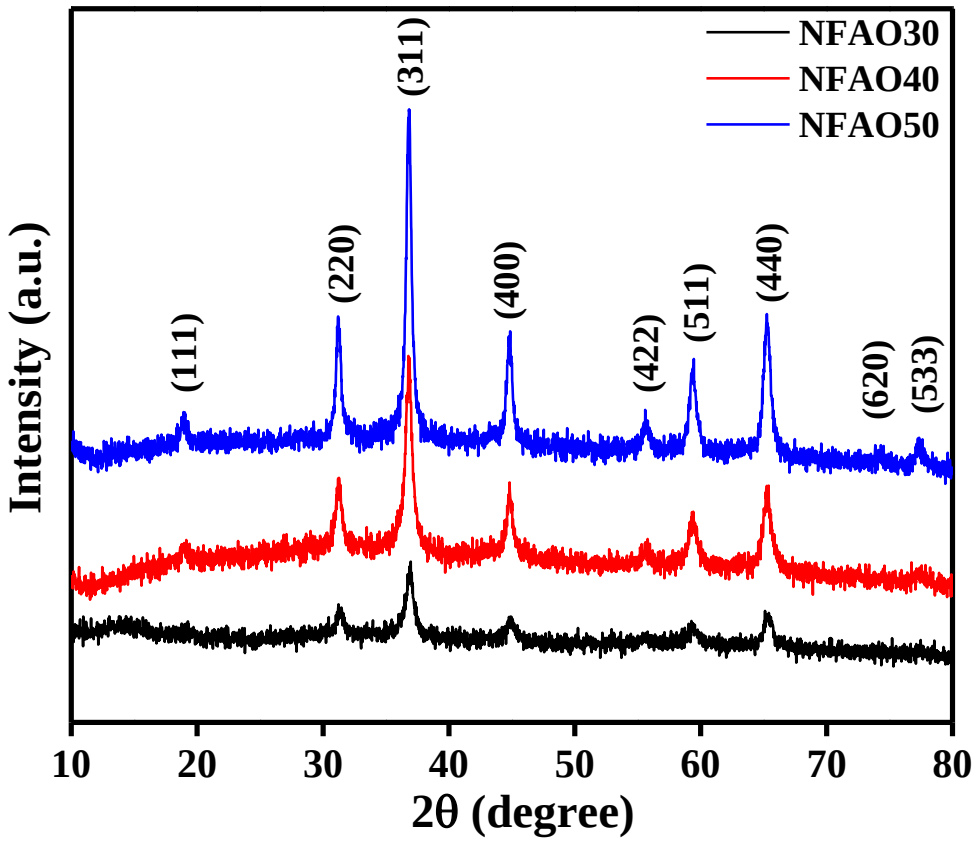

Figure 4.1. PXRD patterns of $Ni_xFe_{1-x}Al_2O_4$ (x= 0.3, 0.4 and 0.5), i.e., NFAOX, where X= 30, 40 and 50.

4.2.2. Screening of materials

Among the NFAOX materials, the highest Ni-doped sample NFAO50 was screened initially for 10 h at different temperatures, 650 °C to 800 °C, to determine the best temperature for DRM. The activity data is shown in **Figure 4.2**. The activity of the catalyst is already high at 700 °C when both CH_4 and CO_2 conversions reached about 85 % with H_2/CO ration more than 0.9. These findings led us to choose a mild temperature of 700 °C for subsequent studies.

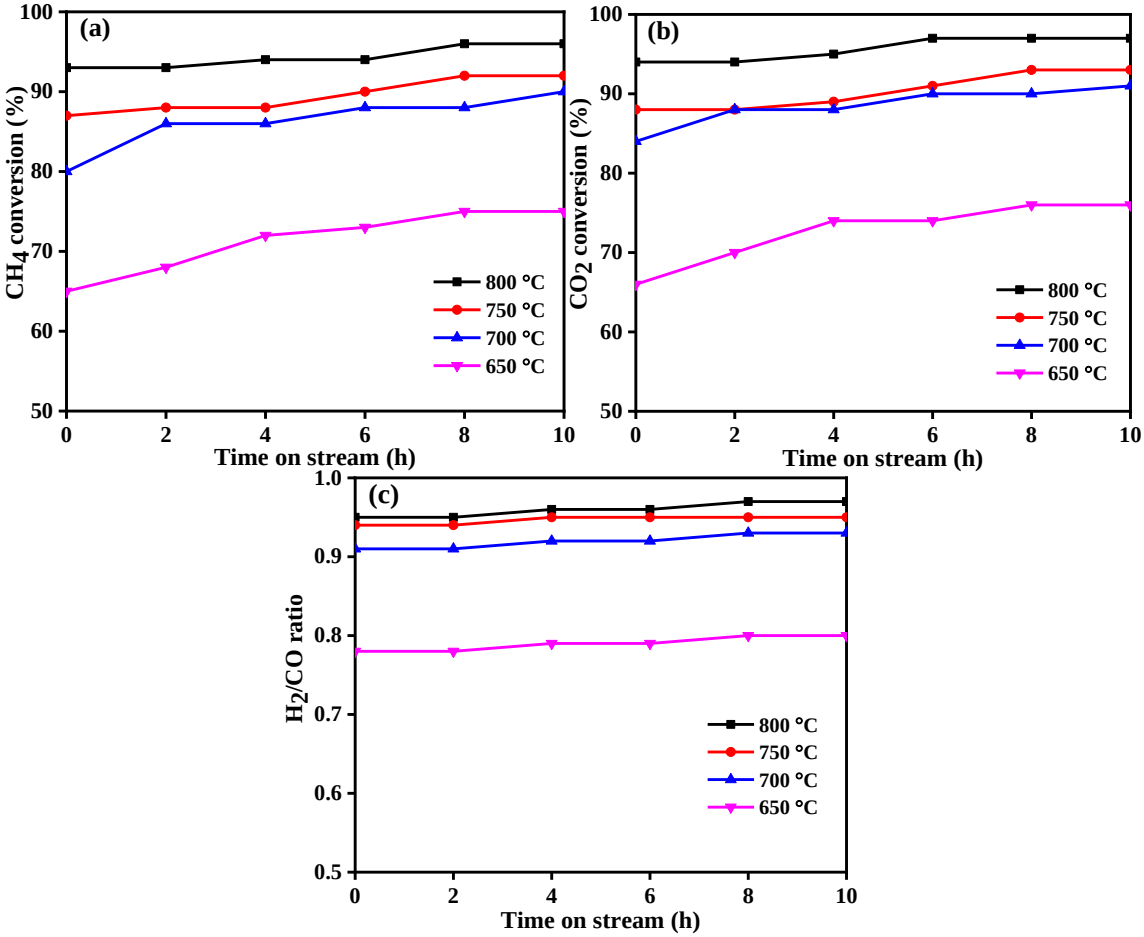

Figure 4.2. DRM activity behavior of NFAO50 in the temperatures range 650 °C to 800 °C (Other reaction conditions: 25 mL each of 10% CH_4 in Ar and 10% CO_2 in Ar and GHSV= 30000 mL g^{-1} h^{-1}).

Figure 4.3 shows the DRM activity behavior of all the NFAOX materials at 700 °C for 20 h of continuous run. The best performing catalyst was found to be NFAO50 that exhibits CH_4 and CO_2 conversions of 93 % and 95 %, respectively with H_2/CO ratio of 0.95, which is very close to the expected theoretical value of unity.

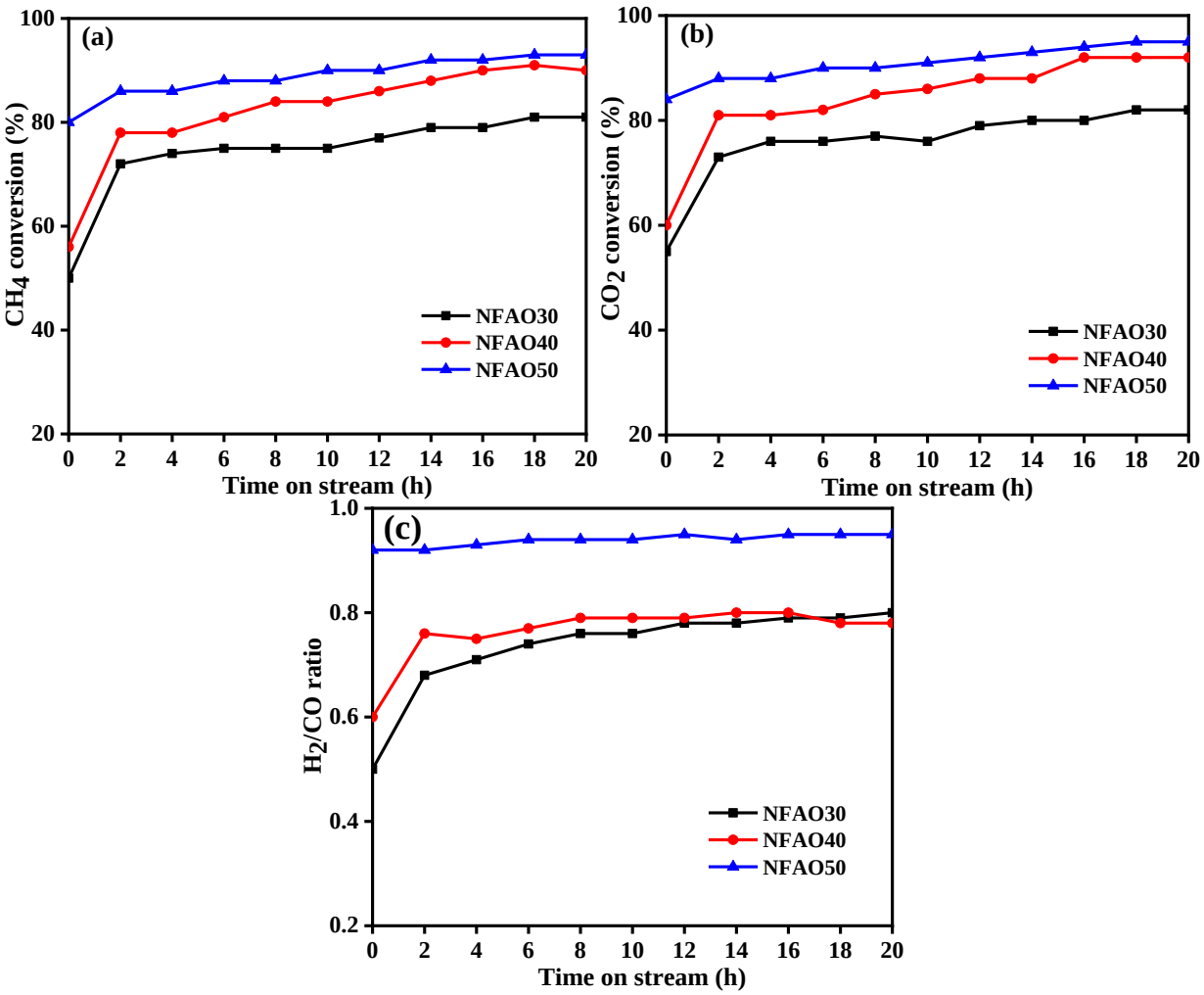

Figure 4.3. DRM activity behavior of NFAOX materials at 700 °C for 20 h (Other reaction conditions: 25 mL each of 10% CH_4 in Ar and 10% CO_2 in Ar and GHSV= 30000 mL g^{-1} h^{-1}).

4.2.3. Time on stream DRM behavior

The long term activity of the best catalyst NFAO50 has subsequently been performed for 50 h of continuous monitoring of CH_4 and CO_2 conversions and H_2/CO ratio at the reaction temperature of 700 °C. Remarkably, the CH_4 and CO_2 conversions were 96 % and 98 %, respectively and the H_2/CO ratio was determined to be 0.96.

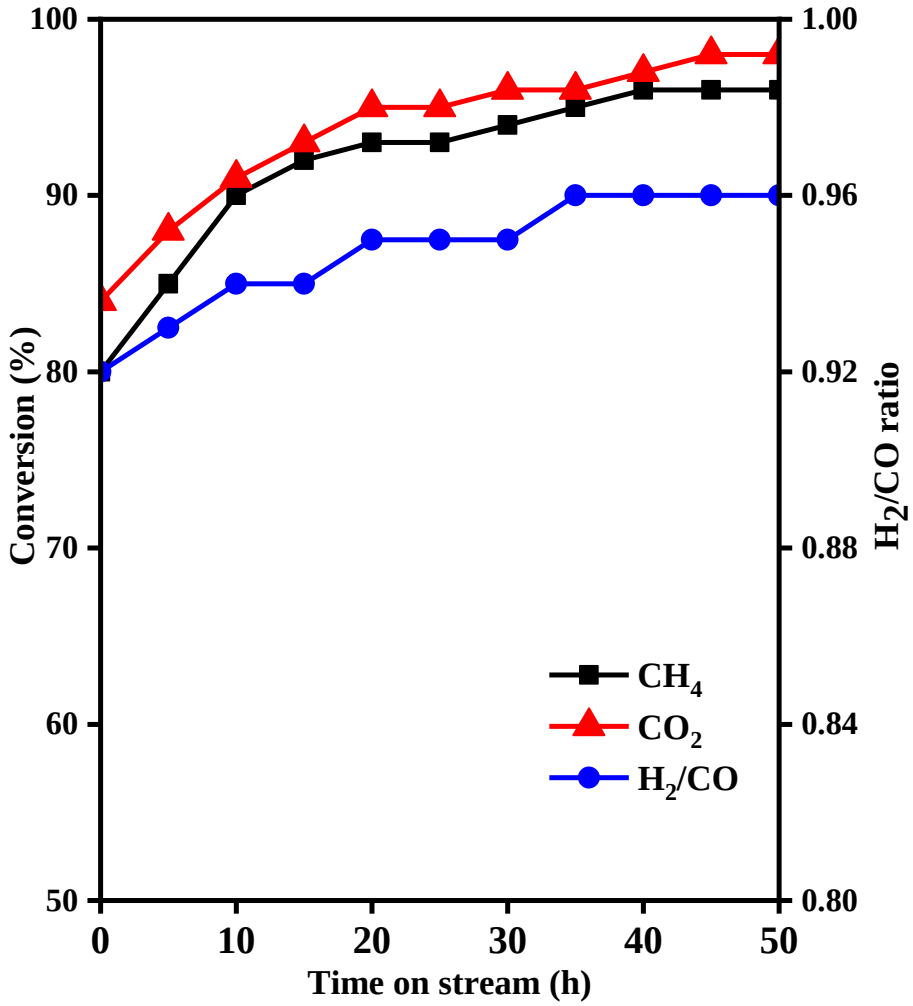

Figure 4.4. Time on stream DRM behavior of NFAO50 for 50 h at 700 °C (Other reaction conditions: 25 mL each of 10% CH_4 in Ar and 10% CO_2 in Ar and GHSV= 30000 mL g^{-1} h^{-1}).

4.2.4. PXRD analysis of aged catalysts: structure-activity correlation

The catalyst sample collected after 20 h and 50 h of continuous operation at 700 ℃ followed by cooling to room temperature in nitrogen flow has been termed as the corresponding aged catalyst. A systematic characterization of the aged forms of catalysts together with the corresponding as-prepared catalysts is needed to reveal the structure-activity correlation of the catalyst. Bulk phase analysis by PXRD study (see **Figure 4.5**)

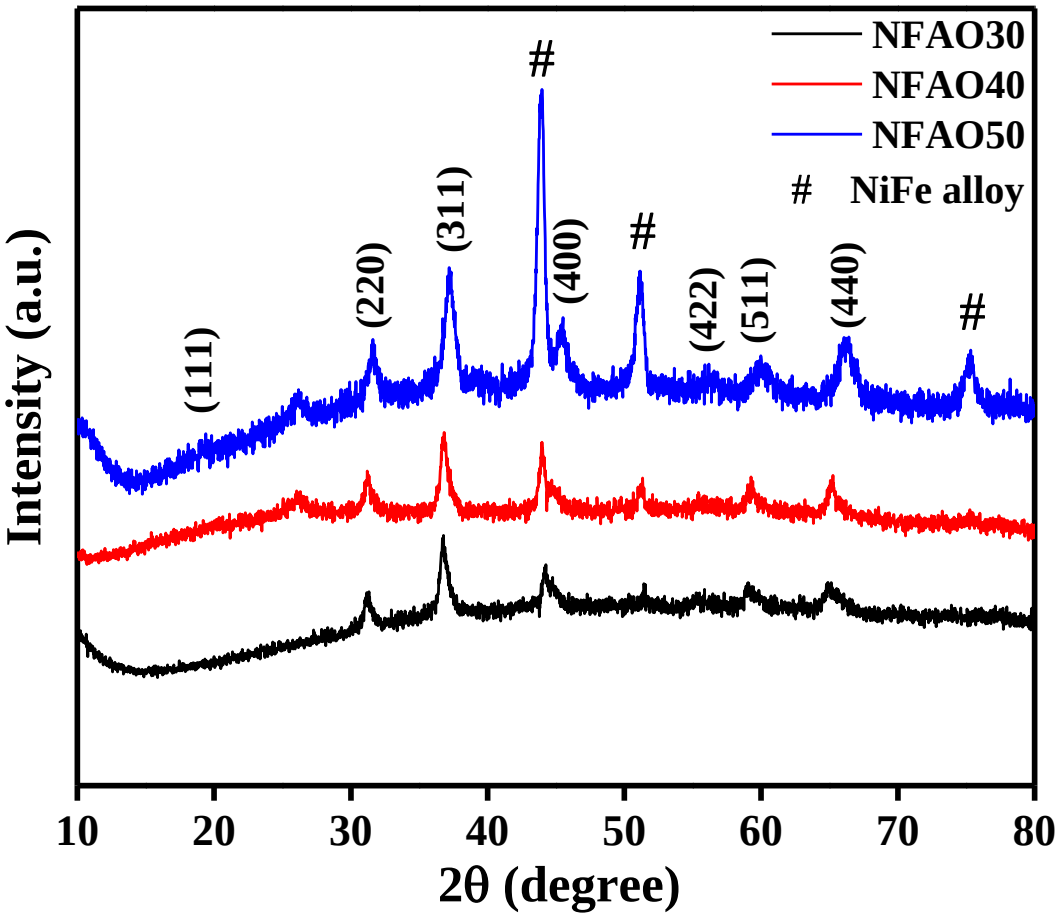

Figure 4.5. PXRD pattern of various $Ni_xFe_{1-x}Al_2O_4$ catalysts collected after 20 h of DRM along with NFAO50 collected after 50 h of DRM reaction.

reveals formation of alloy phase in all the three $Ni_xFe_{1-x}Al_2O_4$ (x= 0.3, 0.4 and 0.5) catalysts, irrespective of whether the ageing in the reforming atmosphere is carried out for 20 h or for 50 h. The diffraction peak due to alloy phase may be attributed to NiFe alloying in analogy with the findings of Ni and Cu co-doped hercynite catalyst discussed in detail in chapter 3. Thus, the present findings point again to "exsolution mediated *in situ* alloying" in Ni-doped hercynite system revealing the prospect of Ni-alloy based catalysts for moderate temperature dry reforming of methane, an industrially demanding reaction of renewed interest to materials community working on this area

4.3. Summary

In this work, we have shown the suitability of solution combustion method to produce Ni-doped hercynite spinel catalysts, where the dopant level has been increased up to 50 at.%. Of the three catalyst formulationss studied here, the NFAO50 is shown to be the most active formulation with significant DRM activity behavior at a moderate temperature of 700 °C and GHSV of 34000 mL g^{-1} h^{-1} without any appreciable loss of activity. The PXRD analysis again highlights a hercynite-based catalyst that offers *in situ* generated NiFe bimetallic alloy contributing to stable DRM activity with H_2/CO ratio close to the stoichiometric value. Thus, $Ni_xFe_{1-x}Al_2O_4$, more importantly NFAO50 performs the role of precursor for *in situ* generation of NiFe alloy particle, which plays the pivotal role in carrying out the reaction along with the hercynite phase. It may thus be proposed that modification of hercynite system, through appropriate tailoring of its chemical composition, is a fruitful ground for further studies. Microstructural analysis by HAADF-STEM coupled with EDS mapping, surface compositional analysis by XPS study along

with the findings on redox, surface acidity and basicity from H_2-TPR, CO-TPD, CO_2-TPD, analysis of carbon content by CHNS and TG-DTA analyses of aged as well as as-prepared catalysts in various environments are needed to understand relationship between structure and activity of the catalyst.

References

1. Bhattacharjee, M.; Bhunia, T.; Hossain, A.; Mandal, C. K.; Sinha, P. K.; Ghosh, S.; Bhaskaran, A.; Roy, S.; Show, B.; Seikh, Md. M.; Bera, P.; Gayen, A. Exsolution mediated *in situ* NiCuFe Alloying in Chemically Tailored Hercynite: A Key to Coke-Free Dry Reforming of Methane. *ACS Appl. Energy Mater*. **2025**, *8*, 10961−10973.

2. Yao, X.; Cheng, Q.; Attada, Y.; Ould-Chikh, S.; Ramírez, A.; Bai, X.; Mohamed, H. O.; Li, G.; Shterk, G.; Zheng, L.; Gascon, J.; Han, Y.; Bakr, O. M.; Castano, P. Atypical stability of exsolved Ni-Fe alloy nanoparticles on double layered perovskite for CO_2 dry reforming of methane. *Appl. Catal. B: Environ.* **2023**, *328*, 122479.

3. Li, Y.; Wang, Q.; Cao, M.; Li, S.; Song, Z.; Qiu, L.; Yu, F.; Li, R.; Yan, X. Structural evolution of robust Ni_3Fe_1 alloy on Al_2O_3 in dry reforming of methane: Effect of iron-surplus strategy from Ni_1Fe_1 to Ni_3Fe_1. *Appl. Catal. B: Environ.* **2023,** 331, 122669.

4. Shah, S.; Sayono, S.; Ynzunza, J.; Pan, R.; Xu, M.; Pan, X.; Gilliard-AbdulAziz, K. L. The effects of stoichiometry on the properties of exsolved Ni-Fe alloy nanoparticles for dry methane reforming. *AIChE J.* **2020**, *66*, e17078.

5. Olowoyo, J. O.; Sharifvaghef, S.; Zheng, Y. Syngas production via microwave-assisted Dry Reforming of Methane over NiFe/$MgAl_2O_4$ alloy catalyst. *CEP:PI*. **2024**, 203, 109899.

6. Song, Z.; Wang, Q.; Guo, C.; Li, S.; Yan, W.; Jiao, W.; Qiu, L.; Yan, X.; Li, R. Improved Effect of Fe on the Stable NiFe/Al_2O_3 Catalyst in Low Temperature Dry Reforming of Methane. *Ind. Eng. Chem. Res.* **2020**, 59, 17250-17258.

7. Motomura, A.; Nakaya, Y.; Sampson, C.; Higo, T.; Torimoto, M.; Tsuneki, H.; Furukawa, S.; Sekine, Y. Synergistic effects of Ni–Fe alloy catalysts on dry reforming of methane at low temperatures in an electric field. *RSC Adv.* **2022**, 12, 28359.

8. Xu, L.; Wen, H.; Jin, X.; Bing, Q.; Liu, J. DFT study on dry reforming of methane over Ni_2Fe overlayer of Ni (111) surface. *Appl. Surf. Sci.* **2018**, 443,515–524.

9. Manabayeva, M. A.; Mäki-Arvela, P.; Vajglová, Z.; Martinéz-Klimov, M.; Tirri, T.; Baizhumanova, T. S.; Grigor'eva, V. P.; Zhumabek, M.; Aubakirov, Y. A.; Simakova, I. L.; Murzin, D. Y.; Tungatarova, S. A. Dry Reforming of Methane over Ni-Fe-Al Catalysts Prepared by Solution Combustion Synthesis. *Ind. Eng. Chem. Res.* **2023**, *62*, 11439−11455.

10. Das, S.; Bhattar, S.; Liu, L.; Wang, Z.; Xi, S.; Spivey, J. J. Kawi , S. Effect of Partial Fe Substitution in La0.9Sr0.1NiO3 Perovskite-Derived Catalysts on the Reaction Mechanism of Methane Dry Reforming. *ACS Catal.* **2020**, *10*, 12466−12486.

11. Chen, X.; Zou, G.; Yuan, Y.; Xu, Z.; Zhao, H. Flame spray pyrolysis synthesized Ni-doped Fe/Ce oxygen carriers for chemical looping dry reforming of methane. *Fuel*, **2023**, 343, 127913.

12. Wan, C.; Song, K.; Pan, J.; Huang, M.; Luo, R.; Li, D.; Jiang, L. NieFe/Mg(Al)O alloy catalyst for carbon dioxide reforming of methane: Influence of reduction temperature and Ni-Fe alloying on coking. *Int. J. Hydrog. Energy*.**2020**, *45*, 33574-33585.

13. Alanazi, Y. M. Patel, N.; Fakeeha, A. H.; Abu-Dahrieh, J.; Ibrahim, A. A.; Abasaeed, A. E.; Kumar, R.; Al-Fatesh, A. Understanding Coke Deposition Vis-à-Vis DRM Activity over Magnesia-Alumina Supported Ni-Fe, Ni-Co, Ni-Ce, and Ni-Sr Catalysts. *Nanomaterials.* **2023**, *13*, 2874.

14. Margossian, T.; Larmier, K.; Kim, S.M.; Krumeich, F.; Müller, C.; Coperet, C. Supported Bimetallic NiFe Nanoparticles through Colloid Synthesis for Improved Dry Reforming Performance. *ACS Catal*. **2017**, *7*, 6942−6948.

15. Meng, Q.; Loughney, P. A.; Joshi, J.; Sunny, A. A.; Kumar, S.; Mohapatra, P.; Kane, A.; Qin, L.; Cheng, Z.; Fan, L. Enhancing dry reforming of methane with engineered SBA-15-supported Fe-Ni alloy nanoparticles for sustainable syngas production. J. of CO_2 Utili. **2024**, *81*,102717.

16. Ray, K.; Sengupta, S.; Deo, G. Reforming and cracking of CH_4 over Al_2O_3 supported Ni, Ni-Fe and Ni-Co catalysts. *Fuel Process. Technol*. **2017**, *156*, 195–203.

17. Dhillon, G. S.; Cao, G.; Yi, N. The Role of Fe in Ni-Fe/TiO_2 Catalysts for the Dry Reforming of Methane. Catal. **2023**, *13*, 1171.

18. Theofanidis, S. A.; Galvita, V. V.; Poelman, H.; Marin, G. B. Enhanced Carbon-Resistant Dry Reforming Fe-Ni Catalyst: Role of Fe. *ACS Catal.* **2015**, *5*, 3028−3039.

19. Theofanidis, S. A.; Galvita, V. V. Poelman, H.; Dharanipragada, N. V. R. A.; Longo, A.; Meledina, M.; Tendeloo, G. V.; e Detavernier, C.; Marin, G. B. Fe-Containing Magnesium Aluminate Support for Stability and Carbon Control during Methane Reforming. *ACS Catal.* **2018**, *8*, 5983−5995.

20. Zhang, T.; Liu, Z.; Zhu, Y.; Liu, Z.; Suia, Z.; Zhua, K.; Zhou, X. Dry reforming of methane on Ni-Fe-MgO catalysts: Influence of Fe on carbon-resistant property and kinetics. *Appl. Catal. B-Environ*. **2020**, *264*, 118497.

21. Kim, S. M.; Abdala, P. M.; Margossian, T.; Hosseini, D.; Foppa, L.; Armutlulu, A.; van Beek, W.; Comas-Vives, A.; Copéret, C.; Müller, C. Cooperativity and Dynamics Increase the Performance of NiFe Dry Reforming Catalysts. *J. Am. Chem. Soc.* **2017**, 139, 1937−1949.

22. Theofanidis, S. A.; Galvita, V. V.; Sabbe, M.; Poelman, H.; Detavernier, C.; Marin, G. B. Controlling the Stability of a Fe−Ni Reforming Catalyst: Structural Organization of the Active Components. *Appl. Catal. B: Environ.* **2017**, *209*, 405−416.

23. Li, L.; Qiu, J.; Bian, Z.; Shao, B.; Liu, Z.; Lian, C.; Liu, H.; Hu, J. Breaking trade-off between catalytic activity and carbon deposit by tailoring d-band center of NiFe alloy for dry reforming of carbonate. *Appl. Catal. B: Environ*. 2025, 368, 125114.

24. Shah, S.; Hong, J.; Cruz, L.; Wasantwisut, S.; Bare, S. R.; Gilliard-AbdulAziz, K. L. Dynamic Tracking of NiFe Smart Catalysts using In Situ X-Ray Absorption Spectroscopy for the Dry Methane Reforming Reaction. *ACS Catal.* **2023**, *13*, 3990−4002.

25. Joo, S.; Seong, A.; Kwon, O.; Kim, K.; Lee. J. H.; Gorte, R. J.; Vohs, J. M.; Han, J. W. Kim, G. Highly active dry methane reforming catalysts with boosted in situ grown Ni-Fe nanoparticles on perovskite via atomic layer deposition. *Sci. Adv*. **2020**, *6*, eabb1573.

26. Hallassi, M.; Benrabaa, R.; Cherif, N. F.; Lerari, D.; Chebout, R.; Bachari, K.; Rubbens, A.; Roussel, P.; Vannier, R.; Trentesaux, M.; Löfberg, A. Characterization and Syngas Production at Low Temperature via Dry Reforming of Methane over Ni-M (M = Fe, Cr) Catalysts Tailored from LDH Structure. *Catal.* **2022**, *12*, 1507.

27. Song, Z.; Wang, Q.; Guo, C.; Li, S.; Yan, W.; Jiao, W.; Qiu, L.; Yan, X.; Li, R. Improved Effect of Fe on the Stable NiFe/Al_2O_3 Catalyst in Low Temperature Dry Reforming of Methane. *Ind. Eng. Chem. Res*. **2020**, *59*, 17250−17258.

Chapter 5

Studies on the DRM behavior of combustion made $(NiCuCoMn)_xFe_{1-x}Al_2O_4$

5.1. Introduction

It has already been discussed in the chapter 1 that design and development of Ni-based catalyst is a requisite for realistic DRM process and alloying is one of the promising techniques ever explored. As mentioned in chapter 3, some chemical tailoring have been done in hercynite for DRM process and have arrived in a scenario that the dopants (Cu and Ni) along with a certain portion of host Fe in hercynite are co-exsolved in the DRM medium and NiCuFe ternary alloy is formed which actually carry out the reaction for prolonged duration. This finding explores that hercynite may have the required potential of providing Ni-based alloy through co-exsolution in the DRM reaction medium and for further confirmation we have deliberately used Ni-doped hercynite toward DRM reaction in more demanding situation and got the same result of NiFe alloying, as discussed in chapter 4. Hence, based on our findings on hercynite engineering for DRM, it may be inferred that hercynite can be considered as a precursor for producing multicomponent alloy of Ni through *in situ* co-exsolution by incorporating different transition metals (including Ni) in 'Fe'/'A' site of the spinel lattice. Except a very few high entropy alloys (HEAs), multmetalic alloys of random compositions and oxide precursors of multimetalic

alloys there are a handful of reports available by far in the literature regarding the methane dry reforming process.[1-12]

Herein, we have rationally chosen four different transition metals viz., Ni, Cu, Co and Mn as dopant for Fe in hercynite, with the general formula $(NiCuCoMn)_xFe_{1-x}Al_2O_4$ (where, x= 0.2 and 0.4), and synthesized the multimetal ion doped system following the facile SCS route in order to check the structural flexibility of hercynite to incorporate several metal ions, although our primary aim of doping was to ensure the formation of Ni-based multimetal alloy in the DRM environment, the theme of this research work.

5.2. Results and Discussion

5.2.1. Powder XRD studies

The powder XRD patterns of Ni, Cu, Co, Mn doped $FeAl_2O_4$ catalysts, $(NiCuCoMn)_{0.2}Fe_{0.8}Al_2O_4$ and $(NiCuCoMn)_{0.4}Fe_{0.6}Al_2O_4$, are shown in **Figure 5.1**. Formation of the pure hercynite spinel phase is clearly evident from the well matched diffraction peaks of JCPDS PDF# 34-0192. No noticeable peak(s) of oxides of individual metals could be identified in the PXRD pattern, which point to successful doping of Ni, Cu, Co, Mn in hercynite. The crystallite size of the as-prepared sample falls in the range 15-20 nm as obtained from Scherrer's equation representing nano-dimensional nature of the synthesized materials.

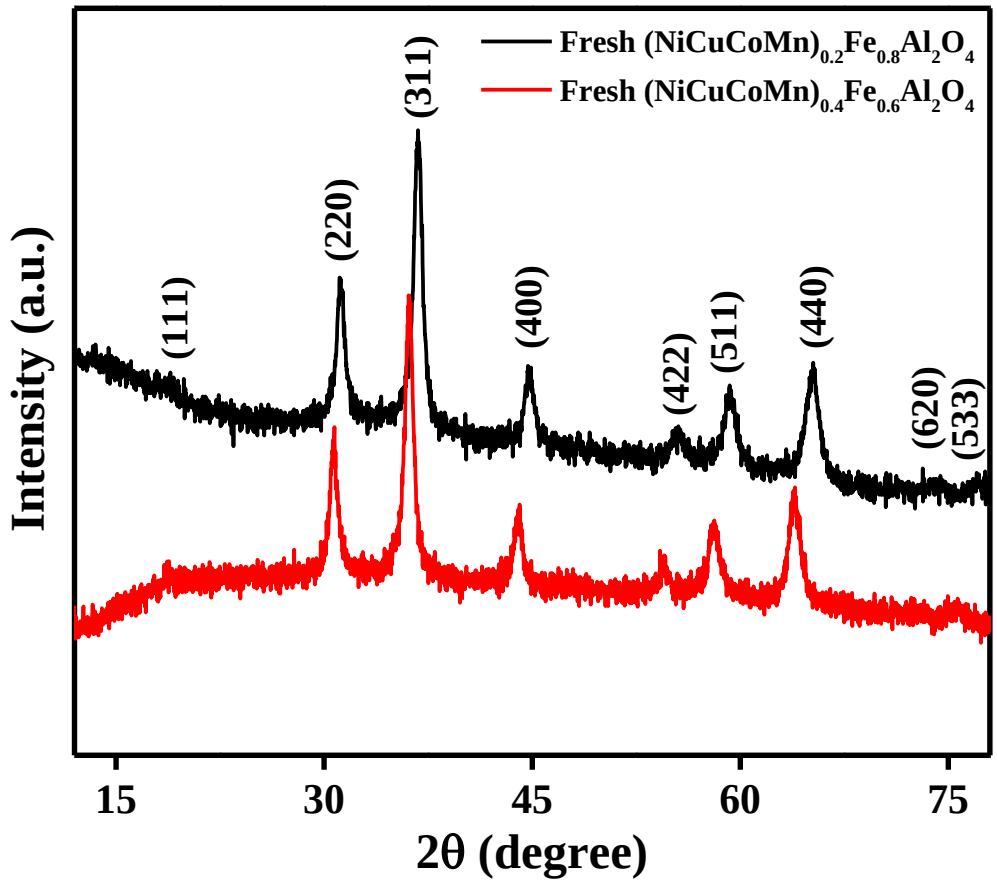

Figure 5.1. PXRD patterns of $(NiCuCoMn)_xFe_{1-x}Al_2O_4$ (where, x= 0.2 and 0.4).

5.2.2. Screening of materials

The $(NiCuCoMn)_xFe_{1-x}Al_2O_4$ (where x= 0.2 and 0.4) materials were screened initially for 20 h at 800 °C, to determine the most active catalyst for DRM. The activity behavior of all the materials is shown in **Figure 5.2**. The most active catalyst is found to be $(NiCuCoMn)_{0.4}Fe_{0.6}Al_2O_4$ that shows CH_4 and CO_2 conversions of 93 % and 95 %, respectively with H_2/CO ratio of 0.96, which is very nearer to the expected theoretical value of unity and suggests negligible contribution from the side reactions.

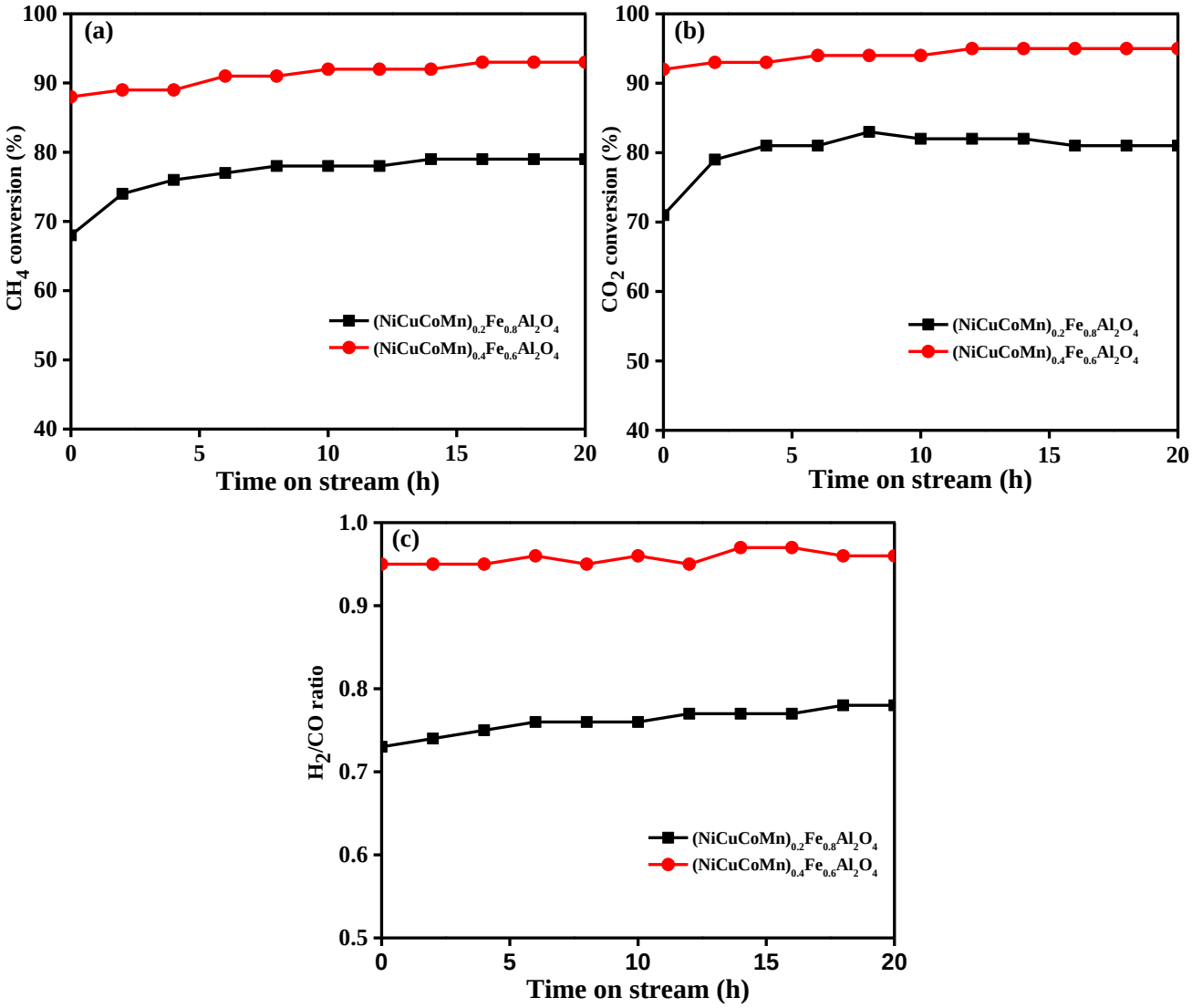

Figure 5.2. DRM activity behavior of $(NiCuCoMn)_xFe_{1-x}Al_2O_4$ (where, x= 0.2 and 0.4) materials at 800 °C for 20 h (Other reaction conditions: 25 mL each of 10% CH_4 in Ar and 10% CO_2 in Ar and GHSV= 30000 mL g^{-1} h^{-1}).

5.2.3. PXRD analysis of aged catalysts: structure-activity correlation

The catalyst samples collected after 20 h of continuous operation at 800 °C followed by cooling to room temperature in nitrogen flow has been termed as the corresponding aged catalyst. A systematic characterization of the aged catalysts together with the

corresponding as-prepared catalysts is needed to shed light on the structure-activity correlation of the catalyst. Bulk phase analysis through PXRD (see **Figure 5.3**) reveals formation of alloy phase in both the $(NiCuCoMn)_{0.2}Fe_{0.8}Al_2O_4$ and $(NiCuCoMn)_{0.4}Fe_{0.6}Al_2O_4$ catalysts upon 20 h aging. The diffraction peak due to alloy may be attributed to NiCuCoMnFe quinary alloying in analogy with the findings of Ni and Cu co-doped hercynite catalyst discussed in detail in chapter 3. Thus, the bulk phase analysis on multimetal (Ni, Cu, Co, and Mn) doped hercynite system again point to "exsolution mediated *in situ* alloying" in the hercynite-based catalyst and hence revealing the prospect of NiCuCoMn alloy based catalysts for moderate temperature dry reforming of methane.

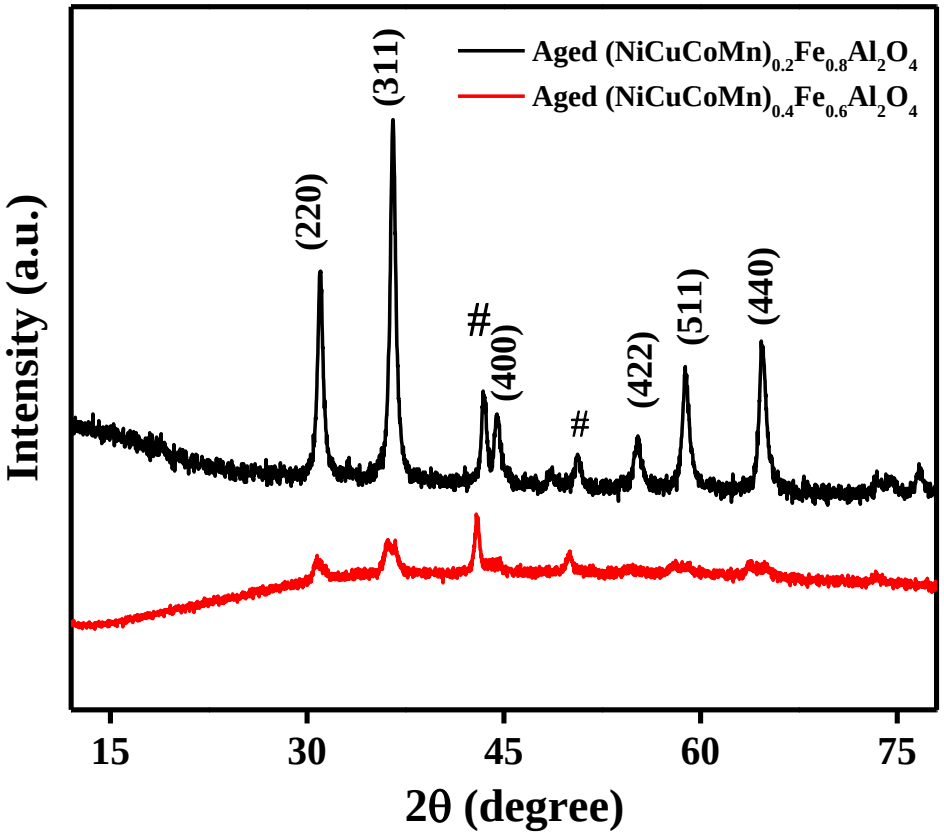

Figure 5.3. PXRD patterns of $(NiCuCoMn)_xFe_{1-x}Al_2O_4$ (where, x= 0.2 and 0.4) catalysts collected after 20 h of DRM reaction.

5.3. Summary

Due to the regulation of structure–activity relationship among various active metals along with Ni, the proposed catalysts portray synergistic effects within a single catalytic framework, which can suppress the amount of carbon deposition and maintain stable conversion during a 20 h of continuous TOS activity. Moreover, the diffraction patterns of the aged catalysts contain an apparent signature of alloying which can be tentatively ascribed to the formation of NiCuCoMnFe quinary alloy ensuring again the phenomenon of "exsolution mediated *in situ* alloying" though further confirmation is necessary to visualize the exact composition of the alloy formed *in situ* in the reforming environment. Detailed microstructural analysis especially, HAADF-STEM coupled with EDS mapping together with surface compositional analysis by XPS and other findings from H_2-TPR, CO-TPD, CO_2-TPD, CHNS and TG-DTA analyses will be more helpful to establish the structure-activity correlation in the complicated multimetal alloy based hercynite catalyst of this study.

References

1. Bhattacharjee, M.; Bhunia, T.; Hossain, A.; Mandal, C. K.; Sinha, P. K.; Ghosh, S.; Bhaskaran, A.; Roy, S.; Show, B.; Seikh, Md. M.; Bera, P.; Gayen, A. Exsolution mediated *in situ* NiCuFe Alloying in Chemically Tailored Hercynite: A Key to Coke-Free Dry Reforming of Methane. *ACS Appl. Energy Mater.* **2025**, *8*, 10961−10973.

2. Liu, K.; Xing, F.; Xiao, Y.; Yan, N.; Shimizu, K.; Furukawa, S. Development of a Highly Stable Ternary Alloy Catalyst for Dry Reforming of Methane. *ACS Catal.* **2023**, *13*, 3541-3548.

3. Shao, Y.; Wu, C.; Xi, S.; Tan, P.; Wu, X.; Saqline, S.; Liu, W. Halite-structured $(MgCoNiMnFe)O_x$ high entropy oxide (HEO) for chemical looping dry reforming of methane. *Appl. Catal. B-Environ.* **2024**, *355*, 124191.

4. Gangwar, B. P.; Tripathi, P.; Das, R.; Sarkar, S.; Singh A. K.; Tiwary, C. S.; Sharma, S. Low-temperature dry reforming using high entropy alloy (Co-Fe-Ga-Ni-Zn)-cerium oxide (CeO2) hybrid nanostructure. *Chem. Eng. J.* **2024**, *495*, 153291.

5. Guo, C.; Zhang, W.; Du, X.; Yu, Y.; Peng, X.; Wu, Y.; Li, J.; Kong, T.; Xiong, Y. Strong Metal−Support Interaction between Layered Double Oxides and High-Entropy Alloys for the Efcient Light-Driven Dry Reforming of Methane. *ACS Materials Lett.* **2025**, *7*, 1336-1343.

6. Riley, C.; Burnside, B.; Alcala, R.; Valdez, N.; Porter, S.; Huang, W.; Riva, A. D. L.; Salinas, P.; Grant, R.; Rodriguez, M.; Miller, J.; Datye, A. Structurally Regenerable High Entropy Aluminate Spinel Catalysts for Dry Reforming of Methane. *ChemCatChem.* **2025**, *17*, e202401949.

7. Utilization of High Entropy Alloy (Co–Cu–Fe–Mn–Ni) and Support (CeO2) Interaction for CO2 Conversion into Syngas. *Adv. Sustainable Syst.* **2024**, *8*, 2400219.

8. Enhancing Thermocatalytic Activities by Upshifting the d-Band Center of Exsolved Co-Ni-Fe Ternary Alloy Nanoparticles for the Dry Reforming of Methane. *Angew. Chem. Int. Ed.* **2021**, *60*, 15912–15919.

9. Exsolution of Embedded Ni−Fe−Co Nanoparticles: Implications for Dry Reforming of Methane. *ACS Appl. Nano Mater.* **2021**, *4*, 8626−8636.

10. Complex Alloy and Heterostructure Nanoparticles Derived from Perovskite Oxide Precursors for Catalytic Dry Methane Reforming. *ACS Appl. Nano Mater*. **2022**, *5*, 17476−17481.

11. Co-Exsolution of Ni-Based Alloy Catalysts for the Valorization of Carbon Dioxide and Methane. Acc. Chem. Res. **2023**, *56*, 3132−3141.

12. Ma, X.; Yang, W.; Tang, X.; He, Y. Efficient catalysis and products regulation of methane dry reforming under mild temperature conditions using novel high-entropy catalyst. *Fuel.* **2024**, *372*, 132263.

Chapter 6

Exsolution-mediated *in situ* alloying: key findings and future outlook

6.1. Introduction

Hercynite-based materials are one among the most explored oxide materials in recent times in various aspects. These are routinely employed for various purposes including mitigation of some prevailing global issues like sustainable energy production through reforming, water treatment, magnetic study, transformation of small organic molecules etc. Brief literature survey and our expertise of dealing hercynite over a decade lead to conclude us that hercynite (iron aluminate) has a prolific nature with the flexibility of incorporating several transition metals in the spinel framework to be employed in different catalytic purposes with specific interest in gas-solid heterogeneous catalysis. Additionally, solution combustion synthesis has been chosen for several reasons including the scope of screening several metal ion-doped compositions in minutes.

6.2. General findings on exsolution-mediated in situ alloying

In chapter 1, we have discussed the relevance of DRM in modern era with its limiting issues, the frequently used state-of-the-art catalysts along with their limitation, role of Ni as a viable substitute and the hurdle behind its successful commercialization, rational design of Ni-based catalysts and significance of Ni-transition metal alloying in DRM. In

this context, the objective of choosing hercynite for compositional engineering through SCS method has been rationally demonstrated.

Chapter 2 deals with the details of the methodologies adopted for the preparation of the materials studied, the details of fabricated reaction set-up used for catalytic evaluation and the varieties of sophisticated instrumental techniques accessed for the characterization of the materials before and after catalysis for drawing structure-property relationship in a conclusive manner.

It is always desirable to get a common recipe for the development of any particular material or process. Herein, three consecutive chapters are focused on developing a protocol for a sustainable DRM process taking hercynite as a model system for engineering.

Our primary aim in chapter 3 was to develop a synthetic strategy alongside its applicability towards high temperature DRM reaction. Herein, we developed general synthesis scheme using facile SCS route operating at a temperature of 350 °C in a preheated furnace using ODH as a fuel for the preparation of Ni and Cu co-doped hercynites with general formula $Ni_xCu_{0.07}F_{0.93-x}Al_2O_4$ (x= 0-0.1 and named as NCFAOX, where X= at.% of doped Ni). Among them, NCFAO8 shows highly promising activity in DRM reaction at 800 °C at a GHSV of 34000 mL g^{-1} h^{-1}. Subsequently, thorough characterization of the as-prepared vs. aged materials, especially the microstructural analysis and chemical analysis, have revealed the coke-free nature of the reaction enabled by *in situ* formed NiCuFe ternary alloy. Here, hercynite becomes a precursor for producing Ni-alloy *in situ*. The true potential of the catalysts is envisaged through

screening at varying GHSVs over various operating temperatures of DRM especially at the coke prone zone.

The evaluation of DRM behavior of Ni-only (without Cu-doping) hercynite with the expectation of *in situ* NiFe alloying actually forms the basis of chapter 4. In addition to this finding, the diminished performance of the catalysts at lower temperatures and at higher GHSVs (i.e., in more demanding situation) also insisted us for further tailoring of hercynite in order to apply in more demanding situations. In chapter 4, we have synthesized Ni-doped hercynite with the general formula $Ni_xF_{1-x}Al_2O_4$ (x= 0.3-0.5) using the very same strategy where we have gone for higher amount of Ni incorporation in hercynite framework using the SCS strategy and subsequently screened the materials in moderate temperature DRM with higher feed gas concentrations to attain the more demanding situation. The series of materials that are screened at 700 °C were found to exhibit superior DRM activity. Diffraction studies done after catalysis, have confirmed the presence of NiFe alloy in all the aged catalysts confirming the formation of *in situ* alloy in tailored hercynite. Among the samples, $Ni_{0.5}F_{0.5}Al_2O_4$ has been selectively chosen for 50 h time-on-stream activity test. The formation of *in situ* alloy through co-exsolution in engineered hercynite is indeed a confirmation of the capability of hercynite as a precursor for *in situ* alloying.

The very pertinent query in this research work, i.e., whether hercynite can be considered as a viable contender for 'exsolution mediated *in situ* alloying', it is necessary to guarantee formation of alloy by incorporating several transition metals into hercynite so as to make a promising catalyst for DRM. This actually initiates the foundation of chapter 5. In chapter 5, we have reported the effects of simultaneous doping of four numbers of

first row transition metals, including Ni and Cu, in the hercynite and its expected activity behavior in DRM. IN this preliminary work, we have underscored the potential performance of hercynite upon multimetal incorporation. The general formula of the materials are $(NiCuCoMn)_xFe_{1-4x}Al_2O_4$ (where, x=0.05-0.10). As expected, the multimetal doped hercynite is also found to be very good performer in DRM. The diffraction pattern of the 20 h aged sample has confirmed the signature of alloying, which is in line with the prediction of 'exsolution mediated in situ alloying' in the iron alumina spinel, i.e., hercynite.

6.3. Comparison of hercynite-based catalysts with other Ni-based DRM catalysts

It is a difficult task to compare the different types of catalysts due to variations in the synthetic protocol, differences in the conditions employed for dry reforming, different duration of the stability test, *ex situ* (as in the previously reported catalysts) versus *in situ* alloying (as we have shown in the works embodied in this thesis) and others. However, we have made an attempt to make a healthy comparison of the already reported state-of-the-art Ni and Ni-alloy based DRM catalysts with the NCFAO8 catalyst of chapter 3 as provided in Table 6.1, which gives a further insight about the true potential of the hercynite-engineered catalyst.

Table 6.1. Comparison of hercynite-based catalyst NCFAO8 with other state-of-the-art Ni and Ni-alloy based DRM catalysts

Catalyst composition	**Method of synthesis**	**Active component**	**GHSV/ WHSV**	**Operating temperature (°C)**	**Alloying technique**	**CH_4 conv. (%)**	**CO_2 conv. (%)**	**H_2/CO ratio**	**Durability (h)**	**Amount of deposited coke**	**Nature of deposited coke**	**Ref.**
Ni/Al_2O_3	Spray pyrolysis-assisted evaporation-induced self-assembly (EISA)	Ni	24000 mL g^{-1} h^{-1}	800 °C	-	92	97	0.97	30	0.277 mmol/g_{cat}	Amorphous, filamentous and inactive graphitic	1
Ni/Al_2O_3	microwave-assisted combustion followed by wet impregnation		72000 mL g^{-1} h^{-1}	700 °C	-	87-72	87-72	1.09	20	13.2%	Filaments (whiskers)	2
6Ni6CuMgAlO-S	hydrothermal crystallization followed by calcination	NiCu alloy	40,000 mL g^{-1} h^{-1}	700 °C	H_2 reduction	85	90	0.96	70	2.7 %	Mainly amorphous	3
$Cu–Ni@SiO_2$	Microemulsion followed by polymerization of TEOS		80000 h^{-1}	700 °C	H_2 reduction	75	…	0.8-0.9	16	-	-	4
$Ni1Fe1/Al_2O_3$ and $Ni3Fe1/Al_2O_3$	Evaporation-induced self-assembly method	NiFe alloy	60000 mL g^{-1} h^{-1}	600 °C	H_2 reduction	28 and 18	40 and 30	0.6 and 0.5	50	9.1 % and 32.1%	Mainly graphitic	5
$Ni_3Fe_1Cu_1$-$Mg_xAl_yO_z$	Co-precipitation followed by calcination	NiCuFe alloy	120000 mL g^{-1} h^{-1}	650 °C	H_2 reduction	27	32	0.6	20	5.4 %	-	6
NCFAO8 ($Ni_{0.08}C_{0.07}F_{0.85}$ Al_2O_4)	Solution combustion synthesis	NiCuFe alloy	34200	800 °C 750 °C	*in situ* exsolution	97 78	99 84	0.8 0.74	100 100	Apparently coke free	-	7

6.4. Conclusive remarks

In a nutshell, following conclusive remarks may be made based on the overall findings:

- Hercynite engineering through Ni, Cu co-doping, Ni-doping and multimetal doping for DRM is indeed very effective and interesting from structural as well as catalytic perspective.
- Additionally, this report highlights a series of hercynite-based catalysts that are capable of offering *in situ* generated Ni-based multicomponent alloy through co-exsolution, introducing a promising approach towards sustainable DRM.
- In particular, chemically tailored hercynites act as the precursor for Ni-based multimetallic alloying, the main carrier of the reaction along with γ-Al_2O_3 and hercynite.
- The improvisation of the active metal(s) and support occur simultaneously during the reaction and may be projected as a suitable contender for industrialization of the currently immature DRM technique.
- The generalized idea of "exsolution mediated *in situ* alloying" can be further employed for mixed metal oxide systems, other than hercynite not only for DRM, but for other heterogeneous catalytic applications.

6.5. Future directions

The present endeavor has led to reach at definitive conclusions as pointed out above. Yet, there are several pertinent issues that are to be addressed in the near future. Some of these may be summarized under the following heads:

- More numbers of catalyst compositions are to be made, specifically in reference to multimetal doped hercynite system. High entropy alloy based catalyst may be considered as a promising contender.
- Exhaustive catalytic tests are to be carried out under various conditions of temperature, GHSVs to conclusively reach at the robust nature of the catalysts. Investigating the kinetic aspects of the reaction will form another integral component in optimizing the catalyst materials.
- Exhaustive characterization of as-prepared vis-à-vis aged catalysts by some high end sophisticated instrumental facilities like HAADF STEM are needed to be carried out to understand the microstructure and to confirm the formation of alloy.
- Surface compositional analysis of as-prepared and aged catalysts by XPS will be needed to understand the various surface species and ther role in catalytic process.
- Chemisorption methods including H_2-TPR, O_2-TPO, CO-TPD, CO_2-TPD will strengthen the understanding of redox behavior along with surface acidity-basicity properties of the materials that will eventually help to tune the material property as per the requirement.
- ICP-AES analysis is needed to have quantitative information of the materials, while CHNS will provide carbon content in the as-prepared as well as the aged form of the catalysts. Role of C present inherently in the catalyst sample needs to be given due importance in the overall assessment of the catalytic property.
- TG-DTA analyses in inert as well as in oxidative and reductive environments will shed more insights about alloy formation and the consequences.

- A few cutting edge technologies like mechanistic study by *in situ* DRIFTS (diffuse reflectance infrared Fourier transform spectroscopy) will be helpful to give a better insight about the structure-property relationship in the complicated multimetal alloy based hercynite catalyst materials of this study.
- The residual carbon present inherently in the SCS made hercynites demands additional investigations to draw any inference whether they have any promotional effect through active participation in catalytic cycle or not.[8]
- Moreover, a trace amount of amorphous C present in the 100 h aged catalyst needs a justification about its source, whether it is coming from the initially present residual C or being deposited during the operating conditions of DRM. Isotopically labeled gases such as $^{13}CH_4$ and $^{13}CO_2$ may possibly be employed to track the origins of C in the aged sample.
- Finally, an initiative is to be taken about the applicability of the catalysts in other versions of the DRM like photo-assisted DRM etc.

References

1. Seo, J.; Kim, H.; Lee, Y.; Nam, S.; Roh, H.; Lee, K.; Park, S. B. One-Pot Synthesis of Full-Featured Mesoporous Ni/Al_2O_3 Catalysts via a Spray Pyrolysis-Assisted Evaporation-Induced Self-Assembly Method for Dry Reforming of Methane. *ACS Sustainable Chem. Eng.* **2021**, *9*, 894−904.

2. Maziviero , F. V.; Medeiros, R.; Melo , D.; Macedo, H. P; Oliveira, A.; Araújo, T. R. Synthesis of alumina by microwave-assisted combustion method using low fuel content

and its use as catalytic support for dry reforming of methane. *Mater. Chem. Phys.* **2021** *264*, 124408.

3. Xiao, Z.; Hou, F.; Zhang, J.; Zheng, Q.; Xu, J.; Pan, L.; Wang, L.; Zou, J.; Zhang, X.; Li, G. Methane Dry Reforming by Ni−Cu Nanoalloys Anchored on Periclase-Phase $MgAlO_x$ Nanosheets for Enhanced Syngas Production. *ACS Appl. Mater. Interfaces* **2021**, *13*, 48838−48854.

4. Wu, T.; Cai, W.; Zhang, P.; Song, X.; Gao, L. Cu–Ni@SiO_2 alloy nanocomposites for methane dry reforming catalysis. *RSC Adv.*, **2013**, *3*, 23976.

5. Li, Y.; Wang, Q.; Cao, M.; Li, S.; Song, Z.; Qiu, L.; Yu, F.; Li, R.; Yan, X. Structural evolution of robust Ni_3Fe_1 alloy on Al_2O_3 in dry reforming of methane: Effect of iron-surplus strategy from Ni_1Fe_1 to Ni_3Fe_1. *Appl. Catal. B: Environ.* **2023**, *331*, 122669.

6. Jin, F.; Fu, Y.; Kong, W.; Wang, J.; Cai, F.; Zhang, J.; Xu, J. Dry reforming of methane over trimetallic NiFeCu alloy catalysts. *Chem. Phys. Lett.* **2020**, *750*, 137491.

7. Bhattacharjee, M.; Bhunia, T.; Hossain, A.; Mandal, C. K.; Sinha, P. K.; Ghosh, S.; Bhaskaran, A.; Roy, S.; Show, B.; Seikh, Md. M.; Bera, P.; Gayen, A. Exsolution mediated *in situ* NiCuFe Alloying in Chemically Tailored Hercynite: A Key to Coke-Free Dry Reforming of Methane. *ACS Appl. Energy Mater*. **2025**, *8*, 10961−10973.

8. Jiménez, J. D.; Lustemberg, P. G. Danielis, M.; Fernández-Villanueva, E.; Hwang, S.; Waluyo, I.; Hunt, A.; Wierzbicki, D.; Zhang, J.; Qi, L.; Trovarelli, A.;. Rodriguez, J. A.; Colussi, S.; Ganduglia-Pirovano, M. V.; Senanayake, S. D. *From Methane to Methanol: Pd-iC-CeO2 Catalysts Engineered for High Selectivity via Mechanochemical Synthesis. J. Am. Chem. Soc.* **2024**, *146*, 25986−25999.

List of publications

1. **Bhattacharjee, M.**; Bhunia, T.; Hossain, A.; Mandal, C. K.; Sinha, P. K.; Ghosh, S.; Bhaskaran, A.; Roy, S.; Show, B.; Seikh, Md. M.; Bera, P.; Gayen, A. Exsolution mediated *in situ* NiCuFe Alloying in Chemically Tailored Hercynite: A Key to Coke-Free Dry Reforming of Methane. *ACS Appl. Energy Mater*. **2025**, *8*, 10961−10973.

2. Hossain, A.; **Bhattacharjee, M.**; Ghorai, K.; Llorca, J.; Vasundhara, M.; Roy, S.; Bera, P.; Seikh, M. M.; Gayen, A. High activity in the dry reforming of methane using a thermally switchable double perovskite and in situ generated molecular level nanocomposite. *Phys. Chem. Chem. Phys*. **2024**, *26*, 5447-5465.

3. Ghorai, K.; Panda, A.; Hossain, A.; **Bhattacharjee, M.**; Chakraborty, M.; Bhattacharya, S. K.; Show, B.; Sarkar, A.; Bera, P.; Kim, H.; Seikh, M. M.; Gayen, A. $LaNiO_3$/g-C_3N_4 nanocomposite: An efficient Z-scheme photocatalyst for wastewater treatment using direct sunlight. *J. Rare Earths*. **2022**, *40*, 725-736.

4. Ghorai, K.; **Bhattacharjee, M.**; Mandal, D.; Hossain, A.; Bhunia, T.; Das, M.; Ray, P. P.; Show, B.; Bera, P.; Mandal, T. K.; Seikh, M. M.; Gayen, A. Facile synthesis of $CuCr_2O_4$/BiOBr nanocomposite and its photocatalytic activity towards RhB and tetracycline hydrochloride degradation under household visible LED light irradiation. *J. Alloys Compd*. **2021**, *867*, 157947.

5. Ghorai, K.; Panda, A.; **Bhattacharjee, M.**; Mandal, D.; Hossain, A.; Bera, P.; Seikh, M. M.; Gayen, A. Facile synthesis of $CuCr_2O_4$/CeO_2 nanocomposite: A new Fenton like catalyst with domestic LED light assisted improved photocatalytic activity for the degradation of RhB, MB and MO dyes. *Appl. Surf. Sci*. **2021**, *536*, 147604.

6. Ghorai, K.; Panda, A.; Hossain, A.; **Bhattacharjee, M.**; Chakraborty M.; Bhattacharya S. K.; Bera, P.; Kim, H.; Seikh, M. M.; Gayen, A. Anatase TiO_2 decorated $CuCr_2O_4$ nanocomposite: A versatile photocatalyst under domestic LED light irradiation. *Appl. Surf. Sci*. **2021**, *568*,150838.